

Holographic Investigation of Azobenzene-Containing Low- Molecular-Weight Compounds

Von der Universität Bayreuth
zur Erlangung des Grades eines
Doktors der Naturwissenschaften (Dr. rer. nat.)
genehmigte Abhandlung

von

Hubert Audorff

geboren in

Weiden in der Oberpfalz

1. Gutachter: Prof. Dr. Lothar Kador
2. Gutachter: Prof. Dr. Werner Köhler

Tag der Einreichung: 15.12.2010

Tag des Kolloquiums: 16.02.2011

Table of Contents

1	Introduction	1
1.1	Analog data storage	1
1.2	Digital data storage.....	1
1.3	Holographic data storage	3
1.3.1	Photorefractives.....	4
1.3.2	Photopolymers.....	4
1.3.3	Azobenzene-containing materials	5
1.4	Aim of the thesis	6
1.5	Outline	7
2	Basic theory	9
2.1	Holography	9
2.2	Holographically induced volume gratings.....	10
2.2.1	Writing and reading of holograms with plane waves	10
2.2.2	Diffraction off thin holographic gratings	14
2.2.3	Diffraction off thick holographic gratings.....	15
2.2.4	Holograms of objects.....	18
2.3	Azobenzene.....	19
2.4	Surface relief gratings.....	23
2.4.1	Holographically induced surface relief gratings.....	23
2.4.2	Gradient force model	25
3	Materials	29
3.1	Azobenzene-containing low-molecular-weight compounds ...	29
3.1.1	Central building blocks of low-molecular-weight compounds.....	30
3.1.2	Azobenzene side groups of low-molecular-weight compounds.....	32
3.1.3	Synthesis of the low-molecular-weight compounds	32
3.1.4	Thermal and optical properties of the low-molecular-weight compounds	33

3.1.5	Reorientation of azobenzene chromophores in low-molecular-weight compounds	36
3.2	Azobenzene-containing polymers	37
3.3	Sample preparation	40
3.3.1	Preparation of thin samples	40
3.3.2	Preparation of thick samples	41
4	Experimental methods	43
4.1	Holography with plane waves	43
4.2	Holography of two-dimensional data pages	46
4.3	Ellipsometry	47
4.4	Atomic force microscopy	48
5	Low-molecular-weight compounds with latent liquid-crystalline properties	51
5.1	Liquid-crystalline phases in low-molecular-weight compounds	51
5.2	Light-induced phase changes	54
5.3	Reorientation of the chromophores on the molecular scale ...	58
5.4	Experiments at elevated temperatures	60
5.5	Bisazobenzene chromophores	64
6	Amorphous low-molecular-weight compounds	67
6.1	Temporal behavior of the refractive-index modulation	67
6.2	Influence of the central building block	69
6.3	Influence of the number of arms	70
6.4	Influence of the substituent	71
6.5	Best azobenzene-containing molecular glass	72
6.6	Holographic experiments at elevated temperatures	74
6.7	Angular multiplexing with molecular glasses	75
7	Molecular glasses as blending materials	79
7.1	Blends with polystyrene	79
7.2	Blends with an azobenzene-containing homopolymer	82
7.3	Blends with an azobenzene-containing diblock copolymer	86

7.4	Temperature dependence of blends with a diblock copolymer	93
7.5	Blends with a diblock copolymer containing mesogenic units	93
7.6	Angular multiplexing	95
7.7	Storage of two-dimensional data	97
7.8	Blends with liquid-crystalline low-molecular-weight compounds	99
8	Surface relief gratings	101
8.1	Temporal evolution of the diffraction efficiency	101
8.2	Influence of the polarization of the writing beams	105
8.3	Influence of the substituents	107
8.4	Influence of the temperature	109
8.5	Influence of the matrix	113
8.6	Replication of surface relief gratings	116
9	Summary	119
10	Zusammenfassung	123
11	Appendix A: Liquid-crystalline polymers	127
12	Appendix B: Determination of the glass transition temperature of the minority segment of diblock copolymers	133
13	Appendix C: Publications	139
14	References	141
15	Acknowledgement	157

List of figures

2.1	Writing and reading of holographic gratings.....	11
2.2	Electric-field vector distribution in the region of interference.....	12
2.3	Diffraction efficiency of thick gratings.....	16
2.4	Isomerization reactions of azobenzene.....	19
2.5	Schematic absorption spectrum of azobenzene.....	20
2.6	Angular hole burning of azobenzene chromophores.....	22
2.7	Schematic side views of surface modulations.....	24
3.1	Schematic building blocks of low-molecular-weight compounds	30
3.2	Functionalized central building blocks.....	31
3.3	Azobenzene side groups attached to the central building block	32
3.4	Final reaction step of the low-molecular-weight compounds.....	33
3.5	Absorption spectrum and chemical structure of compound 7g ..	36
3.6	Angular dependence of the absorption coefficient.....	37
3.7	Chemical structures of polymers 17 , 18 , and 19	38
4.1	Holographic set-up for experiments with plane waves.....	43
4.2	Holographic set-up for experiments with 2d data-fields.....	46
4.3	Schematic set-up of ellipsometry.....	48
4.4	AFM image of an SRG on a film of compound 6g	49
4.5	Set-up of an atomic force microscope.....	50
5.1	Thermal properties of low-molecular-weight compounds.....	52
5.2	Differential scanning calorimetry and polmic pictures.....	53
5.3	Refractive-index modulation during inscription.....	55
5.4	Refractive-index modulation after inscription.....	55
5.5	Step-wise inscription of a holographic grating in 11i	58
5.6	Polarized IR absorbance.....	59

5.7	Refractive-index modulation in 11i as a function of time at different temperatures	60
5.8	Writing time and time to reach the maximum of post-development in 11i as a function of temperature	61
5.9	Maximum refractive-index modulation and amplitude of post-development in 11i as a function of temperature	61
5.10	Refractive-index modulation during a heating cycle.....	62
5.11	Annealing of holographic gratings in 11i	63
5.12	Stability of the refractive-index modulation in 6k and 6l	65
6.1	Build-up and decay of the refractive-index modulation in 7g	69
6.2	Time constant of the build-up and maximum refractive-index modulation in 7g as a function of temperature	74
6.3	Angle-multiplexing of plane-wave holograms inscribed in a thick sample of compound 6g blended with polycarbonate	77
7.1	Schematic view of a blend between a small amount of an molecular glass and a diblock copolymer.....	80
7.2	Time constant of the build-up and normalized refractive-index modulation as a function of the concentration of 7g in PS.....	81
7.3	Absorption spectra of 7g in PS.....	81
7.4	Position of the $\pi\pi^*$ -transition of blends of homopolymer 17 and molecular glass 7g as a function of the concentration of 7g	82
7.5	Maximum refractive-index modulation and time constant of the build-up of blends of homopolymer 17 and molecular glass 7g .	83
7.6	Material sensitivity of blends of homopolymer 17 and molecular glass 7g as a function of the concentration of 7g	84
7.7	Chemical structure of the non-photo-active compound 20	85
7.8	Stability of the refractive-index modulation of blends of homopolymer 17 and molecular glass 7g	86
7.9	Maximum refractive-index modulation and writing time of blends of diblock copolymer 18 and molecular glass 7g	87
7.10	Material sensitivity of blends of diblock copolymer 18 and molecular glass 7g as a function of the concentration of 7g	88

7.11 Schematic view of azobenzene-containing minority segments of a diblock copolymer with molecules of a molecular glass	89
7.12 TEM picture of a blend of diblock copolymer 18 and molecular glass 7m	92
7.13 Maximum refractive-index modulation and writing time of blends of diblock copolymer 18 and molecular glass 7g as a function of temperature.....	93
7.14 Maximum refractive-index modulation and writing time of blends of diblock copolymer 19 and molecular glass 7g	94
7.15 Material sensitivity of blends of diblock copolymer 19 and molecular glass 7g as a function of the concentration of 7g	95
7.16 Angular multiplexing of 80 holographic gratings in a thick sample of a blend containing PS, 7g , and 19	96
7.17 Checkerboard pattern reconstructed from a sample containing PS, 7g , and 19	97
7.18 10 data pages of each 24x18 squares reconstructed from a sample containing PS, 7g , and 19	98
8.1 Temporal evolution of the diffraction efficiency during the formation of a surface relief grating of compound 6c	103
8.2. AFM image of a sinusoidal surface modulation and an egg-crate in compound 6g	104
8.3 Maximum height of the surface relief gratings.....	106
8.4 Build-up and initial decay of surface relief gratings of compound 6c at different temperatures	110
8.5 Maximum height of surface relief gratings of compound 6c as a function of temperature	111
8.6 Decay of the height of surface relief gratings after the end of the writing process in compound 6c at different temperatures	112
8.7 Residual height of surface relief gratings after 1000 s in compound 6c as a function of temperature.....	113
8.8 AFM pictures of a surface relief grating in a blend consisting of 6g and Ultem	115
8.9 Replica molding of a surface relief grating	117

11.1 Chemical structure of the polymers 21-27	127
11.2 Polmic pictures of homopolymer 21	128
11.3 Writing time and refractive-index modulation as a function of temperature of a quenched sample of 25	132
11.4 Rate of the inscription and refractive-index modulation as a function of temperature of a quenched sample of 25	132
12.1 Build-up of the refractive-index modulation at different temperatures	134
12.2 Stability of the refractive-index modulation at different temperatures	135
12.3 Logarithm of the rate constants as a function of $1/T$	136
12.4 Relative amplitude of the decay as a function of temperature .	136

List of tables

3.1	Optical and thermal properties of azobenzene-containing low-molecular-weight compounds.....	35
3.2	Properties of the polymers 17-19	39
5.1	Holographic results of 17 selected compounds.....	56
5.2	Holographic results of bisazobenzene-containing materials.	65
6.1	Holographic results of blends of PS and low-molecular-weight compounds with different central building blocks	70
6.2	Holographic results of low-molecular-weight compounds with different number of arms attached to the cyclohexane core.	71
6.3	Holographic results of low-molecular-weight compounds with different substituents at the azobenzene chromophores.....	72
6.4	Holographic results of blends of PS and low-molecular-weight compounds with different central building blocks and substituents a and g	73
6.5	Holographic results of low-molecular-weight compounds with different central building blocks.	73
7.1	Holographic results of blends of compounds 8i and 7g	99
8.1	Parameters of SRG formation for different polarization configurations of the writing beams	105
8.2	Parameters of SRG formation of five molecular glasses.....	108
8.3	Parameters of SRG formation in samples of 6l	114
11.1	Characteristic data of the polymers 21-27	128
11.2	Optical and holographic properties of the polymers 21-27	130
12.1	Holographic results of temperature-dependent experiments ...	135

1 Introduction

1.1 Analog data storage

From the beginning of its history, mankind had the desire to impart and secure its knowledge for its posterity. Being able to pass all important information from one generation to the next orally and especially in the much more reliable form of recordings has facilitated and accelerated the ascent of *Homo Sapiens* to the dominant species on earth. The techniques to save information have improved over thousands of years. The oldest preserved recordings are cave paintings that are more than 30 000 years old. 6000 years ago, the first writings on clay plates were used by the Sumers. The character sets changed and also the writing surfaces as well as the writing materials. In old Egypt, the hieroglyphs were first written on stone. Later, many other materials for the plates were used, such as iron, gold, tin, wax, or silk. An improvement for making the stored information handier and increasing the storage density was to use thinner and lighter writing surfaces such as papyrus. In the Middle Ages also parchment was used. But it was paper, which was developed more than 2000 years ago in China, which became the prevalent writing material for hundreds of years and is still very important nowadays. For centuries it took much time to copy the information by hand. This problem was solved by the invention of the printing almost 600 years ago. The storage density in the analog age increased from the hieroglyphs written on stone 5000 years ago (1 kb/m²) to a page of written paper (300 kb/m²).

1.2 Digital data storage

In the 1940s, a new era started: the digital age. The first computer was built by Konrad Zuse in 1941. His Z3 was a fully operational and programmable electro-mechanical computer capable of binary arithmetic. Today mankind can no longer live without computers and bits of data are an indispensable resource in the information age. Over the last 70 years, the speed of computers increased by many orders of magnitude. As a consequence, the amount of data which is processed and which needs to be stored also increased enormously. Today, around 1 ZB (10²¹ byte) of digital data exist in the world and this amount of data increases by roughly 50 % every year ^[1]. For efficient storage, also the data density inside the storage media must increase. Whereas in the beginning of the digital age the data was stored on punched cards with a data density of 40 kb/m², nowadays data densities of 500 Tb/m² are state of the art. New methods and materials have to be

developed in the future to replace the current technologies of information storage, so they do not become the bottle neck of computers.

Today, three techniques are applied for the preservation of digital information: magnetic, electrostatic, and optical storage. In the 1960s the era of the first technique started when the magnetic tape replaced the punched cards as established storage system. The data is stored as permanent magnetization in small volumes of the medium. For the private user, the standard storage device today is a magnetic hard-disk drive, which is built in every computer. Magnetic tapes are also still in use, mainly in businesses to archive or back-up huge amounts of data, since the tape has high data capacity and data rates combined with low power consumption. The data densities for magnetic data storage cannot be arbitrarily increased, because there is a fundamental limit for the minimum size of a bit. If the volume of a bit in a magnetic medium is further reduced, it will be soon so small that the magnetization is no longer thermally stable.

To interchange data from one computer to another, magnetic floppy discs were mainly used in the last century but have now been replaced by flash drives, which are also used for data back-up. The data in the flash drives is stored electrostatically. The memory cells are metal-oxide-semiconductor field-effect transistors (MOSFETs) with two gates. On top is the control gate, as in other transistors. The second gate, the floating gate, is positioned between the control gate and the MOSFET channel and insulated by a dielectric. Charges can tunnel to the floating gate if a potential difference is applied. These charges are long-term stable and represent the stored information. The data can be read out by applying a voltage to the control gate. If the floating gate holds a charge, it modifies the threshold voltage which, in turn, influences the measurable current between source and drain.

The third important technique to store digital data is optical data storage. Its story of success started almost 30 years ago, when the compact disc (CD) was introduced. With the first generation of optical discs, a storage capacity of 650 MB and single-speed writing and reading rates of 150 kB/s could be achieved. The CD was first used for the dissemination of data, which today is still the main use for optical data storage, along with data interchange and back-up. The data is stored bit-wise in a two-dimensional layer on a spiral track on the CD. The prerecorded CD consists mainly of polycarbonate, on which a thin layer of aluminum is placed and protected by a cover layer. Along the track, there are pits in the aluminum. The regions between the pits are called land. The reading laser operates at 780 nm and is focused by a lens of numerical aperture 0.45 to a spot of 0.87 μm . The reflected light can be extinguished by destructive interference at the transition between pit and land. Thus, the pits do not directly represent the “0” or “1” of the binary data, but a change from one to the other indicates “1”, while no change indicates “0”. In

recordable CDs, the aluminum is replaced by a photosensitive dye layer and in rewritable CDs by a metallic alloy which can change its phase upon illumination. When illuminating the dye or the alloy, the optical properties of the recording layer are changed, leading to differences in reflectivity between the illuminated and non-illuminated areas representing the inscribed bits. In 1997 the digital versatile disc (DVD) was presented which has a single layer capacity of 4.7 GB and data rates of 1.4 MB/s. This increase in performance was achieved by using the same principle of storage as in the CD, but decreasing the laser spot to 0.54 μm by using a laser at 650 nm and a lens of numerical aperture 0.6. The third generation of optical data storage, blu-ray (BR), was introduced in 2003 which has improved optics as compared to the previous generations. The wavelength of the light has been reduced to 405 nm and the numerical aperture is 0.85, leading to a focal spot of 0.24 μm and resulting in a single layer capacity of 25 GB and data rates of 4.5 MB/s.

The optical data storage system of the fourth generation is expected to have storage capacities of 1 TB and data transfer rates of 1 Gb/s. There are several approaches to achieve this increase in performance. The most obvious approach would be to further reduce the bit size by reducing the beam size. As was done in the generations before, this can be achieved by reducing the wavelength of the reading light or using optics with a higher numerical aperture ^[2,3]. Another possibility is to use near-field optical transducers ^[4] or surface plasmons ^[5]. A further possibility is to store more than one bit per pit, e.g. by varying depth and rotation of each pit. A completely different technique with many advantages as compared to the first generations of optical discs is multidimensional recording. The most promising candidate in this field is holography.

1.3 Holographic data storage

In contrast to all other digital data storage techniques, holographic data storage (HDS) uses all three dimensions of the recording material and not only the surface. The theoretical limit for the size of one bit is roughly λ^3 , resulting in enormous data densities. High data rates are achieved by parallel inscription and read-out of entire data pages with millions of bits. This parallel processing enables associated search rates of 100 Gb/s to find unindexed information and data rates of 10 Gb/s ^[6]. Already in 1963, the great potential of holography as data storage technique was realized ^[7,8]. The laser was the solution for one of the main problems of holography since it emits coherent light which is needed for the inscription of holograms ^[9]. Along with the dramatic improvements of the optical set-up, most notably the advent of sensitive cameras and spatial light modulators, these innovations led to an extended research in the field of holographic data storage ^[6,10]. Finding the right material for HDS is the central problem preventing the success of

holographic data storage up to now. A suitable material has to meet stringent requirements ^[6] such as thickness in the millimeter-range, high sensitivity, high dynamic range, low shrinkage, and low light scattering.

1.3.1 Photorefractives

Inorganic photorefractive crystals, e.g. iron doped LiNbO_3 , were the first class of materials to be intensely investigated for the application in HDS ^[11,12]. Several steps take place during the inscription of holograms in these materials. In the bright regions of the holographic interference pattern, electrons are photo-excited from impurity levels into the conduction band. These electrons can diffuse throughout the crystal. Their net diffusion occurs towards the dark regions of the material. While in the conduction band, the electrons may recombine with holes and return to impurity levels where they are trapped. This leads to a redistribution of electrons from illuminated to non-illuminated regions of the material, causing an electric field, which is known as space charge field. Since the trapped electrons and holes are immobile, the space charge field persists even when the illuminating beams are turned off. Via the electro-optic effect, the internal space charge field causes a change of the refractive index of the crystal. This, in turn, leads to a spatial refractive-index modulation throughout the crystal. The advantages of photo-refractive materials are low light scattering and large refractive-index modulation, but their photo-sensitivity is rather low.

1.3.2 Photopolymers

Another possible material class for HDS are photopolymers ^[13-16] which consist of several components: monomer, photo-initiation subsystem, and a chemically inactive matrix. Upon light exposure, the photo-initiation subsystem triggers the polymerization of the monomer. This generally results in local variations in density, and more monomers diffuse to the region of polymerization. After the diffusion, the polymer is dominant in the illuminated areas, whereas in the dark regions, the chemically inactive matrix prevails. This leads to a refractive-index change if these two components have different optical properties. An advantage of photopolymers is the high chemical reactivity of the monomers which results in very high photo-sensitivities. But, on the other hand, it requires the introduction of additional steps in the inscription process. Before inscribing a grating, the shelf life of the recording material has to be on the order of years. To suppress the polymerization in the dark, an inhibitor must be added which has to be consumed in a precure process before the inscription of the hologram. After the recording, a post-cure step is required to consume any unreacted active recording components and photo-initiator. Additionally, there are problems with shrinkage and the thickness of the samples is limited. Despite all these

undesired properties, the first holographic data storage system ^[17] based on photopolymers has become commercially available in 2010. On a disc with a diameter of 13 cm, 300 GB of data can be stored and data rates of 20 MB/s have been achieved ^[18].

1.3.3 Azobenzene-containing materials

Photochromic materials, especially azobenzene ^[19], can be used as holographic storage medium. Upon electronic excitation, the chromophore performs isomerization and subsequent reorientation processes, leading to a change of the refractive-index. Since this reorientation is reversible, azobenzene is one of the few rewritable holographic materials. The first azobenzene materials to be tested for HDS were liquid-crystalline homopolymers with azobenzene side groups introduced by Ringsdorf ^[20,21] in 1984. The applicability of volume gratings in homopolymers for HDS was described first by Eich and later by other groups ^[22-24].

When an azobenzene-containing homopolymer is illuminated with a holographic light grating, besides the volume grating also a surface relief grating (SRG) ^[25-30] can develop which is detrimental to HDS. This macroscopic material transport below the glass transition temperature (T_g) is a field of intense research. There are numerous theories ^[31-36] describing the formation, but the mechanism is not yet understood. Another problem with homopolymers is the relatively high optical density of samples in the millimeter-range which are required for HDS. There are different approaches to achieve the necessary dilution leading to the optimal optical density of 0.5 - 0.7 ^[37,38]. Blending homopolymers with an inert polymer leads to microphase separation and, therefore, the scattering of light. A more promising way to achieve the dilution are statistical copolymers with azobenzene moieties attached to the polymer backbone ^[20,39] as investigated thoroughly by Natansohn ^[22,40-44]. However, also statistical copolymers tend to develop SRGs and the optical density of thick samples is still too high. Another disadvantage is the loss of the cooperative effect ^[45-47] in statistical copolymers. When the azobenzene chromophores are close to each other, they stabilize their orientation through steric and dipole-dipole interactions. The cooperative effects lead also to an enhanced rate and degree of orientation. When the azobenzene groups are diluted, like in statistical polymers, this positive effect is lost. Amorphous block copolymers ^[48] are a possible solution for the problems discussed above. They are composed of an inert majority block and a photo-active minority block containing the azobenzene side groups. Depending on the ratio of the block lengths, the minority block can develop microphase-separated and uniform spheres with diameter below 100 nm, so the cooperative effects are maintained in the confined geometry of the minority block and no light scattering in the visible range occurs.

Additionally, azobenzene-containing diblock copolymers are rewritable materials with low shrinkage. They can be blended with an inert polymer to obtain thick samples in the millimeter-range with an optical density of 0.6 [49]. In samples of this thickness, up to 200 plane-wave holographic gratings can be angle-multiplexed and also two-dimensional data can be multiplexed [50]. Consequently, the interest in amorphous block copolymers containing azobenzene chromophores as material for HDS has increased substantially over the past years [49,51-53].

The low sensitivity of azobenzene-containing diblock copolymers is a major drawback of those materials. An interesting new class of materials are low-molecular-weight compounds with azobenzene chromophores covalently bound to a central building block. They are expected to show faster response to light and higher sensitivity due to the lack of polymer chain entanglement [54,55]. The first amorphous azobenzene-containing low-molecular-weight compounds were introduced by Shirota [56] and consisted of one azobenzene chromophore which was linked to an arylamine derivative. Since then, many azobenzene-containing low-molecular-weight compounds with different topologies and azobenzene chromophores have been synthesized and studied [54,57-59]. Due to their well-defined molecular structure, they are perfect model systems for comparative investigations and to derive structure-property-relations [60-62]. To date, the focus of experiments with azobenzene-containing low-molecular-weight compounds lies on the formation of surface relief gratings [54,63-65]. It was found that low-molecular-weight compounds develop surface relief gratings very efficiently [54,64,65]. On the contrary, holographic volume gratings in azobenzene-containing low-molecular-weight compounds have rarely been investigated.

1.4 Aim of the thesis

The aim of the present thesis is to investigate azobenzene-containing low-molecular-weight compounds with holographic methods to obtain a deeper understanding of this new class of materials. Using a modular-design-principle, a large library of low-molecular-weight compounds can be synthesized. Their basic building blocks are the central core unit, the azobenzene chromophore with substituent and the linkage group and spacer between azobenzene and core. With holographic experiments, structure-property relations can be derived and the holographic performance of the material -especially the refractive-index modulation and the writing times of the gratings- can be optimized. In general, the photo-sensitivity of azobenzene-containing low-molecular-weight compounds is higher than that of comparable diblock copolymers. Therefore, blends containing low-molecular-weight compounds and polymers will be studied to obtain new materials with all the advantages of diblock copolymers, such as rewritability

and long-term stability, but with a higher sensitivity. Additionally, the orientation of the azobenzene molecules in low-molecular-weight compounds induced by holographic volume gratings is usually not stable over long periods of time. Hence the thesis addresses the question, if and to which degree it is also possible to obtain molecular materials which develop stable holographic gratings. This is especially interesting for applications in holographic optical elements. Besides the formation of volume gratings, also surface relief gratings can develop in holographic experiments. By changing the structure of the low-molecular-weight compounds and the polarization configuration, new insights into the formation of surface relief gratings can be obtained. If the process of their formation is better understood, devices in which surface relief gratings are used (e.g. wavelength filters or wave guide couplers) can be further optimized. On the other hand, surface relief gratings are detrimental to holographic data storage. With a deeper understanding of the involved processes, the formation of surface relief gratings can be promoted or suppressed in a controlled way.

1.5 Outline

The outline of the thesis is as follows: In chapter 2, the principles of holography including the formation of volume gratings in thin and thick media, the azobenzene chromophore, and the formation of surface relief gratings are discussed. In chapter 3, the synthesis, the thermal and optical properties of the investigated azobenzene-containing low-molecular-weight compounds and polymers are presented. Chapter 4 describes the experimental set-up. The influence of the molecular structure, especially the length of the spacer, the linkage group between core and spacer, and the substituent at the azobenzene moiety are systematically investigated in chapter 5. Some of the low-molecular-weight compounds have latent liquid-crystalline properties and the formation of stable holographic gratings in these low-molecular-weight compounds is explored. Chapter 6 deals with the inscription of volume gratings in various amorphous azobenzene-containing low-molecular-weight compounds. Different types of core units and substituents are screened to obtain structure-property relations and to find the material with the best performance in the holographic experiments. This optimized low-molecular-weight compound is used as blending material for polymers, as discussed in chapter 7. In a systematic set of experiments the behavior of blends of azobenzene-containing molecular glasses and polymers is investigated to understand these complex systems. With the optimized blends, holographic data storage experiments are performed. The inscription of surface relief gratings in low-molecular-weight compounds with different polarizations are presented in chapter 8. Additionally, different azobenzene chromophores were investigated to obtain structure-property relations and get new insights on the

mechanism of the formation of surface relief gratings. A summary of this thesis is given in chapter 9 and 10. In appendix A, experiments on liquid-crystalline diblock copolymers are presented in which the phase of the photo-active part can be changed from amorphous to liquid-crystalline by illumination. These systems, which can perform a light-induced phase change, show promising properties for holographic data storage. Finally, the determination of the glass transition temperatures of the azobenzene-containing minority blocks of diblock copolymers is discussed in appendix B.

2 Basic theory

2.1 Holography

Holography was invented in 1948 by Dennis Gabor ^[66] when he investigated electron microscopes. At that time, the de Broglie wavelength of the accelerated electrons was short enough to resolve atomic lattices, but the electron optics was imperfect and prevented resolutions better than 12 Å. The ground breaking idea of Gabor was to take a low-quality electron picture which contains the whole information of the object and correct it by optical means. A standard photograph records only the intensities, but by superimposing coherent electron beams also the phase of the object wave can be stored. The reconstruction of the hologram can be processed with an optical system to correct the aberrations of the electron optics. In 1971, Dennis Gabor received the Nobel Prize for “the invention and development of the holographic method”. The origin of the word “hologram” is Greek and means writing (“γραφειν”) the whole (“όλος”) information.

In the realm of light optics, two coherent laser beams are needed to record a hologram. One beam is incident on the object, where it is reflected, scattered or transmitted. This object beam is superimposed in the holographic medium with a coherent reference beam. All the information of the original object beam, i.e. amplitude and phase, is stored in the resulting interference pattern. Additionally, it is also possible to store the polarization of the object beam ^[67].

Holograms can be classified into different categories ^[68-71]. Gabor used in-line holograms because of the short coherence length of the light of the mercury lamp he used. In this set-up, which only works with transparent objects, the reference and the object beam have the same propagation direction. The object beam is scattered light from the object. This technique has some disadvantages. One is that during reconstruction of the hologram, the reconstructed object wave is overlaid with the usually much more intense reference beam, since both have the same propagation direction. This decreases the quality of the readout. With the invention of the laser and its long coherence length, also off-axis holograms could be inscribed which circumvent this problem. Today, mainly off-axis holograms are used. In this configuration, the light from a laser is split into two coherent parts and the object and reference wave are off-axis meaning that they are incident on the sample at different angles. The angle between the object and reference beam distinguishes between two subtypes. If the angle is between 0° and 90°, a transmission hologram is inscribed. For larger angles, a reflection hologram is generated, in which the reference beam is reflected off the holographic grating

to reconstruct the object beam. In the present thesis, off-axis transmission holograms are examined. The holographic gratings can be inscribed either in the volume or on the surface, as will be discussed in detail in the next sections.

2.2 Holographically induced volume gratings

Holographic volume gratings can be used for HDS, but also for security applications ^[72], holographic displays ^[73], non-destructive inspection of materials by holographic interferometry or illumination engineering. Holographic volume gratings are stored by interaction of the holographic interference pattern with the holographic material. The medium can either store the information of the interference pattern by a change of absorption coefficient (amplitude hologram) or as change of the refractive index (phase hologram). A typical material for amplitude holograms is silver bromide, which was also the first material to be used in holography. For phase holograms, mainly photopolymers or azobenzene-containing materials are used. The maximum diffraction efficiency (DE) of the first order of diffraction of an amplitude hologram is only 6.25 %. Since the diffraction efficiency can reach 100 % in phase holograms, most holograms are stored as phase holograms. All the holograms investigated in this thesis are also phase holograms.

2.2.1 Writing and reading of holograms with plane waves

The simplest hologram one can think of is the symmetric interference of two plane waves with the same wavelength and the same angle of incidence, as shown in figure 2.1a. A hologram generated by two plane waves is also called the hologram of no object. In this case the object and reference are equivalent and lie together with the transmitted beams in the x - z -plane of the coordinate system shown in figure 2.1b. The standard polarization configuration for holographic experiments is ss . In this case both beams are s -polarized meaning that their electric-field vector oscillates perpendicular to the plane of incidence so also the polarization oscillates along the y -axis. For this polarization configuration, the interference of the electric fields of the reference and the object beam causes an intensity grating I :

$$\begin{aligned}
 I &\propto \left| \vec{E}_R(\vec{r}, t) + \vec{E}_O(\vec{r}, t) \right|^2 = \left| \vec{R} e^{i(\omega t - \vec{k}_R \vec{r})} + \vec{O} e^{i(\omega t - \vec{k}_O \vec{r})} \right|^2 \\
 &\propto I_R + I_O + 2\sqrt{I_R I_O} \cos\left(\frac{2\pi x}{\Lambda}\right)
 \end{aligned} \tag{1}$$

with:

- \vec{E}_R electric field of the reference wave
- \vec{E}_O electric field of the object wave
- \vec{R} amplitude of the electric field of the reference beam
- \vec{k}_R wave vector of the reference beam
- ω angular frequency
- \vec{O} amplitude of the electric field of the object beam
- \vec{k}_O wave vector of the object beam
- I_R intensity of the reference beam
- I_O intensity of the object beam

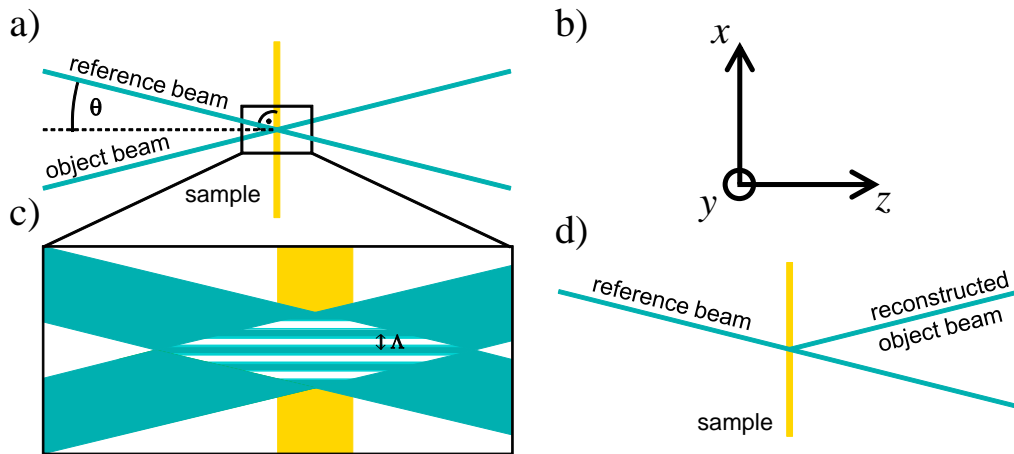


Figure 2.1. Principles of writing and reading of holographic gratings. a) Writing of a hologram with reference and object beam propagating in the x - z -plane. b) Responding coordinate system. c) Enlarged region of interference. d) Reconstruction of the object beam by illuminating the inscribed hologram with the reference beam coming from the upper left corner.

From equation 1 one can see that the phase information of the two beams is stored in the interference term of the intensity distribution.

The resulting grating period Λ is:

$$\Lambda = \frac{\lambda}{2n_0 \sin \theta} \quad (2)$$

with:

- λ vacuum wavelength of the incident laser light
 θ angle of incidence of the laser light inside the material
 n_0 refractive-index of the material

Equation 2 is valid inside and outside the material, the grating period Λ is the same in both cases. Another important parameter is the contrast V defined as:

$$V = \frac{2\sqrt{I_R I_O}}{I_R + I_O} \quad (3)$$

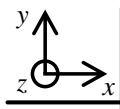
	0	$\frac{\pi}{2}$	π	$\frac{3\pi}{2}$	2π
<i>ss</i>					
<i>pp</i>					
$\pm 45^\circ$					
$\pm 45^\circ$					
<i>rlcp</i>					
<i>rrcp</i>					
<i>sp</i>					

Figure 2.2. Total electric-field vector distribution in the region of interference at five distinct phase differences between the writing beams. The coordinate system in the upper left corner corresponds to the one shown in figure 2.1b (viewed from a different direction).

Thus, equation 1 can be transformed to:

$$I \propto (I_R + I_O) \left[1 + V \cos\left(\frac{2\pi x}{\Lambda}\right) \right] \quad (4)$$

If the contrast V equals unity, both light beams have the same intensity and the light intensity is modulated sinusoidally along the x -axis from 0 in the

dark areas to the maximum in the bright areas. Hence, a pure intensity grating can be obtained in this *ss*-configuration, as shown in figure 2.1c.

Besides the *s*-polarized beams as discussed above, also other polarizations of the beams are possible. In the case of *p*-polarization, the electric-field vector oscillates in the plane of incidence. A 45° polarization corresponds to an angle of 45° with respect to this plane. Furthermore, right-circularly polarized (*rcp*) and left-circularly polarized (*lcp*) light can be used. These polarizations can be combined to achieve different polarization configurations, which are summarized in figure 2.2. If an *s*-polarized and a *p*-polarized wave interfere, the resulting so-called *sp*-configuration generates a pure polarization grating with spatially constant intensity but varying polarization direction. $\pm 45^\circ$ and right and left circularly polarized (*rlcp*) are mainly polarization gratings with only a small amount of intensity variation, whereas *pp*, $++45^\circ$, and right and right circularly polarized (*rrcp*) are mainly intensity gratings with a slight variation of the polarization direction. The most common polarization configuration for holographic experiments is *ss*, a pure intensity grating.

When the holographic grating is read out, as shown in figure 2.1d, there are two limiting cases. The distinction is possible with the help of the two parameters Q' and γ ^[74-78]:

$$Q' = \frac{2\pi \lambda d_0}{n_0 \Lambda^2 \cos \theta} \quad (5)$$

$$\gamma = \frac{\pi n_1 d_0}{\lambda \cos \theta} \quad (6)$$

with:

- d_0 thickness of the sample
- n_1 first spatial component of the refractive-index modulation (cf. equation 9)

Gratings are called thin if:

$$Q' \leq 1 \text{ and } \gamma \cdot Q' \leq 1 \quad (7)$$

The thickness of thick holographic gratings is much larger than the grating period Λ . Thick sinusoidal gratings show Bragg diffraction meaning that the light is only diffracted into one diffraction order. In contrast, thin sinusoidal holographic gratings show Raman-Nath diffraction with many diffraction orders.

2.2.2 Diffraction off thin holographic gratings

To store the intensity grating, a photo-sensitive medium has to be placed in the region of interference. If *ss*-polarization is used, the material is expected to react to the illumination in the bright regions, whereas it stays unaffected in the dark regions. The intensity grating leads to a change of the absorptivity α and refractive-index n . These quantities can be written as Fourier series:

$$\alpha = \alpha_0 + \alpha_1 \cos\left(\frac{2\pi x}{\Lambda}\right) + \dots = \sum_{m=0}^{\infty} \alpha_m \cos\left(\frac{2\pi x m}{\Lambda}\right) \quad (8)$$

$$n = n_0 + n_1 \cos\left(\frac{2\pi x}{\Lambda}\right) + \dots = \sum_{m=0}^{\infty} n_m \cos\left(\frac{2\pi x m}{\Lambda}\right) \quad (9)$$

with:

- α_0 absorption coefficient of the unexposed material
- α_m amplitude of the m -th spatial Fourier component of the absorption coefficient
- n_m amplitude of the m -th spatial Fourier component of the refractive-index

The holograms investigated in this thesis consist of a spatial refractive-index modulation as described in equation 9. The change of the absorption coefficient can be neglected.

The response of the material can be determined by measuring the first-order diffraction of a light beam off the inscribed grating. Only the amplitude of the first Fourier component of the refractive-index, n_1 , determines the diffraction into the first order. The higher Fourier components influence the higher diffraction orders and are only needed to calculate the difference between the minimum and maximum refractive index. The diffraction efficiency η is defined as:

$$\eta = \frac{I_1}{I_0} \quad (10)$$

with:

- I_1 intensity of the light diffracted into the first order
- I_0 intensity of the incident light

The diffraction efficiency of thin volume gratings can be calculated as ^[76]:

$$\eta = J_1^2(2\gamma) = J_1^2\left(\frac{2\pi n_1 d_0}{\lambda \cos \theta}\right) \quad (11)$$

with:

J_1 Bessel function of the first kind of first order

With equation 11 the amplitude of the first spatial Fourier component of the refractive-index, which is the fundamental oscillation of the refractive-index change, can be calculated. In the following the higher orders are neglected and n_1 is called refractive-index modulation. According to the properties of the Bessel function of the first kind of first order, the maximum diffraction efficiency of thin gratings is 33 %.

The definition of the Bessel function by its Taylor series expansion around $x = 0$ is:

$$J_1(x) = \sum_{m=0}^{\infty} \frac{(-1)^m}{m!(m+1)!} \left(\frac{x}{2}\right)^{2m+1} \quad (12)$$

For the case of small γ , equation 11 can be written with the help of the above equation as:

$$\eta = \left(\frac{\pi n_1 d_0}{\lambda \cos \theta}\right)^2 \quad (13)$$

Equation 13 can be used to calculate the light-induced changes of the refractive-index modulation from the measured diffraction efficiency.

2.2.3 Diffraction off thick holographic gratings

If $Q' \gg 1$ and $\gamma \cdot Q' \gg 1$, the gratings are called thick. In contrast to thin gratings, in thick gratings all the light is diffracted into one order only, for all others the Bragg condition is not fulfilled. The Bragg condition for the diffraction into the first order is:

$$2n_0 \Lambda \sin \theta_0 = \lambda \quad (14)$$

The diffraction off thick gratings was calculated by Kogelnik ^[79]. For this calculation the following assumptions have to be made which only have marginal influence on the results of transmission holograms ^[80]. Reflections at the interface between sample and air and higher orders of diffraction are neglected, a homogenous refractive-index grating is present with $n_1 \ll n_0$,

and the grating vector is perpendicular to the surface normal. Then the diffraction efficiency can be expressed as:

$$\eta = \frac{\sin^2 \sqrt{\nu^2 + \xi^2}}{1 + \frac{\xi^2}{\nu^2}} \quad (15)$$

$$\nu = \frac{\pi d_0 n_1}{\lambda \cos \theta} \quad (16)$$

$$\xi = \frac{\pi d_0 \Delta \theta \cos \theta_0}{\Lambda \cos \theta} \quad (17)$$

with:

θ_0 angle for which the Bragg condition is fulfilled

$\Delta \theta$ deviation from the exact Bragg angle

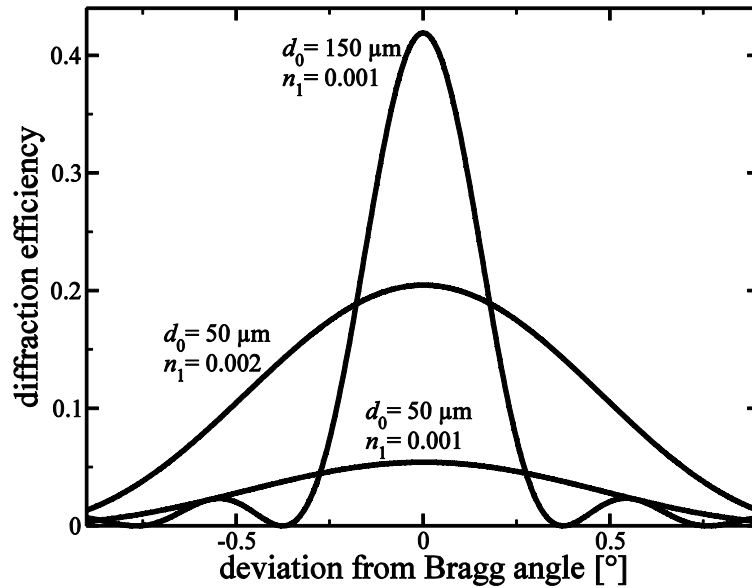


Figure 2.3. Diffraction efficiency of thick gratings as a function of the deviation from the exact Bragg angle for selected values of film thickness and refractive-index modulation.

Figure 2.3 shows a special feature of thick gratings: their angular selectivity. The light of a fixed wavelength is diffracted off the hologram only at a special angle, which can be derived from equation 14 similar to considerations of the Ewald sphere. The angular dependence of this Bragg-mismatch can be calculated with equations 15 - 17. In general, the angular selectivity increases with increasing thickness of the medium, as shown in figure 2.3. This angular selectivity allows the inscription and read-out of many holographic gratings

separately in the same volume of the material. This angular multiplexing is the reason for the enormous data densities which can be achieved in HDS. Other multiplexing techniques such as wavelength-, phase-, or shift-multiplexing are not discussed in the present thesis.

In the special case that the Bragg condition is fulfilled, equation 15 can be simplified to:

$$\eta = \sin \left(\frac{\pi n_1 d_0}{\lambda \cos \theta} \right)^2 \quad (18)$$

From equation 18 it can be seen that the maximum diffraction efficiency for thick gratings is 100%. For small refractive-index modulations, equation 18 becomes:

$$\eta = \left(\frac{\pi n_1 d_0}{\lambda \cos \theta} \right)^2 \quad (19)$$

This formula is equal to equation 13. For light incident at the Bragg angle onto a refractive-index grating with small amplitude, the diffraction efficiencies calculated for thin and thick gratings are the same.

The diffraction efficiency is proportional to $(n_1 \cdot d_0)^2$. To obtain high diffraction efficiencies, the thickness of the material as well as the refractive-index modulation have to be increased, as shown in figure 2.3.

Equation 19 is only valid for a material without absorption. If the material absorbs light, then the writing beams cannot penetrate through the whole sample leading to a reduction of the diffraction efficiency. To account for this absorption -especially in thick samples- the parameter D , the depth of penetration has to be introduced ^[81,82]. It is defined as the length after which the intensity of an incident beam is reduced to a factor e^{-1} :

$$D = \frac{d_0}{OD \ln 10} \quad (20)$$

with:

OD optical density

In strongly absorbing materials, the thickness of the sample d_0 has to be replaced by an effective thickness d_{eff} :

$$d_{eff} = D \left(1 - \exp \left(-d_0 / D \right) \right) \quad (21)$$

In the case of low optical densities, d_{eff} obviously becomes d_0 . The substitution $d_0 \rightarrow d_{eff}$ in equation 13 leads to:

$$\eta = \left(\frac{\pi n_1 d_0}{\lambda \cos \theta} \frac{1}{OD \ln 10} \left(1 - e^{-OD \ln 10} \right) \right)^2 \quad (22)$$

Equation 22 is used to calculate the refractive-index modulation for thick samples, in which the absorption cannot be neglected. For all other cases, equation 13 is used.

In HDS, there are two important benchmarks for the characterization of holographic data storage materials^[6], the dynamic range $M\#$ and the material sensitivity S . The dynamic range is proportional to the refractive-index modulation and is a measure of the storage density. It is calculated by summing up the square-root values of the diffraction efficiency for all N angle-multiplexed gratings in a volume element:

$$M\# = \sum_{i=1}^N \sqrt{\eta_i} \quad (23)$$

The other important property of holographic materials is the recording sensitivity S ^[6]. It describes the slope of the square-root of the growth curve of the diffraction efficiency and is a measure for the writing speed. It can be calculated by the formula:

$$S = \frac{\partial(\sqrt{\eta})}{\partial t} \frac{1}{I_0 d_0} \quad (24)$$

with:

I_0 sum of the intensities of the incident laser beams

Increasing the refractive-index modulation or decreasing the writing time -with all other parameters being constant- leads to an increase of the sensitivity. The latter is usually measured at the beginning of the writing process where it has its maximum value S_{max} . For a material for HDS, values of the dynamic range of 5 and for the sensitivity of 500 cm/J are needed to be competitive to other digital data storage systems.

2.2.4 Holograms of objects

Holograms of three-dimensional objects are a fascinating experience. The reconstruction of the hologram yields an identical image of the original object. When the viewing angle is changed, also the object behind the

hologram changes, as if the original object were present. This effect called parallax is the reason why holograms are not only used in science but also in art.

For the description of the holographic interference of the reference beam with the beam coming from the object, the theory of holography with plane waves discussed above can be used, because any given wave front can be described as a Fourier series of plane waves. The resulting hologram of a three-dimensional object is not a sinusoidal variation of the refractive-index as it was for two plane waves discussed above, but a more complex pattern. The intensity information is stored in the contrast of the holographic pattern, whereas the shape of the pattern is determined by the phase between object and reference beam. In contrast to photography, this holographic pattern has no obvious similarities with the original object.

In HDS, the data is usually stored as an extended two-dimensional object. Data pages consisting of millions of black and white squares are inscribed, whereby a black square represents a digital “0” and a white one a “1”. The parallel inscription of the bits leads to enormous data rates.

2.3 Azobenzene

The isomerization process of azobenzene is essential for understanding the mechanism, how azobenzene-containing materials react to a holographic light grating and build up a refractive-index grating.

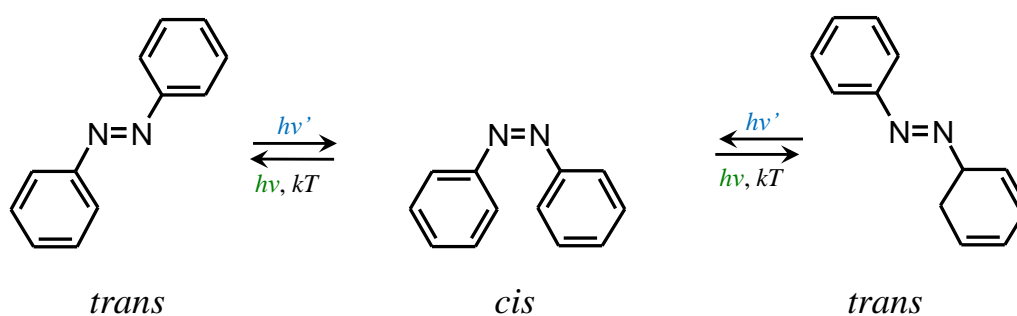


Figure 2.4. Isomerization reactions of azobenzene.

Azobenzene is an aromatic molecule, in which an azo-linkage joins two phenyl rings and the resulting conjugated π -system shows strong electronic absorption. There are two isomers of azobenzene: the stretched *trans*-form (*E*-isomer) and the bent *cis*-form (*Z*-isomer), as shown in figure 2.4. The *trans*-form is energetically more stable by 50 kJ/mol ^[83,84]. The *cis*-state can thermally return to the *trans*-state with an energy barrier for thermal

isomerization of 90 kJ/mol^[85,86]. Therefore, most azobenzene molecules are in the *trans*-form when the sample is stored in the dark. The time constant of the thermal relaxation strongly depends on substituents and surroundings and can reach from seconds to days^[56] or even years^[87]. The *trans*- and the *cis*-form of azobenzene have different properties. For example, the dipole moment is different^[88], only the *trans*-form is a mesogen, *cis*-chromophores occupy a larger fraction of the free volume^[89] and in the *cis*-form the phenyl rings are twisted 90° relative to the CNNC plane^[90]. The photo-isomerization can be used to optically induce phases changes^[91], phase separation^[92], solubility changes^[93], crystallization^[94], and even macroscopic bending of free-standing thin films^[95-97]. The two isomers have also different absorption spectra, making azobenzene a photochromic material. The absorption spectrum can be shifted anywhere from the ultraviolet to the visible red region by push-pull substitutions at the phenyl rings. According to the classification of Rau^[19,98,99], azobenzene chromophores can be classified into three classes depending on the relative energetic order of their $n\pi^*$ and $\pi\pi^*$ states: classical azobenzenes, amino-azobenzenes and pseudo-stilbenes. From the spectra of the chromophores used in the present thesis, it can be concluded that they belong to classical azobenzene chromophores. The *trans*-form absorbs mainly at the $\pi\pi^*$ -transition of the nitrogen double bond. For the materials described in the present thesis, the maximum of the $\pi\pi^*$ -transition is around 350 nm and has a big oscillator strength, as shown in figure 2.5. The weak $n\pi^*$ -transition of the *trans*-isomer has a very low oscillator strength because of its planar shape. The *cis*-form absorbs light mainly at the $n\pi^*$ -transition (maximum around 430 nm) and has almost no oscillator strength at the $\pi\pi^*$ -transition due to geometric reasons.

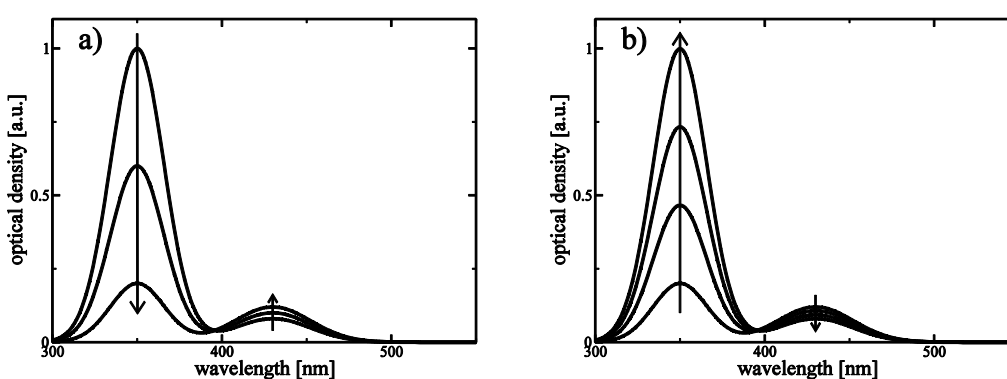


Figure 2.5. Schematic absorption spectra of azobenzene chromophores used in the present thesis. a) Series of simulated spectra during illumination with UV light and b) during thermal or light-induced back relaxation. Along the arrows, the time of illumination with UV light (a) or green light (b) increases.

The photo-induced isomerization occurs usually on a time scale of picoseconds^[100,101]. The energy barrier to the photo-excited state is on the order of 200 kJ/mol^[102]. After the chromophore is electronically excited, it relaxes back to the ground state. This relaxation can lead to an isomerization of the molecule from one form to the other. For the mechanism of isomerization, there are two possible reaction routes^[102-104]: inversion or rotation. In the latter, the double bond is broken into a single bond along which one phenyl ring can rotate. The free volume needed for the isomerization via rotation is 0.38 nm³^[103]. In the other possibility, inversion, the isomerization occurs by an in-plane rearrangement of one phenyl ring, whereby the *sp*²-hybridized nitrogen orbitals become *sp*-orbitals. The free volume for inversion is expected to 0.12 nm³^[104,105]. The small free volume needed for the isomerization process is the explanation why azobenzene can also isomerize in rigid matrices such as glassy polymers. Recently, a new mechanism was proposed, the concerted inversion, where both phenyl rings move at once^[106]. It is generally accepted that the thermal back relaxation occurs via rotation. Although this issue has been controversially discussed for decades, there is still no agreement, which mechanism is responsible for the photo-isomerization. It seems that both mechanisms are possible^[107] and they are competing. Depending on the particular chromophore and its environment, either inversion^[108-111] or rotation dominates^[112,113].

The photo-induced isomerization can take place upon $\pi\pi^*$ - and $n\pi^*$ -excitation with high quantum efficiencies^[114]. When illuminating with ultraviolet (UV) light, mainly the *trans*-isomers are excited which can isomerize to the *cis*-form. This leads to a photo-stationary *cis*-rich state. Therefore, the $\pi\pi^*$ -absorption decreases drastically during the illumination with UV light, whereas the $n\pi^*$ -absorption is increasing, as shown in figure 2.5a. Distinct isosbestic points are present in the sequence of absorption spectra which are characteristically for reversible photochemical reactions. The corresponding back-reaction to a *trans*-rich state can be induced in two ways: either photo-induced (e.g. with green light) or thermally (by keeping the sample in the dark). The height of the $\pi\pi^*$ -transition increases during irradiation of green light to the value before the UV illumination, whereas the $n\pi^*$ -peak decreases, as shown in figure 2.5b. By illuminating the chromophore at a wavelength where both the $\pi\pi^*$ - and the $n\pi^*$ -transition are excited, consecutive *trans-cis-trans* isomerization cycles can be induced.

These continuous isomerization cycles can lead to a reorientation of the long axis of the stable *trans*-form of the chromophore. The transition dipole moment is parallel to its long axis. If polarized light is used, the random reorientation processes of the chromophore in the *trans*-state finally lead to an orientation where the transition dipole moment is perpendicular to the polarization of the incident light. Then the azobenzene chromophore can no longer be electronically excited and remains in that position^[115,116]. This leads

to the so called “angular hole-burning”. The initially isotropically oriented chromophores are all reoriented until they lie in a plane perpendicular to the polarization of the incident light, as shown in figure 2.6. As a consequence, the illuminated areas become birefringent. Due to the anisotropic shape of the chromophores and the corresponding different polarizabilities parallel and perpendicular to the long axis, the refractive index of the illuminated areas becomes different from that of the non-illuminated regions.

In a common holographic set-up, two *s*-polarized laser beams are used which leads to a pure intensity variation. At a writing wavelength of 488 nm both the $\pi\pi^*$ and $n\pi^*$ -transition of the chromophores used in this thesis absorb, meaning that during illumination consecutive isomerization processes from *trans* to *cis* to *trans* are induced in the illuminated areas. This leads to a reorientation whereas the dark areas remain unaffected. When the grating is read out with a laser whose polarization is equal to that of the writing beams, the refractive index in the illuminated areas is smaller (due to the reorientation process during inscription) than that in the non-exposed regions, resulting in a refractive-index modulation n_1 . This refractive-index modulation can be measured by the diffraction efficiency of the grating as discussed in chapter 2.2. Since holography is a zero-background method, very small changes of the refractive-index modulation -on the order of 10^{-7} - can be observed.

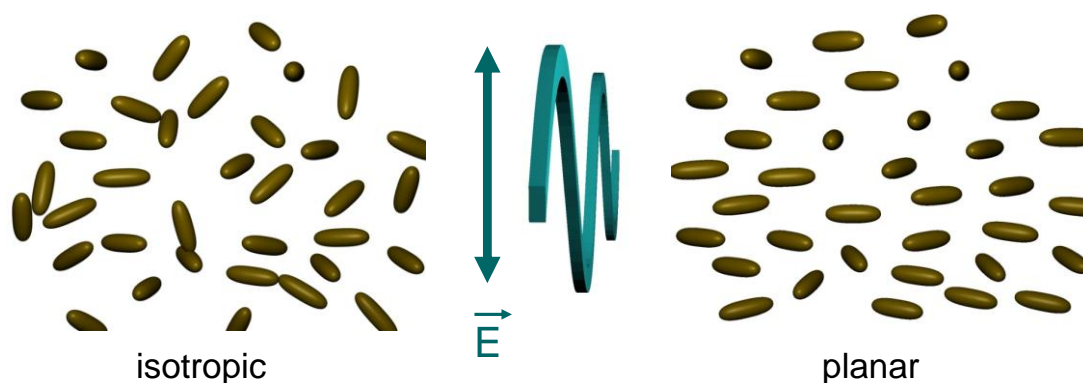


Figure 2.6. Angular hole burning of azobenzene chromophores, here shown as brown cigar-shaped objects.

The temporal behavior of the refractive-index modulation during inscription of a hologram is extremely non-linear with a steep rise at the beginning, then it flattens and slowly approaches a maximum. In the case of intensity gratings, the refractive-index modulation during the inscription of the hologram as a function of time decreases after the maximum. This can be explained by the slow increase of the degree of orientation in the dark regions due to scattered light. At the maximum, the bright regions are already fully oriented.

Therefore the refractive-index modulation -which is the contrast between bright and dark regions- decreases.

Azobenzene has a well-defined photo-chemistry without any side reactions. The chromophore is chemically very stable and can withstand up to 10^6 isomerization cycles without fatigue or damage ^[36]. Azobenzene can be used, e.g. as photo-switch ^[117], photo-probe ^[89,118], and for holographic data storage. But the fact that dozens of isomerization cycles are needed before the chromophore is oriented perpendicularly to the light polarization is a drawback of azobenzene chromophores, since this leads to a low photo-sensitivity. There are many approaches to overcome this problem, such as increasing the quantum efficiency by using bridged azobenzene chromophores ^[119] or increasing the overlap of $n\pi^*$ and $\pi\pi^*$ by using azobenzenes of the pseudo-stilbene-type.

Moreover, azobenzene is a very versatile material. It can induce motions on three length scales. The basic principle of the photo-physics of azobenzene is the reorientation of the chromophore as discussed above, which is a motion on the molecular scale. Motions on the scale of nanometers can be induced by using this reorientation to orient ordered domains in liquid-crystalline materials. The third length scale corresponds to the formation of surface relief gratings which is a macroscopic motion and will be discussed below.

2.4 Surface relief gratings

2.4.1 Holographically induced surface relief gratings

When an azobenzene-containing material is illuminated by a superposition of two coherent laser beams, besides the formation of a volume grating, also modulations of the initially flat surface of the material can occur ^[25,26]. The discovery of this effect in 1995 was completely unexpected, since it is a large-scale mass transport, sometimes hundreds of degrees below the glass transition temperature.

In a typical holographic experiment with plane waves, a sinusoidal surface variation with the same grating period as the interference pattern can develop as shown schematically in figure 2.7a. The grating period in holographic experiments is usually on the order of $1\ \mu\text{m}$ and the height of the SRG from peak to valley can reach the same value. By subsequent inscribing of several holographic gratings at the same location, also more complex structures are possible ^[120-123]. In figure 2.7b an egg-crate structure is shown which can be produced by rotating the material by 90° after the first inscription process and illuminating a second time.

For surface modulations, numerous applications have been proposed, such as liquid-crystal anchoring ^[124], optical polarizers ^[125], wavelength filters ^[126],

waveguide couplers, polarization discriminators ^[120], antireflection coatings ^[126,127], phase masks ^[128], channel waveguides ^[129], or changing the haptic properties of surfaces. So far, surface relief structures are already imprinted on credit cards as a security feature ^[72]. As compared to other techniques for the formation of surface modulations, holographically induced SRGs in azobenzene-containing materials have many advantages. The inscription is an all-optical process which requires only one step and needs no post-treatment. Moreover, the grating period as well as the height can be easily tuned in a wide range.

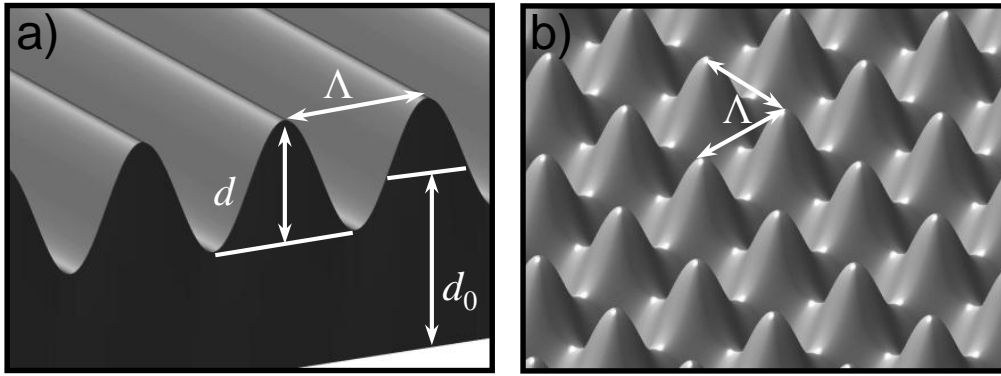


Figure 2.7. Schematic side views of surface modulations: a) surface relief grating and b) egg crate structure.

Surface relief gratings are also thin gratings according to equation 7, so the formalism discussed in section 2.2.2 can also be applied to the description of sinusoidal SRGs. For this purpose, the thickness of the material d_0 has to be replaced by the height d of the SRG from peak to valley and the refractive-index modulation n_1 by Δn :

$$\Delta n = \frac{n_0 - n_{air}}{2} \quad (25)$$

with:

n_{air} refractive index of air

Δn amplitude of the refractive-index change between sample and air

This lead to:

$$\eta = J_1^2 \left(\frac{2\pi \Delta n d}{\lambda \cos \theta} \right) \quad (26)$$

with:

d height of the SRG from peak to valley

With equation 26, the height d of the SRG can be easily calculated in situ from the measured diffraction efficiency.

2.4.2 Gradient force model

The mechanism of the formation of surface relief gratings is not yet fully understood. It is widely accepted that the build-up of an SRG requires a free surface of the material ^[130]. Since the original thickness is recovered by heating above T_g , the observed phenomenon is a reversible mass transport and not ablation. A chromophore performing *cis-trans* isomerization such as azobenzene is a prerequisite for the formation of SRGs ^[120]. There are a number of parameters which influence the formation of surface relief gratings, e.g. the polarization of the laser beams ^[120,128,131,132], the film thickness ^[82], the molecular weight ^[133], the azobenzene concentration ^[134,135], or the glass transition temperature ^[62]. The phase of the material has also an influence on the SRG formation: The build-up is most efficient in amorphous materials ^[136], but also in liquid-crystalline ^[28,137], semi-crystalline ^[54], or even single crystals ^[138] SRGs can develop.

Numerous theories exist which try to explain the formation of surface relief gratings. Although each model describes part of the observed effects correctly, no theory is able to reproduce all observed experimental results. Hvilsted et al. applied a mean-field model ^[33,139] to the formation of SRGs in azobenzene-containing liquid-crystalline polymers. The mean-field potential will align the chromophores parallel to the prevailing molecular direction inside the liquid-crystalline domains. When a light grating is present, the order parameter is modulated due to the spatially varying electric field. This leads to a periodically varying force along the grating vector which causes the mass transport. Henneberg et al. proposed a viscoelastic-flow model ^[34]. Here, the reduction of Young's modulus during light exposure leads to a plastic deformation. Rochon et al. developed a model in which the material transport is ascribed to a pressure gradient ^[32,133] between illuminated and non-illuminated areas, which originates from the larger volume of the *cis*-isomers formed in the bright regions as compared to the *trans*-isomers. The theory of Yager et al. explains the SRG build-up by a competition between photo-expansion and photo-contraction ^[36]. According to the asymmetric diffusion model ^[31] proposed by Lefin et al., the oriented azobenzene chromophores move like an inchworm owing to the isomerization between the stretched *trans* and the bent *cis*-state, so a translational movement can occur resulting in material transport.

The only theory which correctly accounts for different polarization configurations of the laser beams was developed by Kumar et al. It is based on the observation that an electric-field component in the direction of the mass flow is required^[35]. This theory explains the formation of SRG by the presence of a gradient force^[120,140,141]. The spatial variation of the light in the holographic grating leads to a variation of the material susceptibility at the sample surface. In addition, the electric light field polarizes the material. Forces then occur between the polarized material and the light field, analogous to the net force of an electric dipole in an electric-field gradient. The time-averaged gradient force f is:

$$\vec{f} = \langle (\vec{P} \nabla) \vec{E} \rangle = \langle ((\epsilon_0 \chi \vec{E}) \nabla) \vec{E} \rangle \quad (27)$$

with:

- \vec{P} optically induced polarization
- χ electric susceptibility of the material at the optical frequency of the laser

In the following the coordinate system shown in figure 2.1b is used. The x -axis defines the direction of the grating vector, the y -axis is perpendicular to the plane of incidence, and the z -axis is perpendicular to the surface of the sample. The only direction of the macroscopic material transport is along the x -axis, parallel to the grating vector. Therefore, equation 27 can be simplified to^[120,142]:

$$f_x = \epsilon_o \left[\chi'_{xx} E_x \frac{\partial}{\partial x} E_x + \chi'_{yx} E_x \frac{\partial}{\partial x} E_x + \chi'_{zx} E_x \frac{\partial}{\partial x} E_x \right] \quad (28)$$

with:

- χ'_{ix} real part of the electrical susceptibility

The subscript i stands for the spatial coordinates x , y , z . The electric-field vector in the x - y -plane for different polarization configurations of the writing beams at several distinct values of the phase difference between the beams is shown in figure 2.2. The polarization configurations lead to different gradient forces, since the x -component of the electric field in equation 28 is different.

An order-of-magnitude estimate of the strength of the gradient force^[143] leads to a force density of 1000 N/m^3 for the experimental set-up used in this thesis. This value is smaller than the expected value needed for the formation of surface relief gratings. But experiments with AFM^[141] and electromechanical

spectroscopy ^[144] indicate that the action of repeated *trans-cis-trans* isomerization cycles softens and plasticizes the material, thus enhancing the microscopic mobility by orders of magnitude. Due to this photo-softening effect ^[120], the gradient force is sufficient to form SRGs.

The material transport occurs usually from illuminated to dark regions as demonstrated in various experiments ^[25,141,145,146]. But there are also reports that the peaks of the SRGs can form in the bright regions ^[137]. These contrary experimental observations can be explained by the sign of the electric susceptibility in equation 28 which determines the direction of the material transport. For positive values of the susceptibility, which apply to the materials investigated here, the peaks are expected to be in the bright regions. In this case, the light intensity grating and the surface relief grating are in phase. Intensity holograms cause the minima of the refractive-index modulation of the volume grating to be located in the illuminated regions, the maxima in the dark areas as discussed above. Thus, the volume and the surface relief grating are expected to have a phase difference of 180°.

When comparing different materials with positive values of χ' at a given polarization setting, the influence of the electric field is the same for all of them, and only the value of χ' changes f_x in this case. The electrical susceptibility of the material can be written as:

$$\chi = (n_0 - ik)^2 - 1 = n_0^2 - k^2 - 1 - i2n_0k \rightarrow \chi' = n_0^2 - k^2 - 1 \quad (29)$$

with:

k absorption coefficient

The real part of the electrical susceptibility depends on the absorption coefficient k and the refractive index n_0 and can therefore vary for different substituents of the azobenzene moiety.

3 Materials

Pure azobenzene dyes tend to crystallize, which is undesirable for holographic applications. A common approach to circumvent this problem is to covalently attach the azobenzene chromophores to low-molecular-weight materials or polymers. These two concepts are discussed in the next sections. All materials were synthesized at the chair Macromolecular Chemistry I (Prof. H.-W. Schmidt) at the University of Bayreuth.

3.1 Azobenzene-containing low-molecular-weight compounds

An interesting new class of materials are low-molecular-weight compounds. In contrast to functional polymers, low-molecular-weight compounds have the advantages of a well-defined molecular structure, the absence of structural defects and undefined end groups as well as a uniform molecular weight. Like polymers, low-molecular-weight compounds can also form a stable amorphous phase with a glass transition temperature well above room temperature. Different approaches are possible to suppress crystallization and to obtain low-molecular-weight compounds which form a stable amorphous phase. Shirota introduced the name “molecular glasses”^[60-62] for these materials. A non-planar molecular structure is one of the most common concepts. It prevents dense packing of the molecules and, therefore, impedes crystallization. Using bulky substituents which lead to a reduction of the motion of the molecule is another possibility to obtain a glassy state and to improve the long-term stability of the amorphous phase^[60]. Molecular glasses are the subject of intense current studies, mainly with respect to their electronic, optical and optoelectronic properties. They are already used in a number of devices, e.g. in photoconductor drums, organic light emitting devices, organic solar cells, photorefractive materials and anti-reflective coatings^[61,62,147-150].

Azobenzene chromophores can be covalently attached to low-molecular-weight compounds to obtain a light-sensitive material with the advantages mentioned above. An important requirement of azobenzene-containing materials used for holography is the formation of a stable amorphous phase. It is a prerequisite to obtain homogeneous, isotropic, thin films with good optical properties and without light scattering.

Besides the formation of the amorphous phase, the glass transition temperature T_g is another important point. The higher the T_g of the material, the more stable is the amorphous phase. The glass transition temperature can be

increased by introducing rigid substituents or strong intermolecular interactions such as hydrogen bonds. The glass transition temperature in general also increases with the molecular weight or the size of the molecule ^[60,151].

A construction kit principle was used to synthesize a variety of low-molecular-weight compounds. The following structural parameters were changed, as shown in figure 3.1:

- the core unit (light blue triangle)
- the linkage group between core unit and the azobenzene (violet ellipse)
- the spacer between core and azobenzene (brown curve)
- the substituents at the azobenzene, mainly at the *para*-position (red circle)

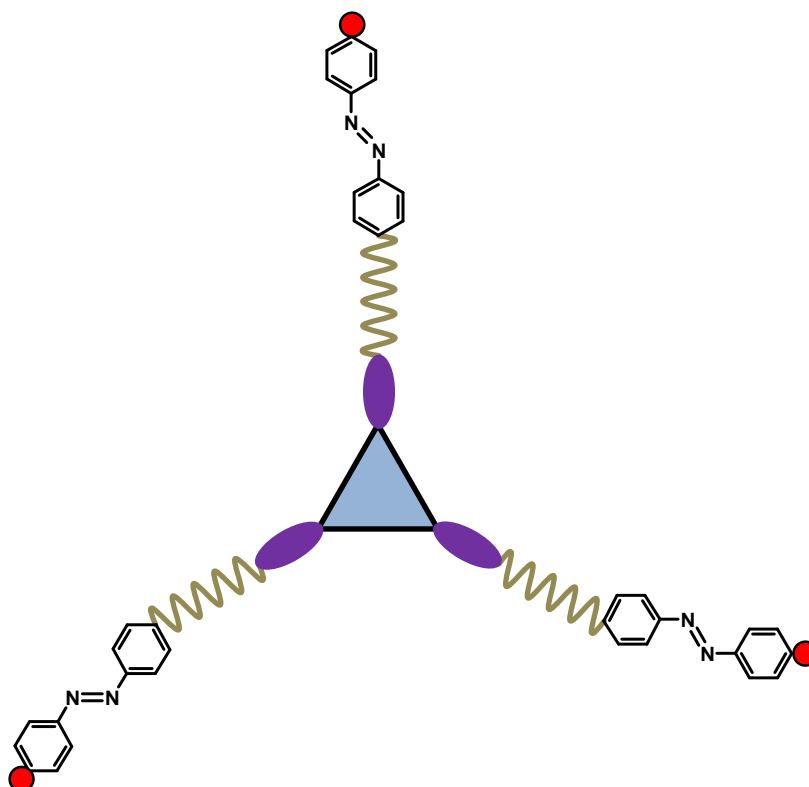


Figure 3.1. Schematic building blocks of an azobenzene-containing low-molecular-weight compound with three arms. For details, see text.

3.1.1 Central building blocks of low-molecular-weight compounds

The central building block consists of the core and the linkage group where the chromophore including the spacer is covalently bound. The core units mainly determine the thermal and glass-forming properties of the low-molecular-weight compounds by their varying weight, bulkiness and

structure. They can be categorized by the number of azobenzene chromophores which are attached: 1 azobenzene (compounds **1**, **14**), 2 azobenzenes (compounds **2-5**, and **15**), 3 azobenzenes (compounds **6-11**), or 4 azobenzenes (compounds **12**, **13**, and **16**), as shown in figure 3.2. The cores **14**, **15**, **7**, and **16** differ only by the number of arms attached to the cyclohexane group. The changes in structure between **3-5** and **12-13** affect only the plane of symmetry, far away from the chromophores. The direction of the ester linkage in **9** is reversed as compared to **8**. In all compounds except **10** and **11**, the azobenzene side group is coupled to the core via an ester linkage. By reversing the direction of the amide bond in **10**, the central building block **11** is obtained.

Most of the azobenzene-containing low-molecular-weight compounds known from literature are synthesized by aryl-aryl and N-aryl coupling reactions. In the present thesis, another route of the synthesis was used, namely linking the azobenzene chromophores to the cores by ester or amide linkages, as shown in figure 3.2. This has several advantages: It allows easy access to a large variety of compounds with commercially available central building blocks and side groups. Azobenzene moieties with more complex substituents are easily accessible via common azobenzene coupling reactions.

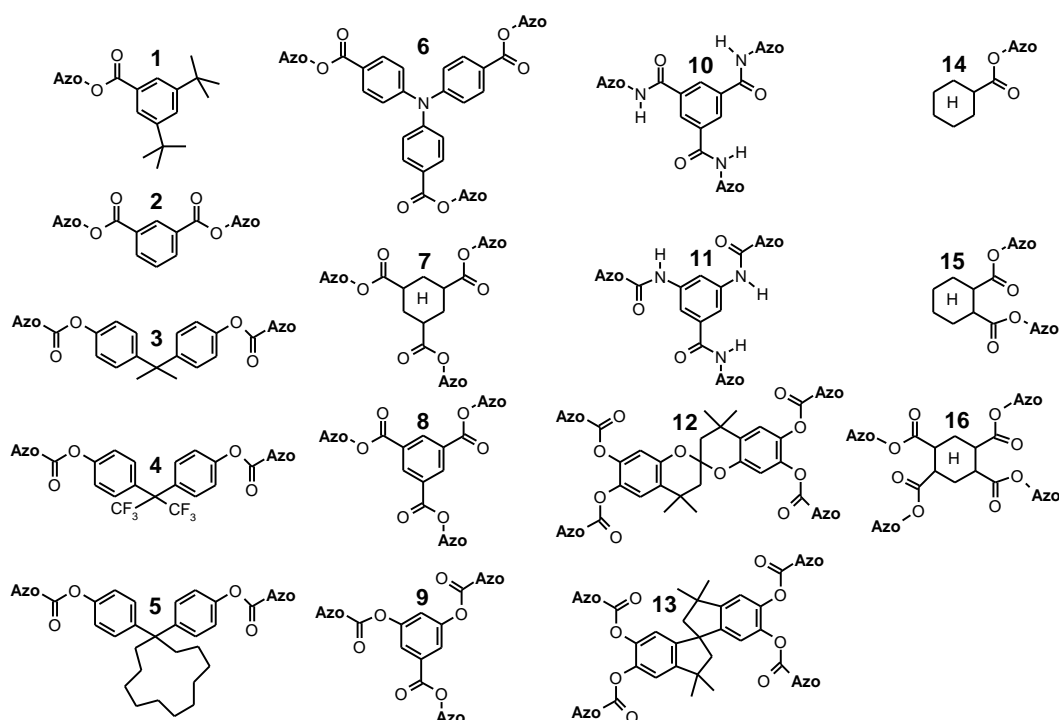


Figure 3.2. Functionalized central building blocks of the low-molecular-weight compounds.

3.1.2 Azobenzene side groups of low-molecular-weight compounds

The side groups consist of the spacer and the azobenzene chromophore with substituent. With the chromophores shown in figure 3.3 it is possible to tailor the optical properties -especially the absorption spectra- of the azobenzene-containing low-molecular-weight compounds. Azobenzene was investigated in unsubstituted form and with trifluoromethyl, cyano, and methoxy substituents at the *para*-position. Additionally, bisazobenzene chromophores in unsubstituted form and with methoxy substituent were examined. Changing the dipole moment affects the intra-molecular forces. The length of the alkane spacer ranges from zero to five CH₂ groups. It has an influence on the glass transition temperature. Moreover, its effect is to decouple the movement of the chromophore from the core. The introduction of long spacers on chromophores with a big dipole moment is expected to favor the formation of a liquid-crystalline phase in low-molecular compounds, as was already shown in polymers ^[81].

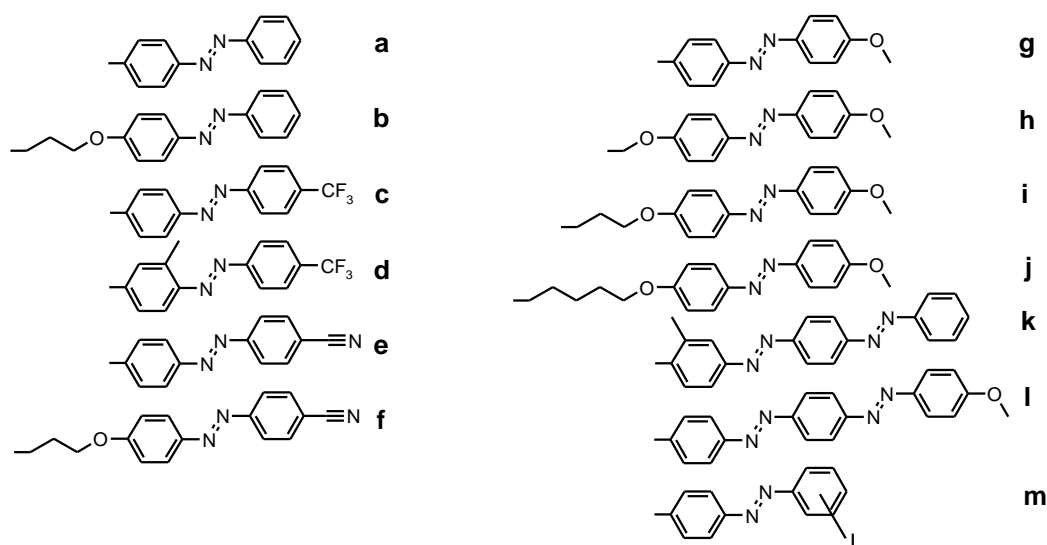


Figure 3.3. Azobenzene side groups which were attached to the central building block.

3.1.3 Synthesis of the low-molecular-weight compounds

Depending on the linkage group and its direction, there are four routes of synthesis. Only the final reaction step is presented in figure 3.4. More details about the syntheses can be found in the literature ^[152-154]. To obtain the low-molecular-weight compounds which are based on the central building blocks **1**, **2**, **6**, **7**, **8**, **14**, **15**, and **16** an aryl-aryl esterification is used, as shown in

figure 3.4a. The hydroxyl-functionalized side groups and the cores functionalized with carboxylic acid chloride react at elevated temperatures and form the ester linkage. By exchanging these functional groups at the side group and the core, the other direction of the linkage group can be obtained. This was performed for compounds based on the central building blocks **3**, **4**, **5**, **9**, **12**, and **13**. To obtain the low-molecular-weight compounds with amide linkage, an amidation reaction was used as the final step. In compounds based on the central building block **10**, the amino group of the chromophore reacts with the carboxylic acid chloride at the core. Low-molecular-weight compounds based on central building block **11** were synthesized by exchanging the functional groups at the azobenzene and the core, leading to an inversion of the direction of the amide linkage.

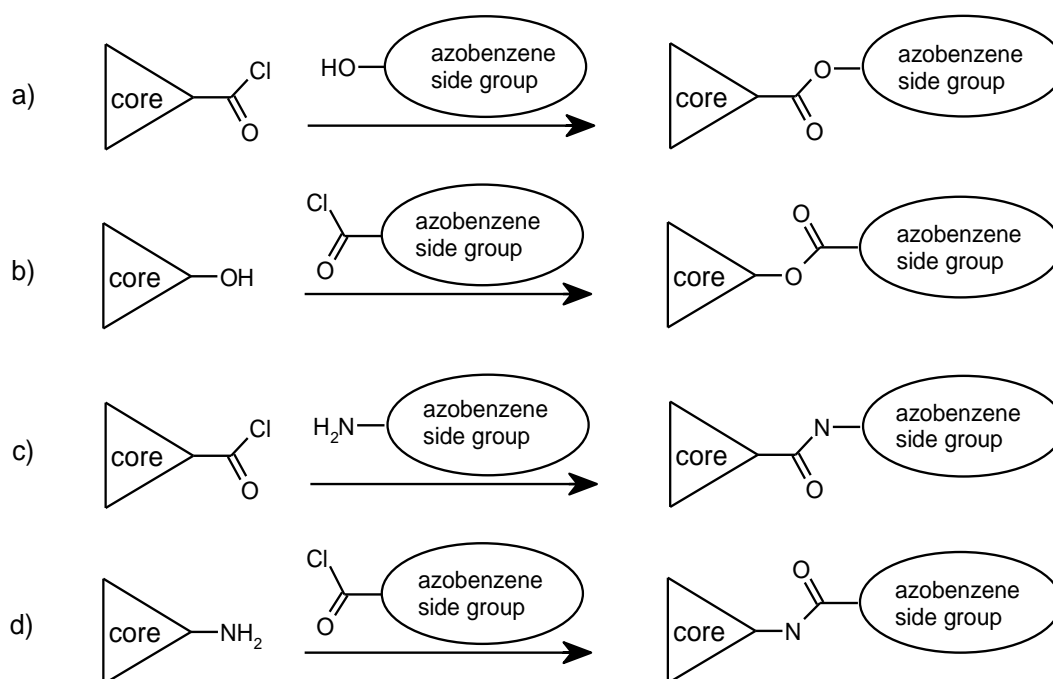


Figure 3.4. Final reaction step to obtain the azobenzene-containing low-molecular-weight compounds based on central building blocks a) **1**, **2**, **6**, **7**, **8**, **14**, **15**, **16**, b) **3**, **4**, **5**, **9**, **12**, **13**, c) **10**, and d) **11**.

3.1.4 Thermal and optical properties of the low-molecular-weight compounds

The thermal and morphological properties of the compounds were investigated by differential scanning calorimetry (DSC). The phase transitions can be identified in the DSC heating and cooling thermograms. All experiments were conducted under nitrogen atmosphere at a scan rate of

10 °C/min. The thermal properties were obtained in two different ways. In the case of materials with central building blocks **8-11**, about 3 mg of the substances were sealed in aluminum standard 40 μ l crucibles, heated to 260 °C, and subsequently quenched from the melt in liquid nitrogen. From the first heating curve, the glass transition temperature and the recrystallization temperature (T_{recr}) were determined. The crystallization temperature (T_c) was measured during the first cooling and the melting point (T_m) during the second heating. Materials comprising the other cores, i.e. **1-7** and **12-16**, were studied from initially crystalline samples. On the first heating cycle, T_m and T_c were determined. The glass transition temperature and the crystallization temperature were measured from the second heating thermogram. The characteristic thermal properties are listed in table 3.1 together with the molecular weights which are in the range of 415 to 1320 g/mol. The decomposition temperatures of the samples are around 300 °C as determined from thermo-gravimetric analysis.

All low-molecular-weight compounds except **2a**, **3a**, and **4a** show a glass transition and for all others except **1a** it is above room temperature. The amide linkage in **10** and **11** leads to higher glass transition temperatures due to the formation of hydrogen bonds. The DSC curves of some compounds show a very complicated thermal behavior. Compound **9a** for example has three recrystallization peaks at 98, 124, and 148 °C. Some compounds such as **6a** and **6c** show a polymorphic melting behavior which is often found in low-molecular-weight compounds^[62]. The triphenylamine core **6** has very good glass-forming properties. In contrast, some compounds have the tendency to crystallize, such as **8-11**. But stable amorphous phases can be obtained from all compounds with suitable preparation techniques such as quenching or blending with an inert polymer, e.g. polystyrene (PS). The presence of amorphous phases was confirmed with polarized microscopy (polmic) and X-ray diffraction, where only a halo around 10° was visible. Some of the low-molecular-weight organic glasses showed in addition a liquid-crystalline phase. For the verification and classification of this phase, polmic and X-ray diffraction were again applied.

The optical properties of thin solid films were measured with a standard absorption spectrometer. Most photochromic low-molecular-weight compounds described in the literature possess an extended conjugated π -electron-system which includes both the azobenzene moiety and the core. The linkage in the low-molecular-weight compounds presented here substantially reduces this conjugation over the entire molecule. This provided the possibility to investigate the optical properties of the azobenzene moiety alone. The absorption spectra have the expected structure, i.e. an intense $\pi\pi^*$ -absorption in the UV and a weak $n\pi^*$ -absorption around 440 nm, as shown in figure 3.5. Since both transitions overlap, it is difficult to determine the exact position of the maximum of the weak $n\pi^*$ -absorption band. This problem can

Table 3.1. Optical and thermal properties of azobenzene-containing low-molecular-weight compounds. M : molecular weight, T_m : melting point, T_c : crystallization temperature, T_g : glass transition temperature, T_{recr} : recrystallization temperature from the glassy state, T_{LC} : temperature of the phase transition from isotropic to liquid-crystalline, $OD/\mu\text{m}$: optical density per micrometer, --: not existing, nm: not measured.

	M [g/ mol]	T_m [°C]	T_c [°C]	T_g [°C]	T_{recr} [°C]	T_{LC} [°C]	$OD/\mu\text{m}$ @ 488 nm	Maximum of $\pi\pi^*$ -tran- sition [nm]	Maximum of $n\pi^*$ -tran- sition [nm]
1a	415	150	--	15	43	--	0.046 ^c	nm	443 ^c
2a	532	nm	nm	--	nm	--	0.061 ^c	nm	448 ^c
3a	645	233	190	--	--	--	0.106 ^c	nm	455 ^c
4a	753	214	190	--	--	--	0.076 ^c	nm	457 ^c
5a	767	234	--	98	--	--	0.074 ^c	nm	457 ^c
6a	918	160,175	--	92	--	--	0.19 ^a	nm	441 ^a
6c	1122	137,145	139,115	99	121	--	0.22 ^a	nm	446 ^a
6d	1164	157	--	93	--	--	0.23 ^a	nm	446 ^a
6e	993	--	--	122	--	--	0.28 ^a	nm	489 ^a
6g	1008	127	--	89	--	--	0.27 ^a	nm	444 ^a
6k	1275	228	--	107	--	--	0.78 ^a	nm	477 ^a
6l	1320	268	--	106	--	243	1.26 ^c	388 ^c	nm
7a	757	185	125	54	--	--	0.08 ^c	nm	442 ^c
7g	847	190	--	58	98	--	0.22 ^a	346 ^a	435 ^a
7m	1135	nm	nm	nm	nm	--	nm	nm	nm
8a	751	241	201	74	102	--	0.23 ^b	322 ^b	447 ^b
8g	841	246	165	66	99	--	0.29 ^b	348 ^b	425 ^b
8i	1015	169	126	38	--	175	0.76 ^b	360 ^b	nm
9a	751	211	124	61	see text	--	0.25 ^b	324 ^b	454 ^b
9g	841	163	109	65	--	--	0.60 ^b	358 ^b	371 ^b
9h	931	208	--	66	98,132	--	0.30 ^b	350 ^b	420 ^b
9i	1015	162	112	58	--	146	0.26 ^b	343 ^b	nm
9j	1099	150	111	40	--	138	0.37 ^b	nm	nm
10a	748	298	--	145	216	--	0.36 ^b	348 ^b	430 ^b
10i	1012	225	143	78	--	180	0.22 ^b	345 ^b	409 ^b
11a	748	252	214	134	172	--	0.32 ^b	329 ^b	450 ^b
11b	922	192	--	68	114,156	--	0.20 ^b	342 ^b	412 ^b
11f	997	251	132	68	--	193	0.32 ^b	351 ^b	434 ^b
11g	838	305	--	134	187,233	--	0.51 ^b	355 ^b	388 ^b
11h	928	262	234	88	--	--	0.23 ^b	355 ^b	393 ^b
11i	1012	232	155	64	--	167	0.12 ^b	349 ^b	424 ^b
11j	1096	199	114	44	--	150	0.17 ^b	352 ^b	419 ^b
12a	1205	257	--	109	212	--	0.08 ^c	nm	459 ^c
12g	1263	--	--	113	--	--	0.47 ^a	360 ^a	nm
13a	1173	247	--	109	--	--	0.09 ^c	nm	459 ^c
14a	311	nm	nm	nm	nm	--	nm	nm	nm
15a	534	150	--	25	75	--	0.13 ^c	nm	443 ^c
16a	980	304	--	72	--	--	nm	nm	nm

^{a)} measured on films containing 100 w% low-molecular-weight compound

^{b)} measured on films containing 5 w% PS and 95 w% low-molecular-weight compound

^{c)} measured on films containing 50 w% PS and 50 w% low-molecular-weight compound

be solved by fitting two Gaussian curves to the spectra which represent the $\pi\pi^*$ and the $n\pi^*$ -absorption. Another possibility is to determine the minimum of the second derivative of the spectrum. It is located at the position of the band maximum^[155]. Both techniques yield the same results. The maximum of the $\pi\pi^*$ -absorption of the investigated low-molecular-weight compounds is in the range 322 to 388 nm and that of the $n\pi^*$ -absorption is between 371 and 412 nm. The optical density per μm thickness is, in principle, proportional to the concentration of azobenzene in the material. Therefore it is possible to normalize optical data, such as the refractive-index modulation in a concentration series with respect to the azobenzene concentration. This normalization procedure is only possible however, if the attenuation of the transmitted beam is solely due to the absorption of azobenzene. In semi-crystalline samples it cannot be applied because of light scattering.

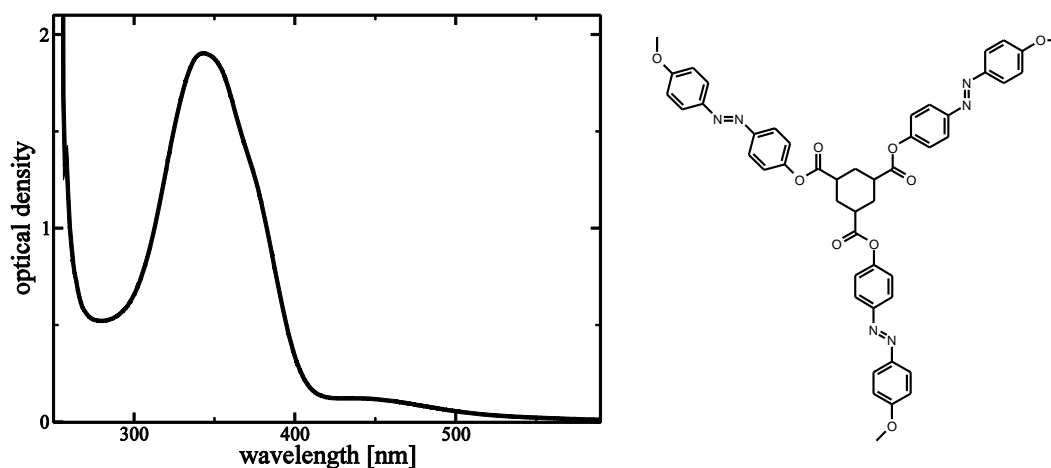


Figure 3.5. Absorption spectrum and chemical structure of compound **7g**.

3.1.5 Reorientation of azobenzene chromophores in low-molecular-weight compounds

It was shown that the refractive-index modulation inscribed in azobenzene-containing polymers^[156] and low-molecular-weight compounds^[54,62,64] with spacers originates from the reorientation of the chromophores. A single-beam experiment was performed to test if also the azobenzene moieties which are linked to the core without a spacer can reorient. A polarized laser beam with a wavelength of 488 nm and an intensity of 1 W/cm^2 was incident on a solid film of a blend containing 50 w% **6a** and 50 w% PS until photo-physical equilibrium -i.e. constant absorption- was reached. Then the polarization-dependent absorption of the sample was measured by rotating the polarization of an attenuated readout beam around its axis of incidence. The dependence follows a sine function, as shown in figure 3.6. If the orientation of the

reading laser is parallel to the polarization of the writing beam the absorption is minimum and maximum if it is perpendicular. This behavior proves the reorientation of the azobenzene chromophores, because neither a *cis-trans* population lattice nor a surface relief grating can explain the sinusoidal variation of the absorption coefficient. From the difference between the minimum and maximum of the sine function, the degree of oriented azobenzene molecules can be calculated. Only about 1 % of the azobenzene chromophores reorient in the solid film upon illumination. This value is smaller than the degree of orientation in systems with a longer spacer^[157].

Another way to proof the orientation are birefringence experiments^[54], since birefringence can only be caused by the reorientation of the azobenzene chromophores. Birefringence could be induced in the film containing compound **6a**. The time constant of its build-up is the same as the time constant of the build-up of the refractive-index modulation obtained from holographic experiments. This is another indication that the diffraction efficiency is solely caused by the reorientation of the azobenzene chromophores.

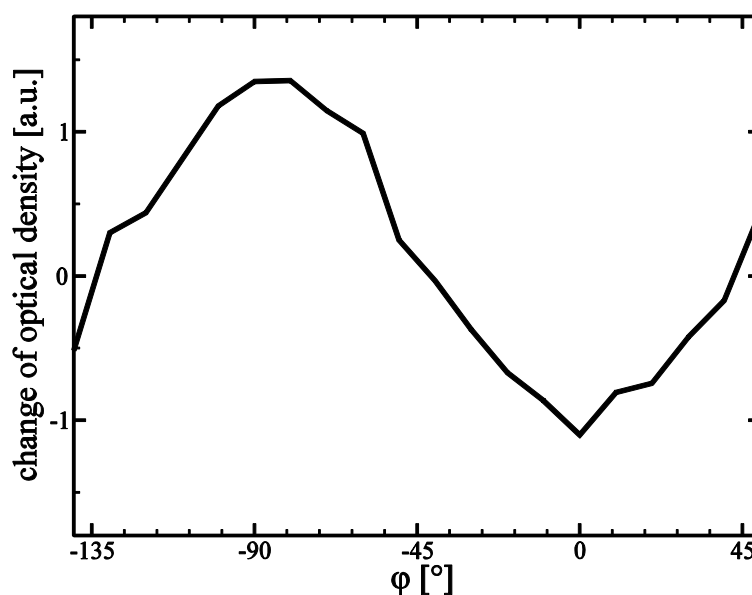


Figure 3.6. Angular dependence of the absorption coefficient of a thin film of compound **6a** diluted with 50 w% polystyrene after illumination with a single linearly polarized laser beam at 488 nm. ϕ is the angle between the polarization directions of the writing beam and the probe beam.

3.2 Azobenzene-containing polymers

In previous studies it had been found that azobenzene-containing diblock copolymers with mesogenic units in the photoactive block are suitable materials for holographic data storage^[52,157,158]. However, a drawback is their

low sensitivity. It was expected that blending the diblock copolymers with low-molecular-weight compounds could increase the sensitivity of the blend as compared to the pure polymer. These blends are very complex systems. A systematic study of concentration series of blends with low-molecular-weight compounds and various polymers has to be performed to understand these systems completely. Therefore, four different types of polymers with increasing complexity were used as material to be blended with the low-molecular-weight compounds: polystyrene, homopolymer **17**, diblock copolymer **18**, and diblock copolymer **19** with mesogenic side groups in the photoactive block. The latter three polymers are shown in figure 3.7.

Important key figures for polymers are the number-average molecular weight (M_n) and the polydispersity index (PDI) which are listed in table 3.2. The number-average weight is the numerical average of all polymer chains in the sample. The polydispersity is a measure for the homogeneity of the weights of the molecules. It is defined as the quotient of the weight-average molecular weight and the number-average molecular weight.

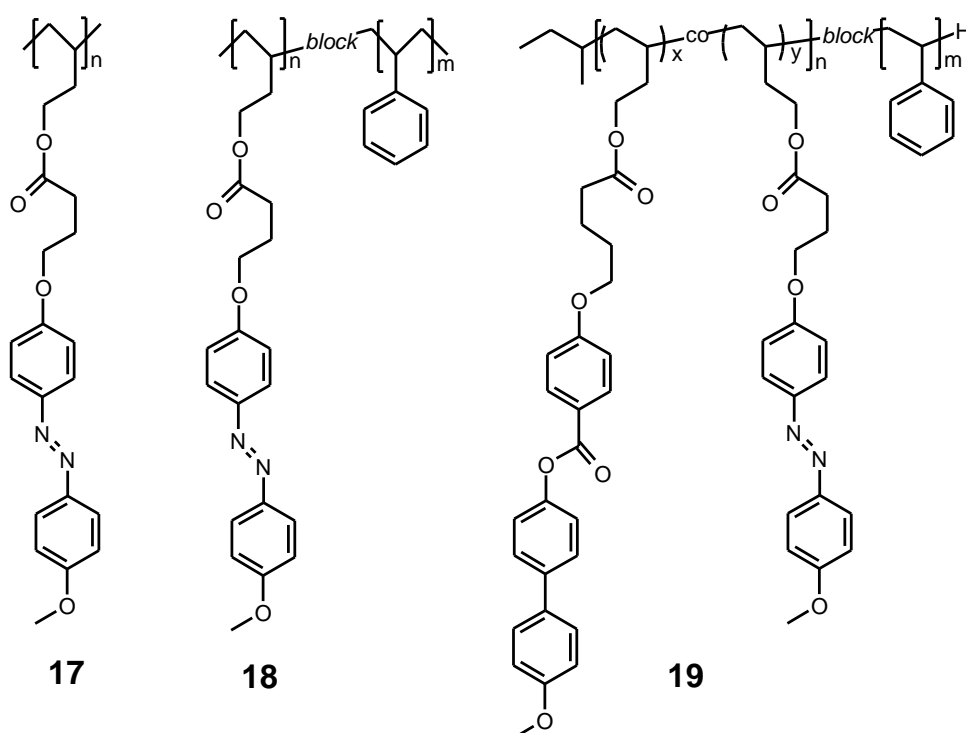


Figure 3.7. Chemical structures of homopolymer **17** and diblock copolymers **18** and **19**.

The optically inert polystyrene was commercially available (BASF 165 H from BASF SE).

Homopolymer **17** is an azobenzene side chain polymer with a poly(1,2-butadiene) backbone, similar as described in the literature ^[159]. The azobenzene-containing acid chloride was bound to the polybutadiene backbone in a polymer-analogous reaction. Compared to the low-molecular-weight compounds, the position of the maximum of the $\pi\pi^*$ -transition is shifted. This is caused by the formation of a liquid-crystalline phase in **17**, as will be discussed in section 7.2.

A more complex system is diblock copolymer **18**, which is an AB-type block copolymer with polystyrene as majority block and poly(1,2-butadiene) functionalized with azobenzene side chains as minority block ^[159]. Due to the relatively high content of the minority block, the azobenzene-containing phase develops a cylinder morphology. The transition temperature T_g of the polystyrene matrix can be determined with DSC and yields around 100 °C as expected for PS. The T_g of the azobenzene-containing minority block is important, since it has an influence on the holographic performance. Standard methods such as DSC are not sensitive enough to determine the glass transition of the minority block since it is buried by the much more intense signal of the majority block. But it is possible to calculate it from temperature-dependent holographic experiments ^[160], as shown in the appendix. The position of the maximum of the $\pi\pi^*$ -transition in **18** is in the same spectral region as for the low-molecular-weight compounds.

Table 3.2. Properties of the investigated polymers. M_n : number-average molecular weight, PDI : polydispersity index, w : weight fraction.

	Mor- phology	T_g [°C]	M_n [g/mol]	PDI	w_{azo} [w%]	w_{PS} [w%]	$w_{mesogen}$ [w%]	Maximum of $\pi\pi^*$ -transi- tion [nm]
PS	--	97	327 000	1.9	--	100	--	--
17	--	47	20 000	1.4	100	--	--	327
18	cylinders	34,103	59 000	1.04	17.5	82.5	--	346
19	spheres	100	150 000	nm	10.8	71.7	17.5	361

The best system for HDS is diblock copolymer **19**. Here, the minority block contains benzoyl biphenyl and azobenzene side chains. The side groups were attached in a similar way as in the homopolymer. A mixture of azobenzene acid chloride and mesogen acid was used in the final step of the synthesis of the polymers. The non-photoactive mesogenic units in the minority block lead to an increase of the long-term stability of the inscribed holographic information. Due to the shorter chain length of the minority segment, it forms spheres with a diameter of a few ten nanometers. The spectral shift of the maximum of the $\pi\pi^*$ -transition is caused by the mesogenic units.

3.3 Sample preparation

The sample preparation technique can have a big influence on the holographic measurements. By applying different preparation methods, the degree of crystallinity, the stability of the amorphous phase, the free volume, and the order parameter varies. Moreover, the preparation can also influence the phase separation between non-miscible components of the sample.

3.3.1 Preparation of thin samples

Three preparation techniques were used to obtain thin samples: spin-coating, doctor-blading, and sandwiching. In spin-coating, the material to be processed is diluted in an excess amount of solvent. This solution is placed on a glass substrate, which is rotating at high speed to spread the fluid by centrifugal forces. The solvent is volatile and evaporates quickly. Thin films of pure azobenzene-containing compounds were prepared by spin-coating 2 - 8 w% of the material in tetrahydrofuran (THF) onto glass slides rotating with 800 - 1000 revolutions per minute. Adding ultra-high-molecular-weight polystyrene to the solution can be used to increase the film thickness to a level required for holographic experiments or to obtain a stable amorphous phase. Blends of the low-molecular-weight compounds with polymers can be produced by dissolving both components at the desired concentrations in THF. Spin-coating this solution yields thin homogenous films.

In doctor-blading, a flat knife blade is held slightly above the substrate onto which the material is to be deposited. Then the blade is moved over the substrate, spreading the material which is placed in front of it through the gap between the blade bottom and the substrate. In contrast to spin-coating, there is almost no loss of material. The blends between the low-molecular-weight compound and polymer were prepared by doctor-blading a filtered 4 w% solution in THF containing both materials over a commercial glass substrate at 20 mm/s.

Typical sample thicknesses of thin films prepared with the first two techniques range from 500 nm to 2 μm . The films were annealed to remove residual solvent, typically at 70 $^{\circ}\text{C}$ for 4 h.

To produce sandwiched samples, two glass plates with a spacer (5 μm thickness) in between were used. The solid low-molecular-weight compound was placed on the edge of the plates and heated above T_m on a heating stage, so the melt was drawn between the glass plates by capillary forces. Since both surfaces of the sample are covered with glass, no SRGs can develop in this configuration.

3.3.2 Preparation of thick samples

Thick samples of low-molecular-weight compounds with an inert polymer in the millimeter-range were prepared by hot pressing. Commercially available polycarbonate (PC) pellets and the azobenzene-containing molecular glass **6g** were ground to fine powder in a freezer mill. Dry-blended powdery mixtures of PC and 1 w% of **6g** were then compounded in a co-rotating mini-twin-screw laboratory extruder for 3 minutes at 260 °C in nitrogen atmosphere. Different concentrations were prepared by dilution of the initial batches with additional PC. The resulting polymer pellets were filled into a circular hole of a 1.8 mm-thick steel plate which was placed between two 125 µm-thick Kapton films and another two steel plates. This set-up was placed in a laboratory press. It was first heated without pressure to 230 °C for 3 minutes to melt the extruded material and then pressed with a force of 18 kN for another 3 minutes. The pressure was released and the hot plates were placed in a second press kept at room temperature to cool the sample under controlled conditions. The diameter of the samples was 25 mm and the thickness 1.7 mm.

Thick samples of blends of PS, azobenzene-containing molecular glass **7g**, and diblock copolymer **19** were prepared by injection molding. To mix the three materials, they were first ground to fine powder. Then the powders were mixed for 5 minutes in a shear extruder rotating at 40 revolutions per minute at a temperature of 220 °C. The injection molding process was performed with a DACA MicroInjector. The blend was heated to 210 °C and pressed through a nozzle with the same temperature into the cylindrical form which had a temperature of 70 °C. The resulting samples had a thickness of 1.1 mm and a diameter of 25 mm. Since shear orientation and frozen-in mechanical stress lead to a strong birefringence, the samples were annealed at 130 °C for 24 hours in vacuum. After this thermal treatment, the birefringence had disappeared. Two sets of samples were prepared. One consisted of 99.5 w% PS, 0.1 w% **7g**, and 0.4 w% **19** and the other of 99.5 w% PS, 0.05 w% **7g**, and 0.45 w% **19**.

4 Experimental methods

4.1 Holography with plane waves

The used holographic set-up is shown in figure 4.1. The set-up is computer controlled and was built during several PhD works ^[82,157,161] and improved steadily. The writing laser is an Argon ion laser (Coherent Innova 307) operating at 488 nm and equipped with an etalon to enhance the coherence length. The laser beam is split with a beam splitter into two coherent waves which are brought to interference at the plane of the sample. The intensities and polarizations of both writing beams can be separately adjusted by polarizers, quarter- and half-wave plates. For most experiments, the power of each beam was 10 mW and the beam diameter 1.4 mm. This results in an intensity of 1 W/cm². The polarization of each beam can be adjusted separately. For linear polarizations, only a polarizer and half-wave plate are used, to obtain circularly polarized light a quarter-wave plate can be added.

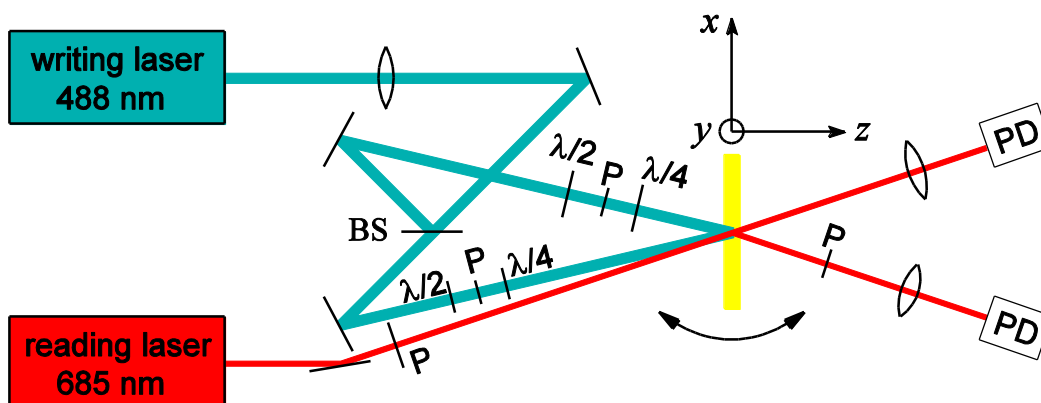


Figure 4.1. Optical set-up for the holographic experiments with plane waves. P: polarizer, BS: beam splitter, PD: photodiode, $\lambda/2$: half-wave plate, $\lambda/4$: quarter-wave plate.

In holographic experiments with azobenzene-containing materials also a *cis-trans* population lattice can develop which also leads to a refractive-index modulation. Contrary to the refractive-index modulation originating from the already discussed reorientation of the chromophores in the volume, the population lattice is an unwanted side effect. The latter is not stable due to the thermal back relaxation of the *cis*-isomer. Additionally, the thermal back relaxation induces motions on a molecular scale, which can lead to a reorientation of the *trans*-isomers. To circumvent the formation of the population lattice, a writing wavelength of 488 nm is used. At this

wavelength, the relative absorption of the $n\pi^*$ -transition of the materials used in the present thesis is much larger than the absorption of the $\pi\pi^*$ -transition. Therefore, during inscription, most azobenzene chromophores are already in the *trans*-state and only few isomers are the *cis*-state.

The inscribed refractive-index grating can be read out with the same wavelength of 488 nm. But this has the disadvantage that the material is sensitive at this wavelength. Thus, the measurement would influence the gratings to be measured. To circumvent this problem, a diode laser operating at 685 nm (Laser 2000 PMT24) with an intensity of 12 mW/cm² and an overall power of 87 μ W is used for reading. At this wavelength, the azobenzene-containing material does not absorb light. The reading laser is diffracted off the inscribed refractive-index grating; from the diffraction efficiency the refractive-index modulation can be determined. The angle of incidence of the reading laser θ_0' must be larger than that of the writing laser to meet the Bragg condition

$$\frac{\lambda}{\sin \theta_0} = \frac{\lambda'}{\sin \theta_0'} \quad (30)$$

with:

- λ wavelength of the writing laser
- λ' wavelength of the reading laser
- θ_0 Bragg angle of the writing laser
- θ_0' Bragg angle of the reading laser

The angle of incidence of the writing laser is around 14° in air and, according to Snell's law, 9° inside the material. This results in a holographic light grating with a grating period of 1 μ m. The corresponding Bragg angle of the reading laser is around 20° in air and 12° in the material.

The signals of the transmitted and the diffracted beam are measured with photodiodes and used to calculate the diffraction efficiency. For the reduction of noise, lock-in detection is used. The reading laser is modulated at 10 kHz and the signals of the photodiodes are processed in lock-in amplifiers (Stanford Research Systems SR830). The typical time constant used in the experiments was 10 ms.

To determine the refractive-index modulation from the equations discussed in chapter 2, the thickness d_0 of the sample must be known. For every hologram, the film thickness was measured with a profilometer (Veeco Dektak 1500).

The inscription of the holographic gratings is very reproducible. All important parameters such as the form of the holographic growth curve, the refractive-

index modulation, the writing time, or the stability can be reproduced even years later. The standard deviation of all holographic parameters is usually less than 10 % of the absolute value.

For maximum contrast of the holographic grating, the phase between the object and the reference beam has to be constant. The significance of the experiments is diminished if this relation changes due to mechanical vibrations, changes of temperature, or fluctuations in the refractive index of air caused e.g. by air draft. Therefore, the whole set-up is placed in the basement on a separate concrete block which is decoupled from the building. On this concrete block, the optical table is placed on air suspension to eliminate the remaining mechanical vibrations. The optical path between beam splitter and sample is placed in a box to prevent air draft. Additionally, the laboratory is equipped with air conditioning to keep the temperature stable.

To perform temperature-dependent measurements, the sample is placed in another holographic set-up inside a temperature-controlled box of anodized aluminum. Inside the walls of the box, water from a thermostat (Julabo F50HC Ultratemp 200) circulates to achieve a homogenous temperature inside. The temperature can be adjusted between 20 and 120 °C with an accuracy of 1 °C. The intensity of the reading laser in this set-up is 19 mW/cm² and the overall power 130 μW. The power of each writing beam of the writing laser is 24.5 mW and the beam diameter 1.9 mm leading to the same intensity of 1 W/cm² as in the standard set-up.

The sample can be placed on a computer-controlled rotational stage to measure the angular selectivity of thick gratings. The stage is moved by a stepper motor in steps of 0.0001°. Inscribing many holograms in multiplexing experiments leads to low diffraction efficiencies of each hologram. Therefore, scattered light is a big problem since it can easily bury the signal. The possibility to reconstruct the polarization from holograms inscribed in azobenzene-containing materials can be used to solve this problem. When the hologram is inscribed with an *s*-polarized object beam and a *p*-polarized reference beam and reconstructed with a *p*-polarized reference beam, the reconstructed object beam is *s*-polarized. By placing a polarizer between the sample and the photodiode which measures the first diffraction order, the scattered light of the reference beam is blocked. This reconstruction of the polarization works also for a reading laser operating at 685 nm. In the polarization configuration *sp*, the modulation is not the difference of oriented to non-oriented regions as in the case of *ss*, but the difference of areas in which the chromophores are oriented perpendicularly. Therefore the maximum achievable refractive-index modulation is larger as in *ss*. A drawback of the *sp*-set-up are the extremely non-uniform diffraction

The sample is shifted from the Fourier plane, so that the object beam has a size of around 2 mm^2 . The sample is again placed on a rotating sample holder to allow for angular multiplexing. The object beam is sent through a spatial filter and is imaged onto a charge coupled device (CCD) (PCO Pixelfly qe) with a resolution of 1392×1024 . The position and orientation of the lenses was optimized to obtain an image of the SLM with minimized aberrations on the CCD ^[161]. The most straightforward approach for the design of the optical set-up would be pixel matching, i.e. to image every pixel of the SLM onto one pixel of the CCD. But this is almost impossible in practice. Additionally, the optical set-up and especially the optical quality of the sample reduce the maximum resolution of the SLM which can be read out without errors. Therefore oversampling is a much easier way to unambiguously read out the data of the SLM. Scattered light from the reference beam is an even more severe problem in this set-up as compared to plane waves. To circumvent this problem, an *s*-polarized object beam and a *p*-polarized reference beam are again used to suppress the scattered light with a polarizer after the sample. This greatly improves the quality of the reconstructed images.

4.3 Ellipsometry

According to equation 28, the gradient force depends on the real part of the electrical susceptibility χ' . The latter depends on the absorption coefficient k and the refractive index n_0 , as shown in equation 29. Optical ellipsometry can be used to measure these two parameters with high accuracy in thin homogenous samples with a flat surface. A typical set-up is shown in figure 4.3. From the changes of the polarization state of the reflected light, the complex reflectance ratio δ can be calculated ^[164]:

$$\delta = \frac{r_p}{r_s} = \tan(\Psi) e^{i\Delta} \quad (31)$$

with:

- r_p amplitude reflection coefficient for *p*-polarized light
- r_s amplitude reflection coefficient for *s*-polarized light
- Ψ amplitude ratio
- Δ phase difference between *s*- and *p*-polarized waves

In general, the measured parameters cannot be converted directly into the optical constants of the sample. Therefore, iterative calculations based on the Fresnel equations are required to obtain k , n_0 , and the thickness of the sample d_0 from the reflectances r_p and r_s . Usually this fit is performed not only at a

single wavelength but for a wavelength range. For that reason, spectra of Ψ and Δ are usually measured.

The experiments were performed with a Sentech SE 850 Spectral Ellipsometer equipped with a Xenon arc lamp as light source at the chair Physical Chemistry II at the University of Bayreuth.

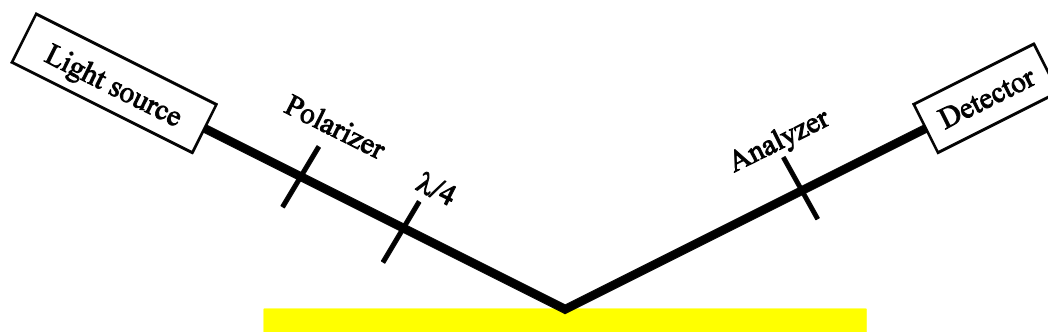


Figure 4.3. Schematic set-up of ellipsometry. $\lambda/4$: quarter-wave plate used as compensator.

4.4 Atomic force microscopy

For a non-destructive measurement of the height of surface relief gratings, atomic force microscopy (AFM) can be applied. It is used for an independent validation of the heights obtained from equation 26. A typical AFM picture of the surface modulation formed in holographic experiments is shown in figure 4.4.

The central element of an AFM is a cantilever with a sharp tip, which has a radius of about 20 nm. It is placed on piezo translators which permit the movement of the cantilever parallel to the surface with a resolution in the nanometer regime. The vertical displacement of the cantilever is determined by measuring the reflection of a laser beam at the top of the cantilever with a photodiode, as shown in figure 4.5. There are several modes to operate an AFM. The best techniques for measuring SRGs are non-contact and tapping mode, which were both used in the present experiments.

In tapping mode, a cantilever with a high spring constant (>10 N/m) is used. It oscillates at a frequency close to its resonance frequency of approximately 300 kHz. This is usually accomplished with an additional piezo translator at the cantilever. The amplitude of the oscillations is around 100 nm. These large oscillations have the advantage that the cantilever cannot stick to the surface. When the cantilever interacts with the sample, the amplitude and the phase between the cantilever and its excitation change. Typically, a control circuit attempts to keep the amplitude of the oscillation constant by moving

the sample perpendicular to its surface. The amplitude of this displacement is the desired height information. The resolution of the height is on the order of a few nanometers. An AFM image consists of lines along which the cantilever moved over the sample. The typical size of the measured area is on the order of $100 \mu\text{m}^2$. Although the observed SRGs were more than 600 nm deep, the cantilever could measure the valleys without any artifacts, as shown in figure 4.4. Atomic force microscopy in tapping mode was performed with a Veeco dimension 3100 AFM equipped with a Nanoscope IV Controller and Closed Loop XY Dimension Head at the chair of Physical Chemistry II at the University of Bayreuth.

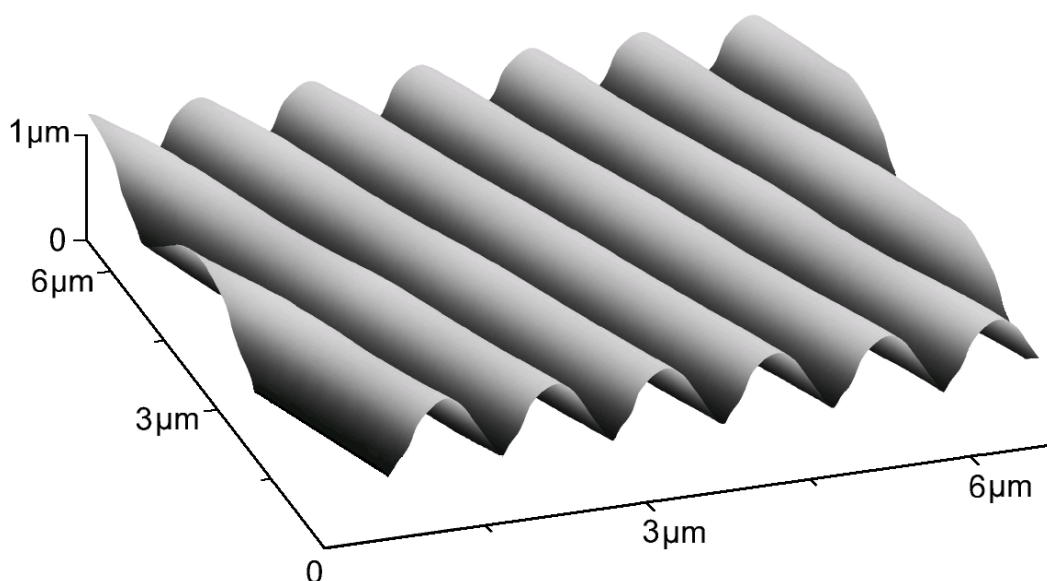


Figure 4.4. AFM image of an SRG on a thin film of compound **6g** recorded in tapping mode. The modulation height of the SRG is 610 nm, its grating spacing 1 μm . The SRG was generated with the polarization configuration $\pm 45^\circ$.

The non-contact mode works very similarly to the tapping mode. Here, the cantilever oscillates with small amplitude at the resonance frequency. Attractive Van der Waals forces act between the tip and the sample. A control circuit regulates the distance of the tip to the surface of the sample to keep the amplitude or the frequency of the oscillation constant. Atomic force microscopy in non-contact mode was performed with a nanoSurf easyScan E-AFM from the “Fortgeschrittenen-Praktikum Physik” at the University of Bayreuth.

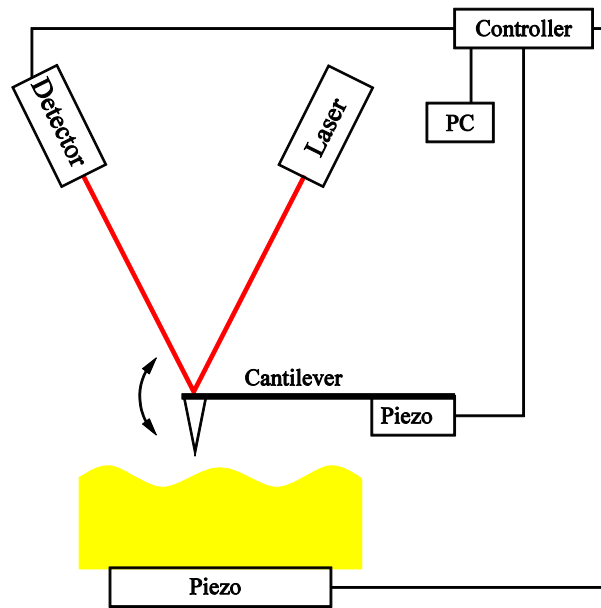


Figure 4.5. Set-up of an atomic force microscope.

5 Low-molecular-weight compounds with latent liquid-crystalline properties

The possibility of inscribing long-term-stable volume gratings in azobenzene-containing materials is of fundamental interest. So far, stable holographic gratings have been obtained only in liquid-crystalline (LC) polymers ^[165-170]. A typical approach to construct an azobenzene-containing liquid-crystalline material is to decouple the mesogenic chromophore from the backbone via flexible spacers. This allows the independent movement of the chromophore and a liquid-crystalline phase can appear. Increasing the dipole moment and, thereby, the intermolecular forces, is also helpful to obtain a liquid-crystalline phase. So far the concept of liquid-crystallinity has not yet been applied to low-molecular-weight compounds. The fundamental requirements for the formation of a liquid-crystalline phase are investigated by systematic changes of the chemical structure of low-molecular-weight organic materials in this chapter.

5.1 Liquid-crystalline phases in low-molecular-weight compounds

The small molecules discussed in this section are based on the central building blocks **8-11**. In a C₃-symmetric shape, three photoactive side groups are linked to the central building block. Additionally, the azobenzene chromophores are decoupled from the core with spacers of different lengths. The lengths ranged from zero to five CH₂ groups. To counteract the drop of the glass transition temperatures induced by the decoupling spacers, polar groups, i.e. amides or esters, are incorporated as linkage group between the side groups and the core. In addition to spacers, the introduction of end standing dipolar substituents, e.g. methoxy- or cyano-groups, is another effective tool to enhance the mesogenic character of the molecules. Besides, these substituents also have an influence on the optical properties. All low-molecular-weight compounds investigated in this chapter are shown in figure 5.1.

The thermal properties of the trisazobenzene derivatives were explored with DSC and supported by polmic. Higher melting, crystallization, and glass transition temperatures were found for the amide homologues as compared to their ester counterparts, as shown in table 3.1 and figure 5.1.

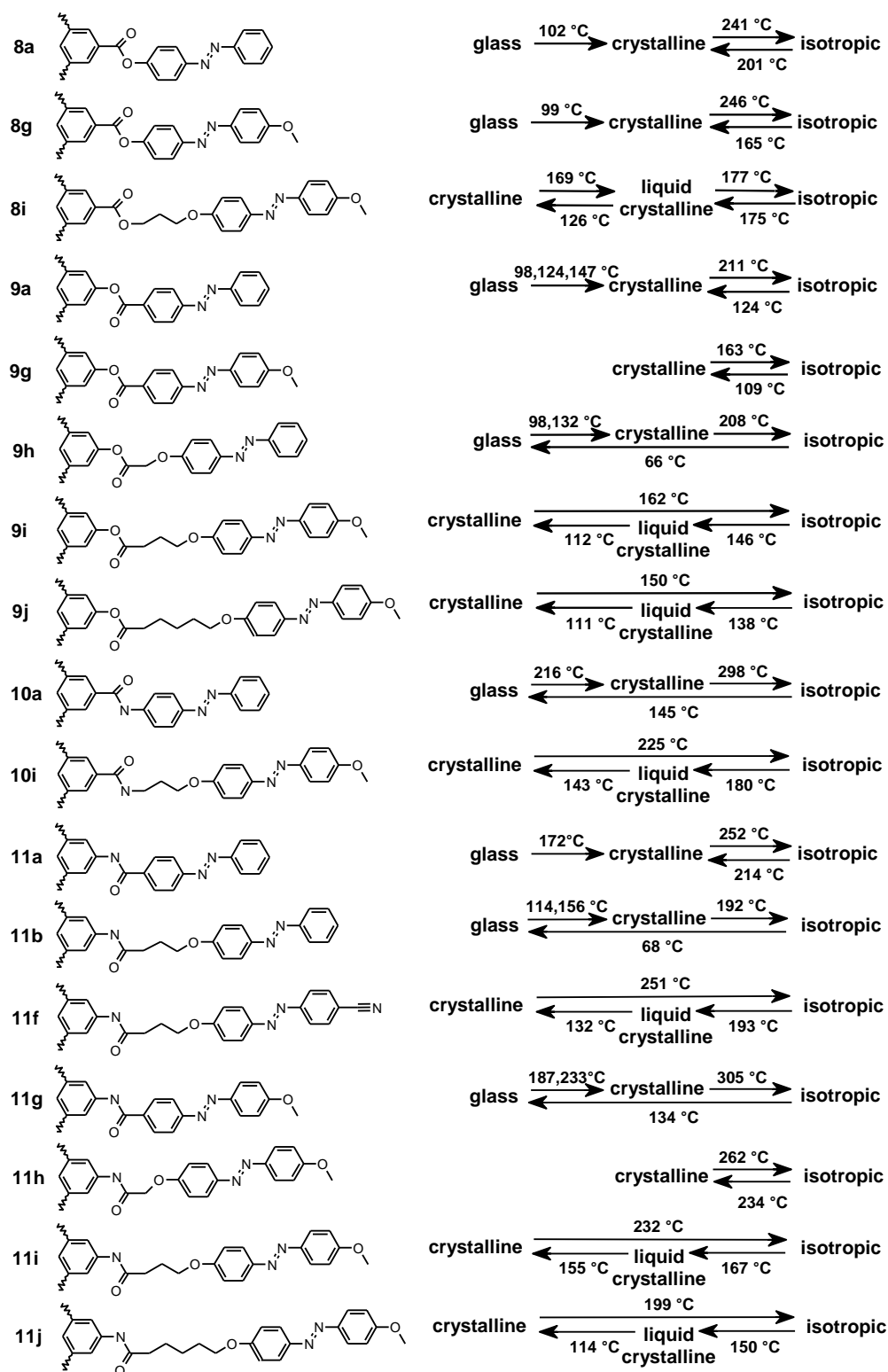


Figure 5.1. Chemical structures and thermal properties of 17 selected low-molecular-weight compounds forming in part liquid-crystalline phases.

This effect demonstrates the influence of a potential hydrogen bond formation in the former species. With increasing spacer length, however, this factor weakens and, owing to strongly increased conformational arrangement possibilities, the influence of the spacers becomes more dominant. The glass transition temperature decreases when the spacer length increases, as can be seen in the series of compounds **11g**, **11i**, **11j** or **9g**, **9i**, **9j**. Compounds **9h**, **10a**, **11b**, and **11g** displayed vitrification and trisester **8a**, **8g**, **9a**, **9g**, and **11a** were found to crystallize upon cooling. Since the T_g of all trisazobenzene derivatives is above room temperature, amorphous phases that are stable at ambient conditions can be obtained by quenching. At room temperature, they are in thermodynamic nonequilibrium.

All compounds without decoupling spacers between the linkage group and the azobenzene chromophore, i.e. all compounds with side groups **a**, **b**, **g**, and **h**, show only an amorphous and, in some cases, a crystalline phase. When heating from the solid state with a relatively moderate rate of 10 °C/min, compound **8i** features a LC phase prior to melting. For compounds **8i**, **9i**, **9j**, **10i**, **11f**, **11i**, and **11j**, liquid-crystalline phases are observed when cooling from the isotropic phase at 10 °C/min, as shown in figure 5.1 and figure 5.2. These molecules are the first azobenzene-containing liquid-crystalline low-molecular-weight compounds reported in literature. For the investigated molecules a spacer length of at least three CH₂ groups and a substituent at the azobenzene chromophore are required for the formation of a liquid-crystalline phase. The enthalpies of the isotropic to liquid-crystalline transition are relatively small and range from -1.2 to -4.0 kJ/mol. In combination with typical defects in the Schlieren textures as observed with polmic, this suggests the presence of nematic phases for trisazobenzenes **8i**, **9i**, **9j**, **10i**, **11f**, **11i**, and **11j**.

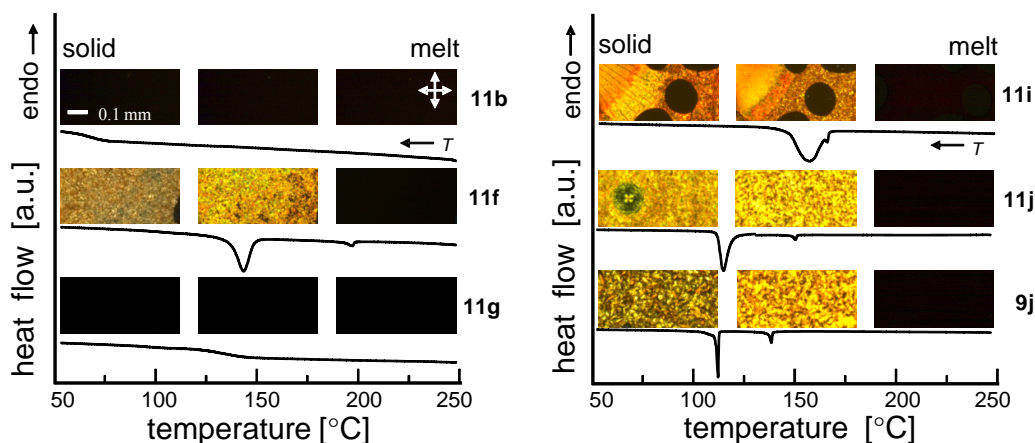


Figure 5.2. Differential scanning calorimetry and representing polarized microscopy pictures of selected compounds indicating a liquid-crystalline phase in compounds **11f**, **11i**, **11j**, and **9j**.

5.2 Light-induced phase changes

The formation of volume gratings in films of the low-molecular-weight compounds listed in figure 5.1 was investigated in holographic experiments. The films were prepared by spin-coating at room temperature. To increase the thickness of the films to a level required for holographic experiments, the viscosity of the solutions used for spin-coating was increased by adding around 5 w% polystyrene ($M_w \approx 30\,000$ kg/mol). For all compounds, the spin-coating led to the formation of an amorphous phase which was long-term stable at ambient conditions. Also those compounds which showed a liquid-crystalline phase in DSC experiments were quenched into an amorphous nonequilibrium state. Therefore, the latter are called latent liquid-crystalline in the following. The holographic experiments were performed with two *s*-polarized beams at 488 nm with an intensity of each 0.5 W/cm². This polarization configuration is known to produce surface relief gratings very ineffectively^[58,171] and the irradiation times were kept very short. Therefore SRGs did not develop and only the photo-physical response of the volume gratings in the material was investigated. All compounds show a photo-orientation, leading to holographic phase gratings in the volume.

The 17 low-molecular-weight compounds discussed in this section permit a systematic study of structure-property relations. The build-up of the refractive-index modulation during inscription is shown in figure 5.3 and the temporal behavior after the writing process in figure 5.4. A consistent fit which is simultaneously valid for the amorphous and the latent liquid-crystalline low-molecular-weight compounds could not be found. Therefore, the absolute values -i.e. the maximum refractive-index modulation and the writing time required to reach this value- as determined from the holographic experiments are discussed in this chapter. The writing times of compounds **9i** and **9j** are very large as compared to the other compounds. DSC measurements showed a complicated polymorphous behavior for these two compounds. Light-induced phase changes in the materials could be the explanation for the long writing times. When comparing the spacer length, e.g. in **11g**, **11i**, **11j** or **9g**, **9i**, **9j**, one finds a clear correlation to the holographic parameters as listed in table 5.1. With increasing spacer length, the maximum refractive-index modulation, the maximum refractive-index modulation divided by the optical density per μm and the writing time increase. The chromophore is decoupled from the core more efficiently and can move more freely when the spacer is longer. This results in a higher degree of orientation and a larger optical anisotropy. Increasing the dipole moment of the chromophore by substitution at the *para*-position with a methoxy or cyano groups also results in higher refractive-index modulation and longer writing times. The refractive-index modulation was found to decay for **8a**, **8g**, **9a**, **9g**, **9h**, **10a**, **11a**, **11b**, **11g**, and **11h** after the writing beams

were shut off, as shown in figure 5.4b. This is the typical behavior of small-molecular species and commonly observed ^[54,64].

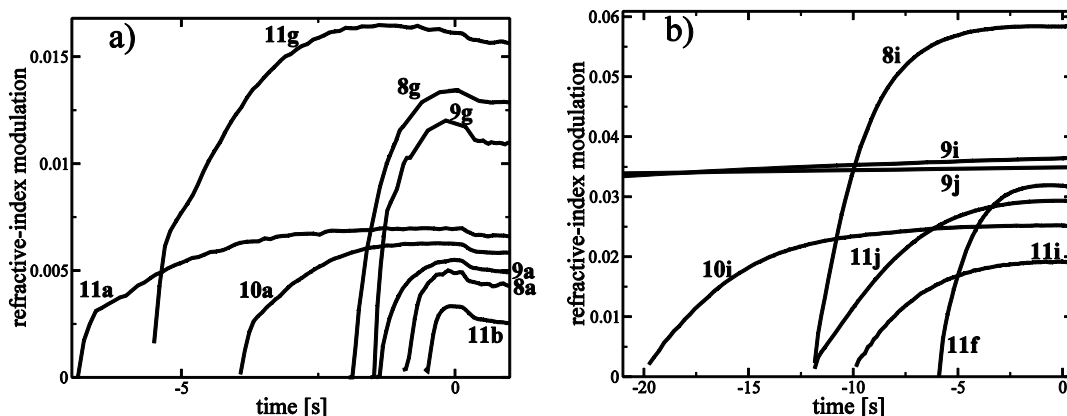


Figure 5.3. Refractive-index modulation during inscription of the holographic grating as a function of time. The writing laser was turned off at time zero. a) Purely amorphous low-molecular-weight compounds and b) latent liquid-crystalline low-molecular-weight compounds.

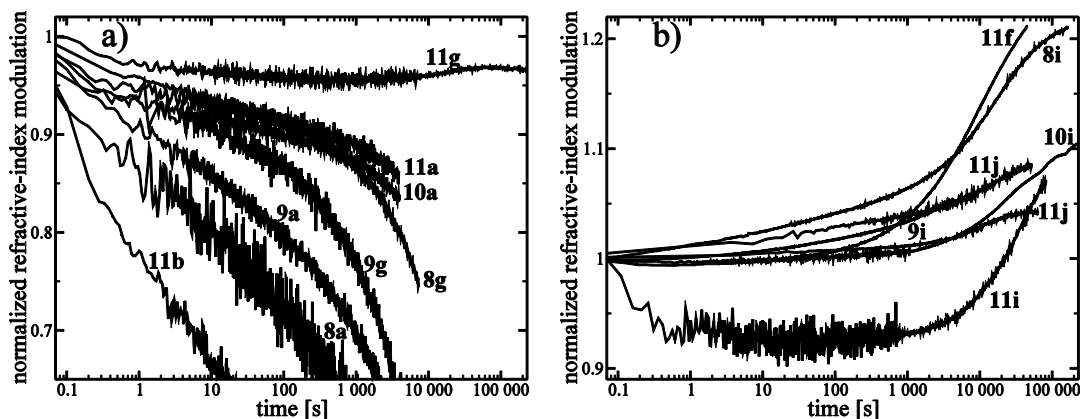


Figure 5.4. Refractive-index modulation after the inscription of the holographic grating as a function of time. The refractive-index modulation when the laser was shut off is defined as unity. Note the logarithmic time axis. a) Purely amorphous low-molecular-weight compounds and b) latent liquid-crystalline low-molecular-weight compounds.

On the other hand, most intriguingly, highly stable photo-orientation was observed for the other materials as can be seen in figure 5.4b. These compounds also displayed a remarkable post-development, i.e. a spontaneous increase of the refractive-index modulation after the writing laser was turned off. This post-development can also be seen in the relative refractive-index modulation after 4000 s, as listed in table 5.1. This relative value is calculated by dividing the refractive-index modulation after 4000 s by the refractive-index modulation when the writing laser was shut off. Substitution of an ester

by an amid linkage leads to an increase of the writing time to the maximum of the refractive-index modulation and the degree of post-development. This can be explained by the higher glass transition temperature of the amide, which slows molecular motions down. But the substitution did not affect the presence of the stability or the post-development. Accordingly, the formation of hydrogen bonds in the amide homologues cannot be the origin of the observed stability found for selected species. Inversion of the amide or ester sequence had only a minor influence on the holographic data. With increasing dipole moment (stronger chromophore interaction) or with increasing spacer length (increasing mesogenic character), the stability of the holographic grating increases, as shown in figure 5.4b. An increase of the dipole moment or the spacer length alone is not sufficient for this effect, as compounds **11g** or **11b** demonstrate. Both components, spacers and substituents, are crucial for a stable photo-induced alignment of the trisazobenzene derivatives.

Table 5.1. Summary of holographic data of 17 selected compounds.

	writing time to maximum of n_1 [s]	n_1 [10^{-3}]	$n_1 / (OD/\mu\text{m})$ [10^{-3}]	rel. value of n_1 4000 s after the inscription [%]
8a	0.9	4.3	17	18
8g	2	11.2	40	64
8i	10.5	56	78	116
9a	1.5	4.8	22	33
9g	1.6	8.9	15	42
9h	6.5	1.7	6	90
9i	350	42	171	110
9j	200	22.6	65	101
10a	3.7	5.9	17	70
10i	20	23	115	102
11a	6.5	22	68	73
11b	0.6	3	16	10
11f	5.3	28.8	94	119
11g	6	14.8	29	91
11h	9	6.2	26	78
11i	8	20	76	95
11j	12	27	163	110

Interestingly, the species featuring post-development are also those which are latent liquid-crystalline. Stable holographic gratings are only observed in liquid-crystalline materials. The light-induced reorientation of the azobenzene

chromophores in the initially amorphous samples must, therefore, induce the formation of an ordered domain (a quenched liquid-crystalline phase). Such an optically induced phase change is of great technical interest. Usually the refractive-index modulation is either low and not stable but is quickly reached as in the case of the amorphous low-molecular-weight compounds. Or the maximum refractive-index modulation is high and long-term stable but develops slowly (in liquid-crystalline materials). The latent liquid-crystalline low-molecular-weight compounds however, combine both advantages: Fast build-up of the refractive-index modulation in samples quenched to an initially amorphous state and long-term stability due to the formation of an ordered domain. This concept of phase change materials can also be applied to diblock copolymers and is a very promising approach to enhance the performance of azobenzene-containing materials for HDS as discussed in the appendix.

Also in blends which consisted of 50 w% PS and 50 w% of a latent liquid-crystalline low-molecular-weight compound, e.g. **11i**, stable holographic gratings can be inscribed. Therefore, the ordered domain must also be present in these blends. If both materials were distributed homogeneously, the polystyrene chains would act as impurities and prevent the formation of an ordered domain. This indicates a phase separation between the inert PS and the low-molecular-weight compound. In regions with high local concentration of the low-molecular-weight compound, an ordered domain can develop.

An experiment to prove that the ordered domain is light-induced was performed at elevated temperatures. At 70 °C, a holographic grating was stepwise inscribed in compound **11i**. When the writing laser was turned off after the first two writing steps, the inscribed grating was not stable. Only after a third step the grating was stable and showed post-development, as shown in figure 5.5. This indicates that a certain threshold of the degree of orientation in the illuminated areas is needed. Only if a sufficient number of chromophores are oriented, the mean field force on neighboring chromophores is strong enough to align them parallel, which leads to the formation of an ordered domain.

The dichroic ratio is another quantity indicating the orientation of azobenzene chromophores. It was measured by Pascal Wolfer at the ETH Zürich. When linearly polarized light is incident on the sample, the azobenzene chromophores reorient perpendicularly to the polarization direction. This changes the absorption of light polarized perpendicular (90°) and parallel (0°) to the polarization direction of the incident beam. In an illuminated sample, the 0° absorption decreases, whereas it increases at 90°. The ratio of the absorbances at 90° and 0° is called dichroic ratio. It is unity for isotropic samples and is usually measured at the maximum of the $\pi\pi^*$ -transition. Measurements of the dichroic ratio showed good agreement with the

holographic measurements presented here ^[153]. It was proven that the orientation of the chromophores is stable for more than a year and shows no decay.

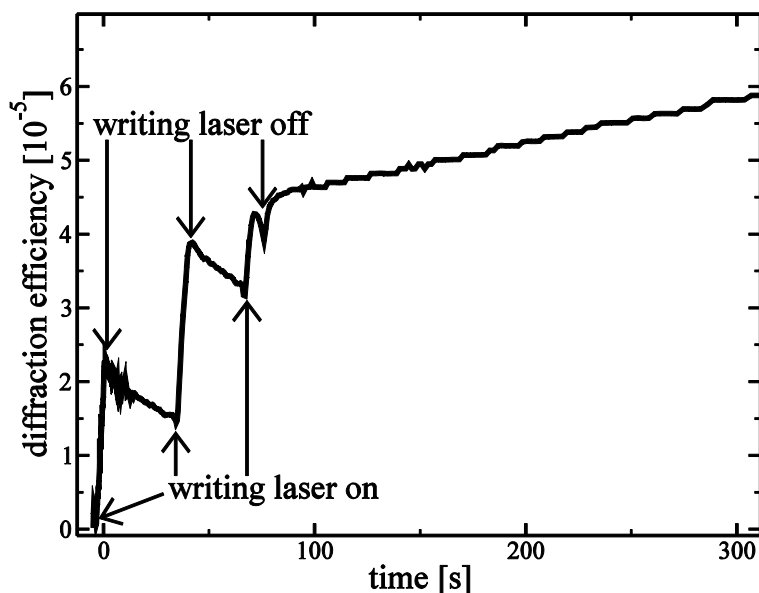


Figure 5.5. Step-wise inscription of a holographic grating in **11i** at 70 °C.

5.3 Reorientation of the chromophores on the molecular scale

From the holographic experiments it can only be concluded that the chromophores are oriented. Other movements on the molecular scale, such as an orientation of the core or the whole molecule, cannot be determined. The absorption of vibrational degrees of freedom lies in the infrared (IR) region. Each bond has characteristic and well-defined absorption bands. When polarized IR light is irradiated, the absorption depends on the relative orientation of the chemical bonds to the polarization direction. Thus, polarization-dependent absorption of specific IR bands can be used to determine the molecular orientation and yields a deeper understanding of the orientations on the molecular scale.

The molecular origin of the photo-alignment of compounds **11g**, **11i**, and **11j** was investigated with IR spectroscopy by Pascal Wolfer at the ETH Zürich. For this purpose, these three materials were spin-cast from solution into largely amorphous thin films, and subsequently illuminated at room temperature with polarized light from a day-light-source for 20 hours. The polarization direction of this light is called 90°.

The molecular orientation of the carbonyl groups located at the core of the trisazobenzene derivatives and of the methoxy end groups was investigated, as shown in figure 5.6. For all three compounds, the strongest absorption was observed for a polarization along the 0° -direction. This was expected, since it is perpendicular to the polarization direction of the writing beam. The deviation of the maximum from exactly 0° originates from the uncertainties of manual calibrating and setting of the polarizer. The stretching vibrations of the carbonyl moieties ($\nu_{\text{C=O}}(\mathbf{11g}) = 1655 \text{ cm}^{-1}$, $\nu_{\text{C=O}}(\mathbf{11i}) = 1669 \text{ cm}^{-1}$, $\nu_{\text{C=O}}(\mathbf{11j}) = 1664 \text{ cm}^{-1}$)^[27-31] at the core were virtually not affected by the exposure with linearly polarized visible light. In contrast, a strong anisotropy was found for the absorption of the stretching vibrations of the methoxy substituent ($\nu_{\text{OMe}}(\mathbf{11g}) = 1255 \text{ cm}^{-1}$, $\nu_{\text{OMe}}(\mathbf{11i}) = 1248 \text{ cm}^{-1}$, $\nu_{\text{OMe}}(\mathbf{11j}) = 1249 \text{ cm}^{-1}$)^[27-31] located at the end of the azobenzene groups. This anisotropy increased with spacer length because of the decoupling of the chromophore discussed above. But the anisotropy is even present in compound **11g** without spacer. The linkage itself seems to provide enough flexibility so that the chromophore can reorient independently of the core.

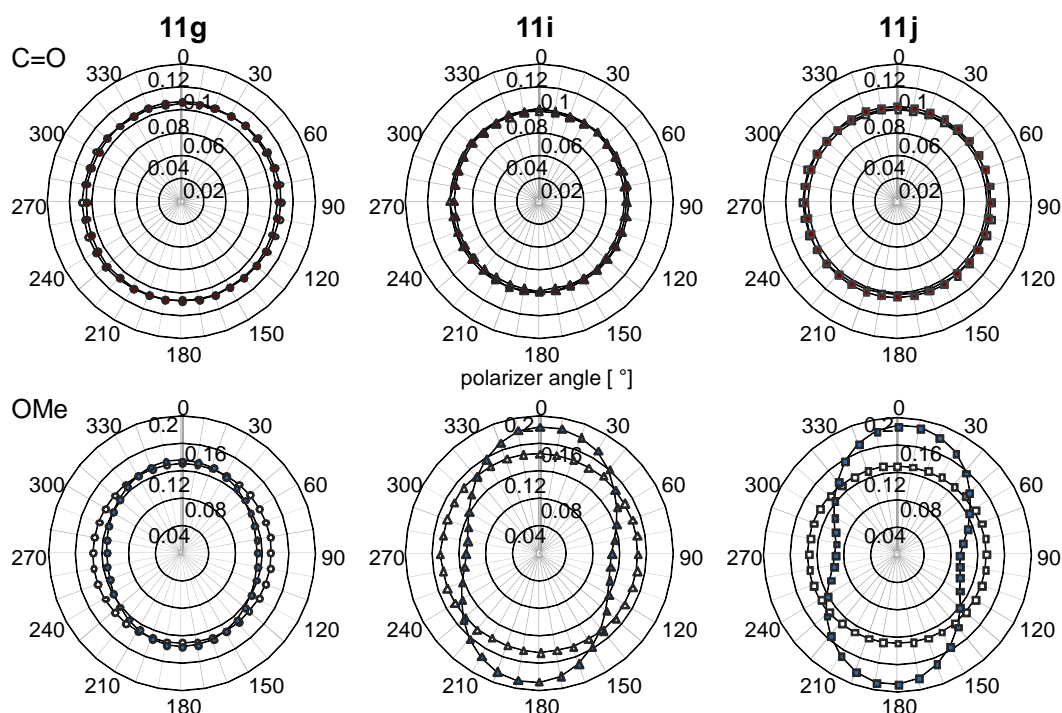


Figure 5.6. Polarized IR absorbance of the carbonyl (C=O; top) and the methoxy group (OMe; bottom) of compounds **11g**, **11i**, and **11j**. Spectra were recorded before (open symbols) and after (filled symbols) exposure to a linearly polarized day-light-source for 20 h.

5.4 Experiments at elevated temperatures

The post-development effect discussed above is a highly useful tool for creating holographic gratings with higher contrast than that achievable with optical methods alone. To enhance this post-development and for a deeper understanding of the system, holographic gratings were inscribed at elevated temperatures.

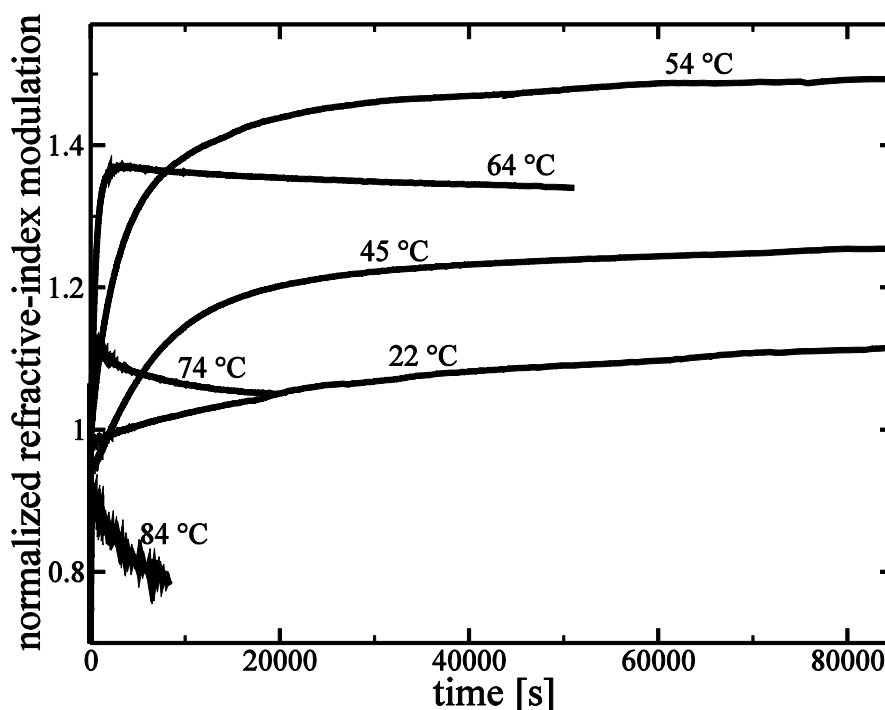


Figure 5.7. Amplitude of the refractive-index modulation as a function of time for thin films of compound **11i** at different temperatures. The refractive-index modulation has been normalized to unity when the writing laser was turned off.

A first set of experiments was performed with compound **11i** which has a glass transition temperature of 64 °C. Inscription and observation of the stability of the inscribed gratings as a function of time were conducted at isothermal conditions, as shown in figure 5.7. The writing times required to reach the maximum refractive-index modulation decrease from ~10 s at ambient temperature to 1.5 s at 85 °C, as shown in figure 5.8. However, this benefit comes at the expense of stability. At higher temperatures, the stability decreases, indicating that the formation of ordered domains is hampered. The maximum refractive-index modulation also decreases at higher temperature, as shown in figure 5.9.

After the inscription of the holographic grating, the thermal reorientation of the chromophores and the post-development effect compete with each other.

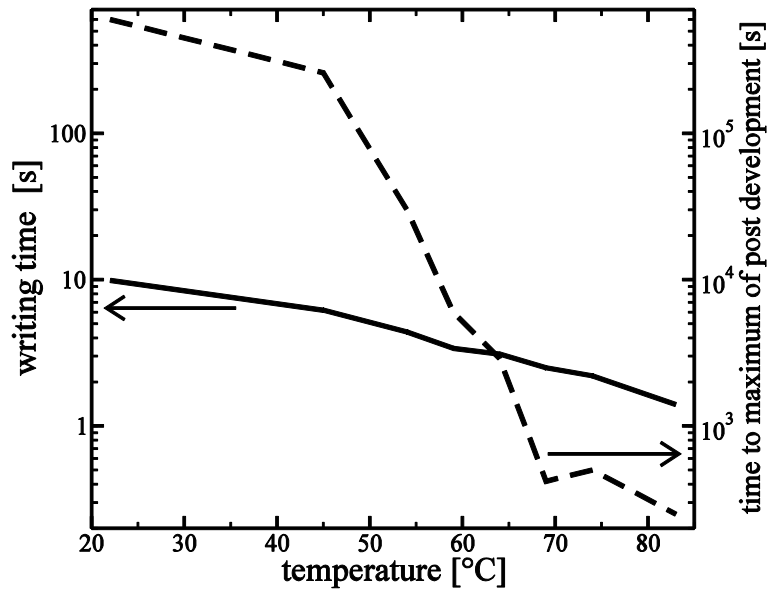


Figure 5.8. Writing time and time to reach the maximum of post-development for **11i** as a function of temperature. Note the logarithmic time scale of the ordinate-axes

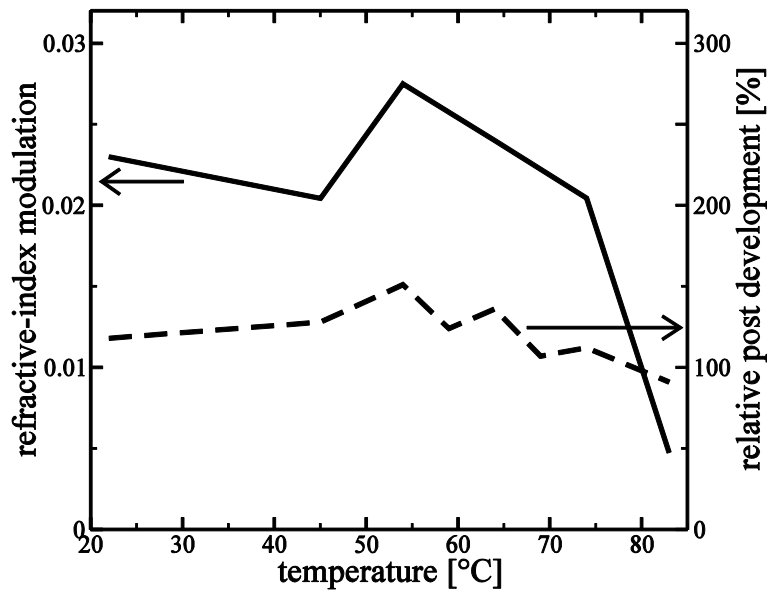


Figure 5.9. Maximum achievable refractive-index modulation and relative amplitude of the post-development for **11i** as a function of temperature.

At room temperature, the effect of the thermal reorientation is very small and slow, so the refractive-index modulation slowly rises to a saturation level, since the parallel alignment in the ordered domain is dominant. The relative post-development, as shown in figure 5.9 is defined as the ratio of the refractive index at the maximum and its value immediately after turning the writing laser off. At elevated temperatures, the time to reach the maximum of

the post-development decreases by three orders of magnitude due to the improved mobility, as shown in figure 5.8. At temperatures higher than 64 °C, the refractive-index modulation increases in the first minutes after the writing process when the process of parallel alignment in the ordered domain dominates. Later, the thermal reorientation dominates, leading to a decrease of the refractive-index modulation. Nonetheless, inscription of holographic gratings at elevated temperatures may be exploited to shorten the writing times, if the writing process is followed by subsequent rapid cooling to room temperature where the gratings are stable.

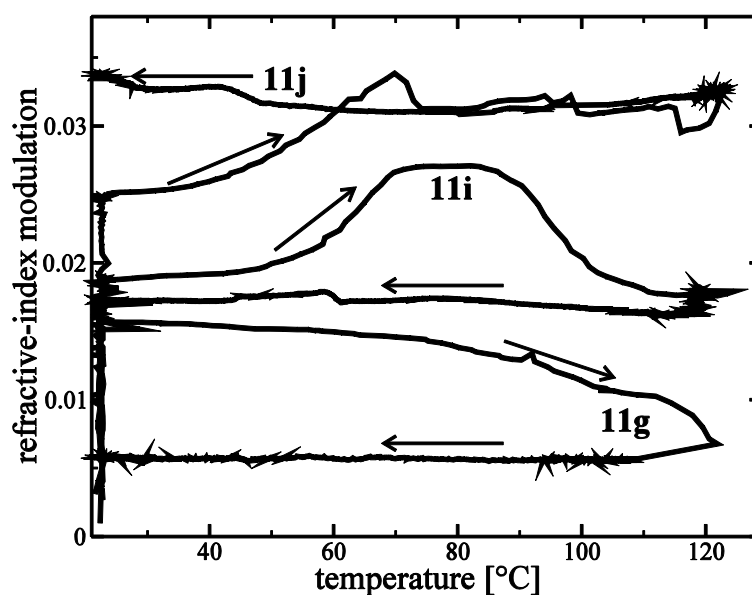


Figure 5.10. Development of the inscribed refractive-index modulation during a heating cycle of films of **11g**, **11i**, and **11j**

To explore the effects of annealing on the photo-alignment in the trisazobenzene structures, a holographic grating was inscribed at room temperature in **11g**, **11i**, and **11j** to the maximum of the refractive-index modulation. Subsequently, the samples were heated with a heating rate of 0.4 °C/min and the refractive-index modulation was monitored in-situ. The gratings inscribed in compound **11g** were severely affected already at $T < T_g$, as manifested by a rapid, continuous decrease of the refractive-index modulation, which is typical for amorphous materials. On the contrary, pronounced amplification of the refractive-index modulation at elevated temperatures was observed for the latent liquid-crystalline compounds **11i** and **11j**, as shown in figure 5.10. During the heating process, the refractive-index modulation increased by more than 40 % for **11j**. The maximum of the refractive-index modulation was reached for **11i** at 80 °C and for **11j** at 70 °C. Both temperatures are above the glass transition temperature of the respective

compound. Additionally, the inscribed holographic gratings are stable above the glass transition temperature. This shows that T_g is not the crucial parameter dictating the behavior at elevated temperatures for the two initially amorphous compounds **11i** and **11j**. This also proves that upon illumination with a holographic grating, an ordered domain is formed. The important parameter for the thermal behavior is then the clearing temperature T_c . Only when the films are heated to higher temperatures -close to T_c - the optical anisotropy is lost. The gratings begin to decay somewhat below T_c , because the ordered domain induced by the light grating is not as stable as in the DSC experiments where this phase is present in the whole bulk of the sample. This behavior was confirmed by measuring the dichroic ratio in UV-Vis spectroscopy.

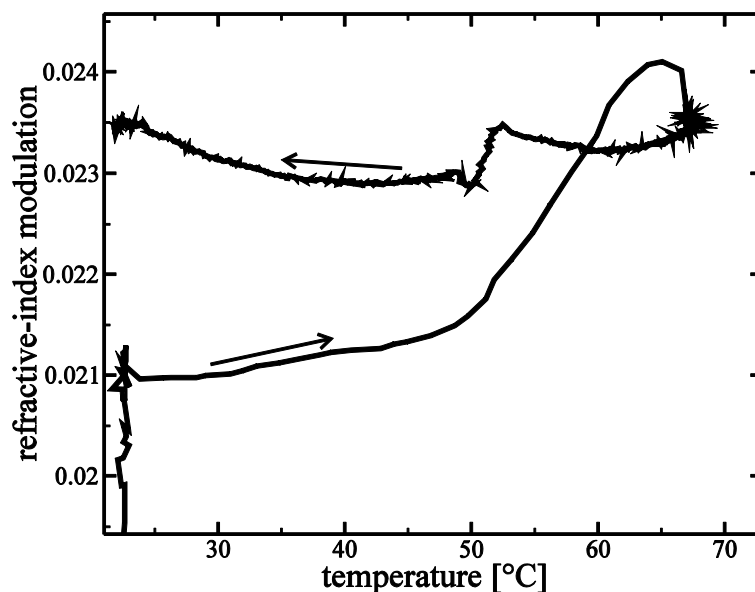


Figure 5.11. Annealing of holographic gratings inscribed in **11i** at room temperature. The maximum excursion temperature was optimized to maximize the post-development effect.

When a holographic grating is inscribed at room temperature and the sample is subsequently heated, the refractive-index modulation increases. If the sample is cooled to room temperature before the thermal reorientation process becomes dominant, the refractive-index modulation after the thermal treatment can be increased as compared to the untreated sample. This gain is long-term stable. By optimizing the temperature profile of the annealing process, the gain of the refractive-index modulation can be higher than 10 %, as shown in figure 5.11. The sample was heated to a maximum temperature of 67 °C with a heating rate of 0.4 °C/min and then quickly cooled to ambient temperature.

5.5 Bisazobenzene chromophores

It is also possible to obtain latent liquid-crystalline materials with bisazobenzene chromophores. They consist of virtually two azobenzene groups, since there are two azo-linkages between three phenyl rings. Due to the stronger anisotropy of the chromophore, the formation of a liquid-crystalline phase is facilitated.

Compound **6k** forms a stable amorphous phase with moderate cooling rates of 10 °C/min without crystallization after the first melting. In the case of **6l**, a liquid-crystalline phase is observed upon cooling with the same rate. The liquid-crystalline phase vitrifies after reaching the glass transition temperature and shows no crystallization upon further cooling or subsequent heating. Polmic investigations of the compound show a mosaic-like texture which remains unchanged between room temperature and the clearing temperature. Shearing is possible above T_g , and the compound solidifies below the glass transition. The existence of the liquid-crystalline phase is also confirmed by X-ray diffraction. As described in the sections before, a polar substituent is required for the formation of a liquid-crystalline phase in bisazobenzene-containing materials, but a spacer is not necessary.

Holographic experiments with *ss*-polarization and a total intensity of 2 W/cm² were conducted to investigate the holographic properties in the solid state. For this purpose thin amorphous films with good optical quality and without light scattering have to be prepared. Since compound **6l** is not a molecular glass, it was blended with 10 w% of the amorphous polymer Ultem in order to promote the solidification in an amorphous phase. Ultem is a commercially available polyetherimide with superior thermal stability ($T_g = 215$ °C) and is used in various high-performance applications, e.g. as electret material [172]. For comparison, both **6l** and **6k**, were blended with 10 w% Ultem.

The refractive-index modulations and the writing times are listed in table 5.2. As presumed, the maximum refractive-index modulation is about five times higher than in the amorphous azobenzene-functionalized low-molecular-weight compounds described earlier in this chapter. Comparing the blends containing 10 w% Ultem and 90 w% of compounds **6k** or **6l**, it can be seen that **6l** exhibits a higher refractive-index modulation. The writing times to the maximum of the refractive-index modulation are 8.9 s for **6k** and 11.8 s for **6l**, respectively. After the writing laser was shut off, compound **6k** exhibits a slow decay of the refractive-index modulation which is much slower than for usual amorphous low-molecular-weight compounds like **8a**. The latter shows a decay to 18 % of its initial value after 4000 s. In contrast, a long-term-stable photo-orientation was observed for compound **6l**. Hence, the introduction of a polar methoxy group enhances also the stability of holographic gratings in

bisazobenzenes. Furthermore, compound **6l** exhibited also the post-development effect, as can be seen in figure 5.12.

Table 5.2. Results of holographic measurements in bisazobenzene-containing materials.

	writing time to maximum of n_1 [s]	n_1 [10^{-3}]	rel. value of n_1 60 000 s after the inscription [%]
90w% 6k in 10 w% Ultem	9	33.3	96
90w% 6l in 10 w% Ultem	11	45.7	104
80w% 6l in 20 w% Ultem	11	48.5	104
60w% 6l in 40 w% Ultem	11	31.8	103

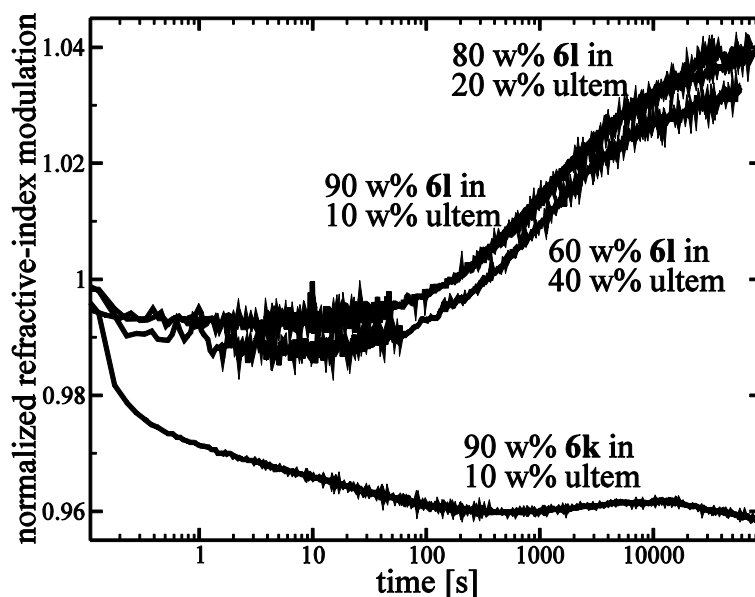


Figure 5.12. Long-term stability of the refractive-index modulation inscribed in films of **6k** and **6l** blended with different amounts of Ultem. The writing laser was turned off at time zero. Note the logarithmic time axis.

Post-development of holographic gratings has not yet been reported for low-molecular-weight compounds functionalized with bisazobenzene chromophores. It is assumed that the long-term-stable photo-orientation arises from a latent liquid-crystalline phase in the blends of compound **6l**, as proposed in the previous chapter. To achieve a deeper understanding of the blended systems, holographic investigations at lower concentrations of **6l**

(60 - 90 w%) in Ultem were also conducted. In the concentration series of **6l**, the writing time stays nearly constant and the refractive-index modulation increases with the azobenzene concentration as expected. As can be seen in figure 5.12, a long-term-stable photo-orientation could even be achieved for the lowest concentration of **6l**. This indicates that the latent liquid-crystalline phase is still present, even when the blend contains of only 60 w% of the photochromic material. This indicates that a phase separation between low-molecular-weight compound and Ultem may take place upon the inscription of the holographic gratings.

6 Amorphous low-molecular-weight compounds

In the previous chapter the influence of the spacer length in low-molecular-weight compounds and the associated formation of liquid-crystalline phases were investigated in detail. In this part, low-molecular-weight compounds are investigated in which the azobenzene is directly bound to the core via an ester linkage without spacer. Due to the absence of the spacer, all materials presented in this chapter are purely amorphous and show no liquid-crystalline phase. The focus in this chapter lies on the central core and the substituent at the azobenzene chromophore. Since the amorphous azobenzene-containing low-molecular-weight compounds show a much faster build-up of the refractive-index modulation, they can be used as blending material to improve the photo-sensitivity of azobenzene-containing diblock copolymers. In a systematic study, different materials are screened to find the compound with the best holographic performance. For this purpose, the building blocks core and substituent along with the number of azobenzene side groups at the core are modified.

6.1 Temporal behavior of the refractive-index modulation

The experiments were performed with two *s*-polarized beams at 488 nm of an intensity of each 1 W/cm². SRGs did not form under these conditions, since the irradiation times were very short and therefore only the volume grating was investigated. The growth of the refractive-index modulation in the volume during inscription can be well fitted with a stretched-exponential function, which is common for the kinetics in disordered systems ^[173,174]:

$$n_1(t) = n_{1\max} \left(1 - \exp \left(- \left(\frac{t}{\tau_1} \right)^{0.9} \right) \right) \quad (32)$$

with:

- $n_{1\max}$ maximum achievable refractive-index modulation
- τ_1 time constant of the build-up

The necessity of introducing a stretching exponent < 1 indicates a size distribution of the voids of free volume around the chromophores. Since the exponent turned out to be constant for all fits, it is assumed that the size distribution is roughly independent of the substituent and the core. The build-up of the refractive-index modulation results from an orientation lattice of the thermally stable *trans*-form of azobenzene and -to a small degree- from the formation of a *cis-trans* population lattice. Both processes occur in consecutive steps and are expected to have similar time constants. Therefore, it is impossible to distinguish between them in holographic experiments.

The temporal decay of the refractive-index modulation after turning the writing laser off shows a more complex behavior than the growth. It can be fitted with two stretched-exponential functions:

$$n_1(t) = n_{1\max} \left[A \exp \left(- \left(\frac{t}{1s} \right)^{0.25} \right) + (1 - A) \exp \left(- \left(\frac{t}{\tau_2} \right)^{0.4} \right) \right] \quad (33)$$

with:

- A relative amplitude of the fast relaxation process
- τ_2 time constant of the slow decay process

The fast relaxation component with amplitude A has a time constant of 1 s and the slower one has amplitude $(1-A)$ and the variable time constant τ_2 which is longer than 1 s by several orders of magnitude. The fast process of the decay usually has a relative contribution around 20 %. It is interpreted as the thermal relaxation of the molecules from the metastable *cis* to the *trans*-state. In solution, where the relaxation is usually measured, the *cis*-state has much longer lifetimes than 1 s. In the investigated molecules it is on the order of minutes. In a solid environment, however, the *cis*-isomers are trapped in constrained geometries, so a faster relaxation appears reasonable^[62]. Also mutual influences of adjacent molecules which increase the thermal *cis-trans* relaxation rate are possible^[175].

The slow process originates from the thermally induced reorientation of the *trans*-azobenzene moieties, which can involve either the chromophore units separately or the whole molecules. In most publications, the decay is reported to occur only during a few minutes and the refractive-index modulation is assumed to be constant for longer times^[42,43,54,57]. Here, the decay has been recorded for at least one day and it was found that the refractive-index modulation in the amorphous low-molecular weight compounds is not stable at long times but decays to zero. The growth and decay curves of the refractive-index modulation as a function of time could be well fitted with equations 32 and 33, respectively. As a typical example of the build-up and

decay of an inscribed grating, the holographic growth and decay curves in a film containing 50 w% **7g** and 50 w% polystyrene are shown in figure 6.1.

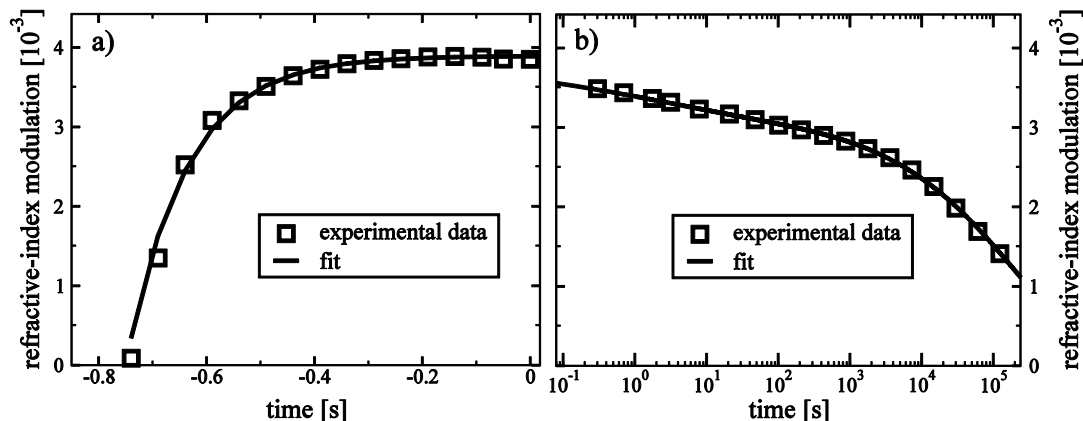


Figure 6.1. a) Build-up and b) decay of the refractive-index modulation of a volume phase grating as a function of time in a film containing 50 w% **7g** and 50 w% polystyrene. Symbols represent the experimental data, smooth curves the fit. The writing laser was turned off at time zero. Note the logarithmic time axis in (b).

6.2 Influence of the central building block

Photochromic low-molecular-weight compounds with different central building blocks were compared in a systematic set of experiments. To improve the optical quality of the amorphous phase, films containing 50 w% of the azobenzene-containing compound and 50 w% polystyrene were prepared, since especially the central building blocks **2**, **3**, **4** and **8** have the tendency to crystallize. All samples showed good optical quality and absence of undesired light scattering, except **2a** which was polycrystalline. The photo-physical properties of the materials diluted in polystyrene remain almost the same as in the pure materials.

A correlation exists between the glass transition temperature and the time constants τ_1 and τ_2 as can be seen in table 6.1. Lower values of T_g result in higher molecular mobility at room temperature and, therefore, lead to faster molecular reorientation processes. Compounds **1a** and **7a**, for example, have the lowest glass transition temperatures and also the shortest time constants of the build-up. This is desired since it leads to high sensitivities. But since the time constants of build-up and decay are coupled, the time constants of the decay are also short in this case, which is undesired. Therefore, one has to find the best compromise between fast inscription and stability for the specific application.

Of particular interest is the maximum sensitivity of the materials -as defined in section 2.2.3- since it is the most important parameter when the low-molecular-weight compounds are used to improve the photo-sensitivity of diblock copolymers. The central building block **7** has the highest S_{\max} . Hence, it is the most promising candidate for increasing the sensitivity of diblock copolymers.

Table 6.1. Summary of the experimental data of blends containing 50 w% polystyrene and 50 w% low-molecular-weight compounds with different central building blocks. The glass transition temperature has been determined in the pure material.

	T_g [°C]	n_1 [10^{-3}]	A	τ_1 [s]	τ_2 [s]	S_{\max} [cm/J]
1a	15	2.5	0.5	0.09	$3 \cdot 10^4$	656
2a	--	2.0	0.36	7	$330 \cdot 10^6$	7
3a	--	3.0	0.2	0.44	$1.3 \cdot 10^6$	161
4a	--	3.4	0.22	0.62	$9 \cdot 10^5$	130
5a	70	3.3	0.2	0.80	$3 \cdot 10^6$	98
6a	92	2.7	0.19	0.91	$5 \cdot 10^6$	66
7a	54	3.2	0.28	0.10	$2 \cdot 10^5$	756
8a	74	4.6	0.17	0.29	$7 \cdot 10^5$	366
12a	109	2.8	0.14	0.28	$6 \cdot 10^6$	225
13a	109	2.5	0.23	0.19	$1.5 \cdot 10^6$	311

6.3 Influence of the number of arms

The cyclohexane core seems to be a very promising building block to construct a low-molecular-weight compound with high sensitivity and sufficient stability of the inscribed holographic grating. In this section the influence of the number of arms attached to the cyclohexane core will be investigated. In compound **14a** one arm is bound to the central ring; **15a** has two arms in *ortho*-position; **7a** has three arms in 1,3,5-position; and **16a** carries four azobenzene side groups at the 1,2,4,5-positions of the core. The glass transition temperature decreases with decreasing number of arms due to the decrease of molecular weight as listed in table 6.2. The samples were prepared either by sandwiching or by spin-coating. Surprisingly, in compound **16a** no holographic gratings could be inscribed at all. The reason for this result is unclear. With decreasing number of arms the molecules become more linear and, therefore, crystallization is facilitated. Pure **7a** forms a stable

amorphous phase, whereas pure **15a** is polycrystalline and in the case of compound **14a**, even blending with PS is not sufficient to obtain a stable amorphous phase. For the desired holographic applications, amorphous materials show superior performance. In a crystalline material, the degree of orientation is higher, but the reorientation is more difficult as compared to a glass because of the smaller free volume which leads to slower time constants. The time constant for the build-up of the refractive-index modulation is shorter in **7a** as compared to **15a** and especially **14a** by several orders of magnitude, which can be explained by polycrystalline phases in the latter two. Compound **7a** with three arms at the cyclohexane core is the most suitable material, since it is a molecular glass and has a high sensitivity.

Table 6.2. Summary of the experimental data for low-molecular-weight compounds with different number of arms attached to the cyclohexane core. The glass transition temperature has been determined in the pure material. nm: not measured.

	dilution	preparation method	T_g [°C]	n_1 [10^{-3}]	τ_1 [s]	rel. value of n_1 4000 s after the inscription [%]	S_{\max} [cm/J]
14a	1:1 in PS	spin-coated	nm	9.5	214	57	1
15a	pure	sandwiched	25	5.3	2.3	nm	54
7a	1:1 in PS	spin-coated	54	3.3	0.1	21	756
7a	pure	sandwiched	54	5	0.08	29	1477
16a	pure	spin-coated	72	--	--	--	--

6.4 Influence of the substituent

In this section, a detailed comparison of the substituents at the chromophore in amorphous low-molecular weight compounds is given. Central building block **6** was used, since it has very good glass-forming properties. Therefore, all materials could be used in pure form to prepare films which show no light scattering. The introduction of several end groups at the azobenzene chromophore allows studying their influence on the photo-physical properties. It is known that a polar end group at the azobenzene moiety ^[176,177] changes the absorption maximum and the transition dipole moment of the molecule. Hence, slight modifications of the molecular structure by different substituents at the azobenzene chromophore will also influence the growth of phase gratings in the bulk ^[41,178].

The experimental data of the glass formers with different substituents are listed in table 6.3. Permanent dipole moments seem to enhance the cooperative effects ^[43,178] resulting in slower decay and higher refractive-

index modulations. Substituent **g** is the best combination of short τ_1 , high refractive-index modulation and sensitivity and reasonable long-term stability.

Table 6.3. Summary of the experimental data of pure films of the photo-addressable low-molecular-weight compounds with different substituents at the azobenzene chromophores.

	T_g [°C]	dipole moment [D]	$OD/\mu\text{m}$	n_1 [10^{-3}]	A	τ_1 [s]	τ_2 [s]	S_{max} [cm/J]
6a	92	0	0.19	5.9	0.17	0.14	$8 \cdot 10^5$	996
6c	99	4.0	0.22	12.1	0.09	0.75	$7 \cdot 10^6$	381
6d	92	3.9	0.23	8.7	0.19	0.38	$2 \cdot 10^6$	553
6e	122	3.9	0.28	15.0	0.06	0.73	$2 \cdot 10^8$	485
6g	89	1.3	0.24	10.3	0.10	0.27	$2 \cdot 10^6$	901

6.5 Best azobenzene-containing molecular glass

In the previous sections, the influence of the core and the substituent was investigated separately. It is believed that the influences of both structural units are largely independent of each other, since they are decoupled by the ester linkage. From these results one can conclude that the best azobenzene-containing low-molecular-weight glass former would be a combination of the core **7** and the substituent **g**. The resulting compound **7g** forms a stable amorphous phase and is therefore a molecular glass.

To verify the above assumptions, a series of four cores without and with methoxy substituent were investigated. Since not all of the low-molecular-weight compounds are molecular glasses, blends consisting of 50 w% of the compound and 50 w% polystyrene were used to produce films with good optical quality for the holographic experiments. The results are listed in table 6.4.

Shirota ^[60] reported an increased *cis*-population in materials with no substituent at the *para* position as compared to the substituent OCH_3 . The fit parameter A , which is a measure of the relative contribution of the *cis-trans* population lattice to the total refractive-index modulation, is therefore also a measure of the overall *cis*-concentration. The value of A is higher for samples with substituent **a** as compared to substituent **g**.

All compounds with chromophore **g** show a higher refractive-index modulation than the corresponding compound with chromophore **a** as discussed in the section before. Additionally, the methoxy substituent leads to a blue shift of the $n\pi^*$ -transition and a red shift of the $\pi\pi^*$ -transition as

compared to the unsubstituted chromophore. The resulting increase of the overlap of both absorption bands can, in part, explain the decrease of time constant τ_1 describing the build-up. The sensitivity which mainly depends on τ_1 and the refractive-index modulation also increases when substituent **g** is used.

Table 6.4. Summary of the experimental data of blends of 50 w% polystyrene with 50 w% low-molecular-weight compounds with different central building blocks and substituents **a** and **g**. The glass transition temperature has been determined in the pure material.

	T_g [°C]	n_1 [10^{-3}]	A	τ_1 [s]	τ_2 [s]	S_{\max} [cm/J]
6a	92	2.7	0.19	0.91	$5 \cdot 10^6$	66
7a	54	3.2	0.28	0.10	$0.2 \cdot 10^6$	647
8a	74	4.6	0.17	0.29	$0.7 \cdot 10^6$	366
12a	109	2.8	0.14	0.28	$6 \cdot 10^6$	225
6g	89	5.6	0.1	0.32	$19 \cdot 10^6$	381
7g	58	3.8	0.08	0.09	$0.2 \cdot 10^6$	846
8g	70	2.8	nm	0.14	nm	536
12g	113	2.5	nm	0.11	nm	518

When comparing the values of τ_2 of the unsubstituted low-molecular-weight compounds, one finds again a correlation to the glass transition temperature. Compounds with methoxy substituent have longer time constants of decay than unsubstituted compounds, which indicates stronger cooperative effects between the chromophores due to the increased dipole moment.

Table 6.5. Summary of the experimental data of pure films of low-molecular-weight compounds with different central building blocks.

	T_g [°C]	n_1 [10^{-3}]	A	τ_1 [s]	τ_2 [s]	S_{\max} [cm/J]
6g	89	10.3	0.1	0.27	$2 \cdot 10^6$	901
7g	58	7.8	0.1	0.1	$1 \cdot 10^6$	1843
8g	70	11.2	0.19	0.24	$3 \cdot 10^4$	1102
12g	113	4.7	0.12	0.12	$4 \cdot 10^4$	925

In a second set of experiments it was tested, if the dilution with polystyrene has an influence on the holographic experiments. For this purpose, the pure materials with methoxy substituent **6g**, **7g**, **8g**, and **12g** were investigated. All

four compounds are molecular glasses. The results of the pure materials listed in table 6.5 are very similar to those obtained from the diluted materials. The refractive-index modulation and the sensitivity are twice as large as compared to the blends, as expected. The time constant τ_1 of the build-up and the parameter A are almost the same for the diluted and undiluted case. Therefore, one can conclude that the photo-physical properties in a blend containing 50 w% polystyrene remain almost the same as in the pure material and the results obtained for the blended materials are also valid for the pure materials.

As was already indicated by the previous sections, also this set of experiments affirms that molecular glass **7g** is the material with the best holographic properties. It combines reasonable stability with a sensitivity of 1800 cm/J. As compared to diblock copolymers with the same optical density per μm , the sensitivity is five times higher. Additionally, the time constant of hologram inscription is faster by a factor of $10^{[51]}$. Therefore, the low-molecular-weight compound **7g** is an interesting material to be used as blending material for photo-addressable polymers to improve the photo-physical response, especially the sensitivity, of the latter.

6.6 Holographic experiments at elevated temperatures

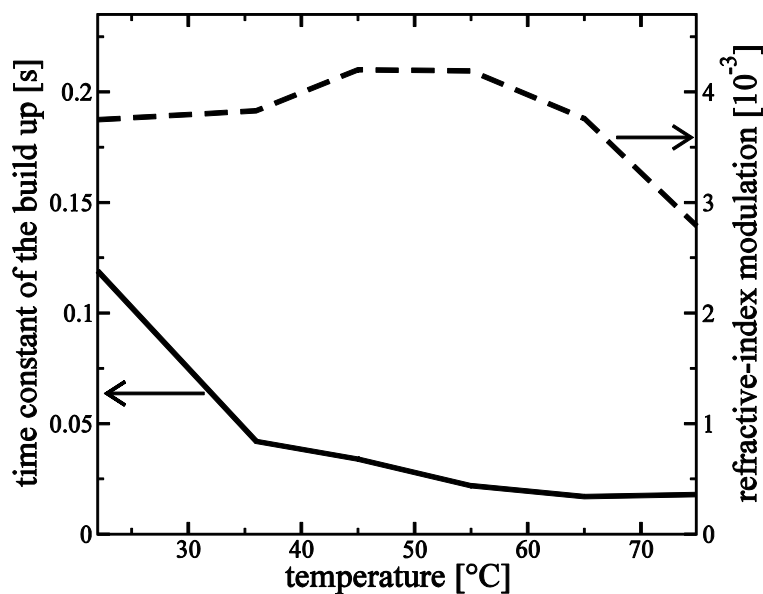


Figure 6.2. Time constant τ_1 of the build-up of the holographic grating and maximum refractive-index modulation as a function of temperature for blends of **7g** with 50 w% polystyrene.

To test the temperature-dependent behavior of the optimized low-molecular-weight organic glasses **7g**, holographic experiments were performed in blends

containing 50 w% of the molecular glass and 50 w% PS. The growth curves of the refractive-index modulation at elevated temperatures could be fitted with equation 32. The time constant τ_1 decreased with increasing temperature, as is shown in figure 6.2. This result can be explained by an increased mobility of the azobenzene chromophores in the photochromic amorphous molecular material. The maximum refractive-index modulation stayed constant up to 65 °C and then showed a steep decrease around T_g . The slow time constant τ_2 of the decay, followed an Arrhenius law with an activation energy of 32 kJ/mol. This value is in the same order as the energies calculated for azobenzene-containing block copolymers ^[160].

6.7 Angular multiplexing with molecular glasses

For high-density data storage, several holograms should be inscribed at the same spot of the material by angular multiplexing. In order to check, if the molecular glasses are, in principle, suitable for angular multiplexing and if the azobenzene chromophores can reorient in a strongly diluted environment, thick samples of a molecular glass diluted with polycarbonate were prepared by compression molding. A large quantity of the molecular glass is needed for the preparation of thick samples. Since a relatively large amount of material **6g** was present, this compound was used. The angular selectivity is determined by the thickness of the holographic gratings. Due to the strong optical absorption of the azobenzene chromophore, the photochromic low-molecular-weight compounds must be highly diluted to obtain thick samples with sufficiently low optical density at the writing wavelength, so the writing laser can penetrate the whole sample. The samples were 1.8 mm thick and of good optical quality and had an optical density of 1.4 at 488 nm.

The experiments were performed with *sp*-polarized writing beams. This configuration has the advantage, in addition to its high achievable refractive-index modulation, that it yields the possibility of easily suppressing scattered light with a polarizer, since the diffracted beam is polarized perpendicularly to the reading beam and scattered light. A disadvantage of *sp*-polarization is the large disparity of the DEs between the inscribed gratings ^[52]. This difference can reach several orders of magnitude, since the inscription of each new grating partly erases previously written holograms.

An optimized exposure scheme, however, yields the possibility to greatly reduce this variation ^[162,179]. The exposure times leading to uniform diffraction efficiencies can be determined by an iterative approach. First a series of angle-multiplexed holographic gratings are inscribed, e.g. with equal exposure times. From this experiment, the DE of the *m*th grating and the corresponding total energy per area that was incident on the sample before and during inscription of the *m*th grating, E_m , can be obtained. From these DEs as a function of exposure energy, the cumulated grating strength C at the

energy E_m can be calculated by cumulating the square-root of all DEs up to E_m . The obtained data points for the cumulated grating strength can be fitted with a polynomial:

$$C = a_0E + a_1E + a_2E^2 + a_3E^3 + a_4E^4 + \dots \quad (34)$$

with:

- C cumulated grating strength
- E exposure energy per sample area
- a_i fit parameters

Usually a polynom of sixth order is sufficient to describe the cumulated grating strength. The maximum of the cumulated grating strength is equal to the available saturation grating strength. Equal grating strengths are obtained by dividing the available saturation grating strength by the number of holograms to be multiplexed. The desired exposure schedule is then:

$$\frac{C_{sat}}{N} = E_n \cdot \left. \frac{dC}{dE} \right|_{E=\sum_{i=1}^{n-1} E_i} \quad (35)$$

with:

- C_{sat} saturation grating strength
- N total number of holograms
- E_i energy per area irradiated for the inscription of the i th grating
- E_n energy per area that will be required to inscribe the n th grating

By rearranging equation 35 with the factors obtained from equation 34, the new exposure scheme can be calculated as:

$$t_n = C_{sat} \left\{ N I_0 \left[a_1 + 2a_2 \left(\sum_{i=1}^{n-1} E_i \right) + 3a_3 \left(\sum_{i=1}^{n-1} E_i \right)^2 + \dots + 6a_6 \left(\sum_{i=1}^{n-1} E_i \right)^5 \right] \right\}^{-1} \quad (36)$$

with:

- t_n exposure time of the n th grating
- I_0 total intensity of the laser beams

A second set of angle-multiplexed gratings is then inscribed according to this new scheme which yields more uniform DEs, and new exposure times are

calculated from this inscription. After a few steps of iteration, largely uniform DEs are obtained. Thus, it was possible to reduce the variation of the DE between the first and the last inscribed grating of a series from a factor of 20 to 1.2. The writing times leading to equal diffraction efficiencies are best described by an exponential law. The writing time of the k th grating was 90 % of that for the $(k+1)$ th grating. This description, however, is not valid for the very first and very last gratings.

Up to 19 gratings can be inscribed at the same spot, as shown in figure 6.3. This demonstrates that light-induced reorientation of the azobenzene chromophores is possible in strongly diluted systems and that angular multiplexing is possible in molecular glasses. This is the first report of angular multiplexing in low-molecular-weight organic glasses containing azobenzene moieties. From the experiments, the maximum sensitivity of the sample was calculated as $S_{\max} = 19 \text{ cm/J}$ and the dynamic range as $M\# = 0.15$.

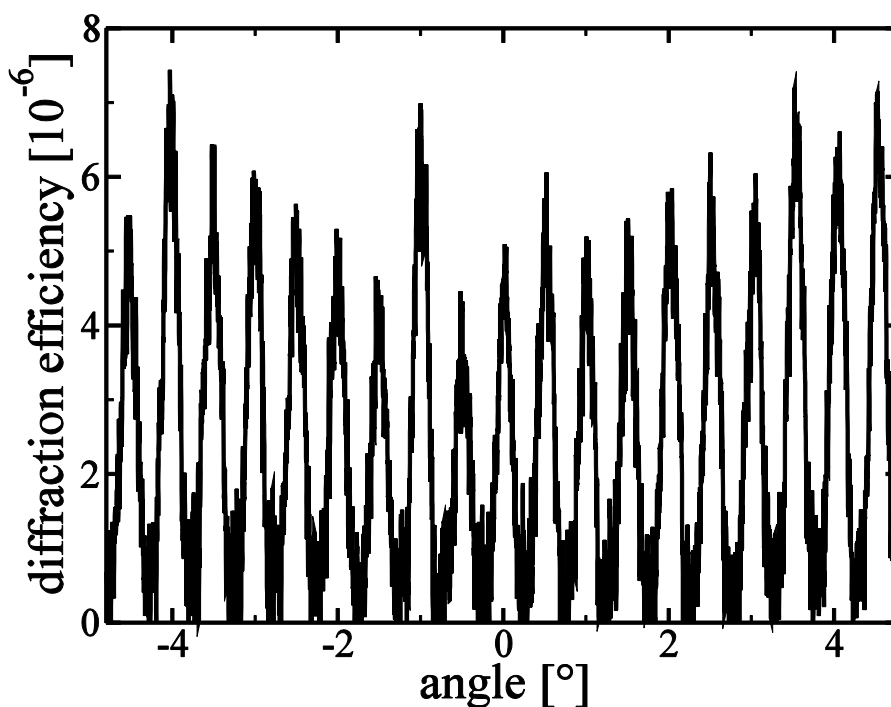


Figure 6.3. 19 angle-multiplexed plane-wave holograms inscribed in a thick sample of compound **6g** blended with polycarbonate. Writing was performed with *sp*-polarized beams. The exposure times were optimized as described in the text.

7 Molecular glasses as blending materials

Azobenzene-containing diblock copolymers are a promising material class for holographic data storage. However, a drawback of these materials is their low sensitivity to light. In the previous chapter, the low-molecular-weight compound with the best holographic performance was identified in a systematic set of experiments. Material **7g** has a high sensitivity combined with reasonable stability. It has no spacer between the methoxy-substituted azobenzene groups and the core allowing for a very fast reorientation of the chromophore. As for all low-molecular-weight glasses, the orientation is not long-term stable. In this chapter, molecular glass **7g** will be tested as a blending material for diblock copolymers. The advantage of the molecular glass is, in particular, its high sensitivity and the main advantage of the diblock copolymers is, among other things, the long-term stability of the inscribed holographic gratings. It is investigated if it is possible to combine the advantages of both classes of materials to obtain a blend with superior properties.

The blend of a low-molecular-weight compound and a diblock copolymer is a complex system. To fully characterize it, a systematic set of experiments are presented in the following sections. The investigated diblock copolymer **18** consists of two parts: an inert polystyrene block and a photo-sensitive block containing azobenzene units. When a molecular glass is added to diblock copolymer **18**, the former is expected to be present in both blocks, as shown in figure 7.1a. The photo-response of the two blocks should be independent. Thus, the behavior of both parts can be investigated separately. The model system for the molecular glass in the majority block is a molecular glass diluted in polystyrene, as shown in figure 7.1b. The molecular glass in a homopolymer with the same structure of the azobenzene side group can be used to investigate the photo-physics of the minority block with the added molecular glass, as shown in figure 7.1c. The complete photo-response of the blend should be characterized by these two contributions.

7.1 Blends with polystyrene

To understand the behavior of molecular glass **7g** in the majority block, a concentration series of compound **7g** blended with commercially available polystyrene (BASF 165 H) was studied. All spin-coated films were amorphous and showed good optical quality without undesired light

scattering. The concentration of **7g** ranged from 6 to 50 weight %. The differences between blends containing 50 w% polystyrene and the pure material **7g** are small as already shown in section 6.5.

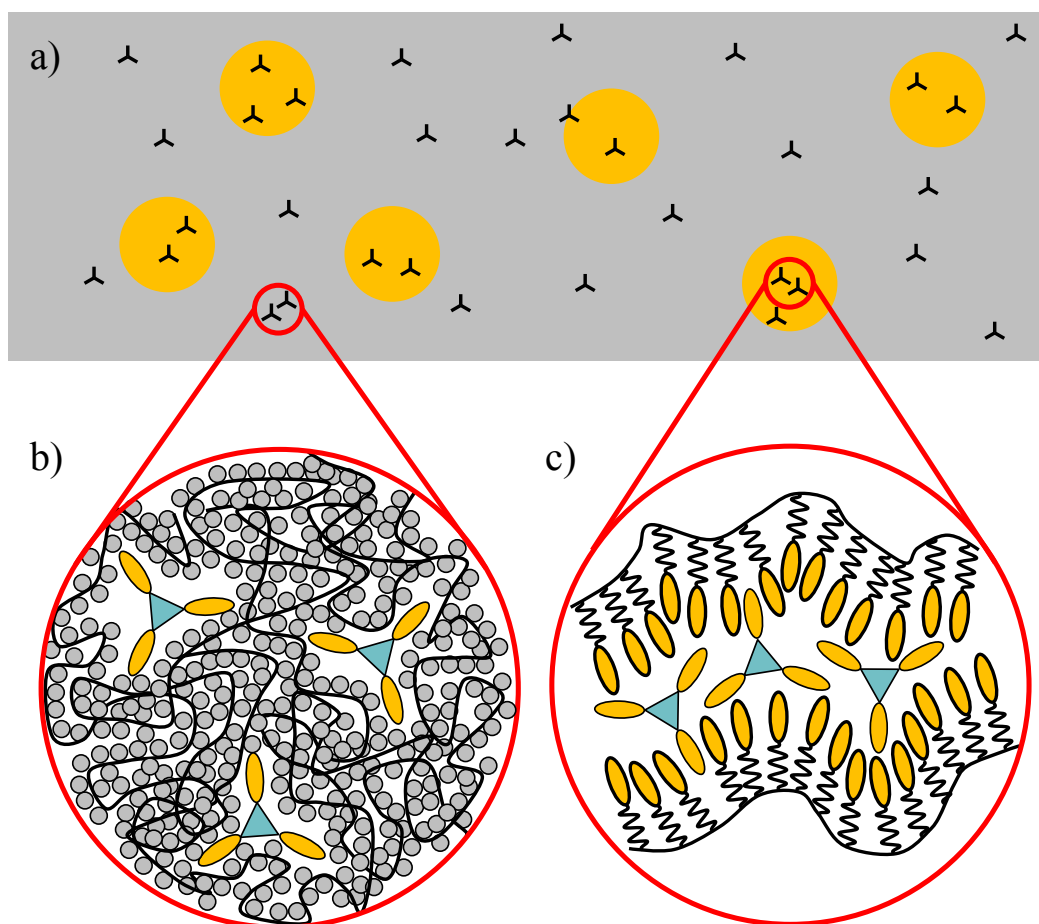


Figure 7.1. a) Schematic view of a blend between a small amount of an azobenzene-containing molecular glass (black triangles) and a diblock copolymer consisting of the spherical azobenzene-containing minority block (orange circles) and the inert majority block forming the matrix (grey). b) Detailed view of the majority block consisting of polystyrene (black lines with grey circles) and the added molecular glass (blue triangles with orange ellipses). c) Detailed view of the minority block consisting of the azobenzene chromophores (orange ellipses with bold edge) attached to the backbone (black line) of the polymer via a spacer (black curl) and the added molecular glass (blue triangles with orange ellipses).

The build-up of the refractive-index modulation in the concentration series can be fitted according to equation 32. The corresponding time constants of the build-up feature a very strong increase with decreasing azobenzene content, especially at low concentrations as can be seen in figure 7.2. The time constants differ by more than two orders of magnitude due to the loss of the cooperative effects. To compare the maximum refractive-index modulations of the blends, one has to normalize them with respect to the total

azobenzene content. The optical density per μm thickness is proportional to the concentration of azobenzene. Therefore, it can be used to normalize the refractive-index modulations of the concentration series. The normalized refractive-index modulation decreases with decreasing azobenzene content.

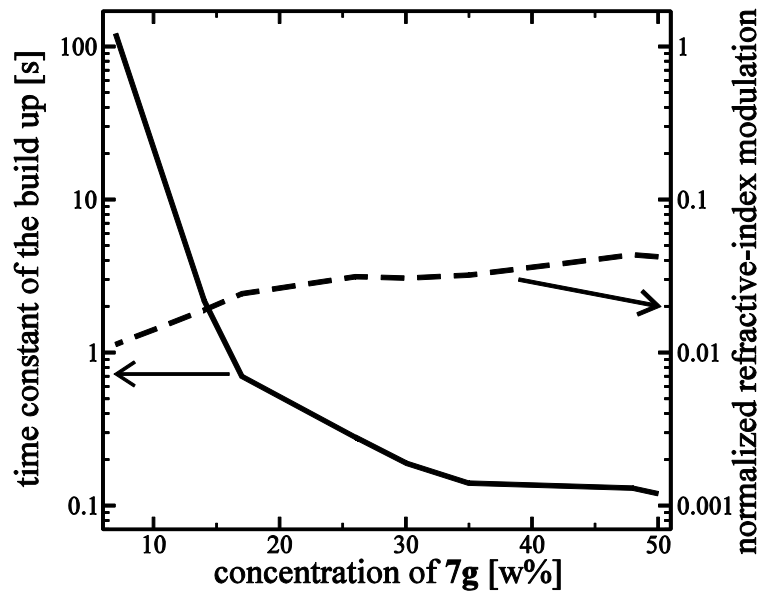


Figure 7.2. Time constant of the build-up of holographic gratings and normalized refractive-index modulation as a function of the concentration of 7g in PS. Note the logarithmic scale of the ordinate axes.

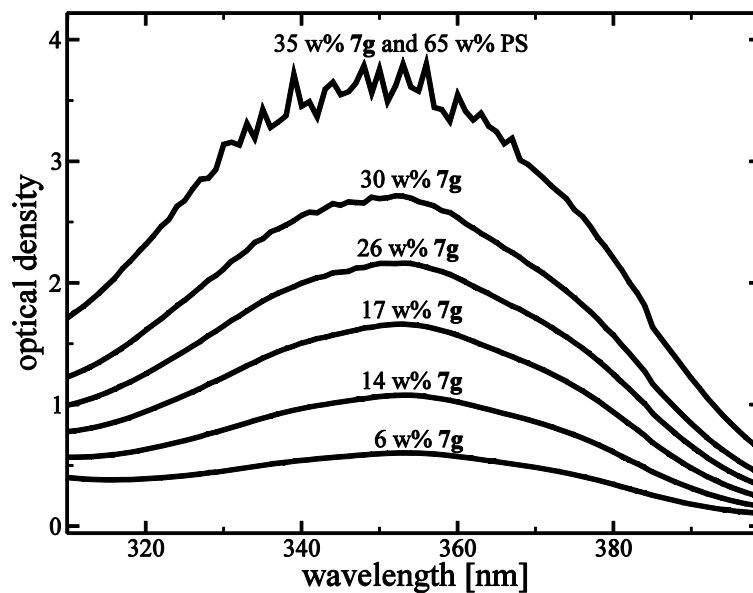


Figure 7.3. Absorption spectra of 7g in PS.

Furthermore, the wavelength of the maximum of the $\pi\pi^*$ -transition shifts from 353 nm at 6 w% to 348 nm at 50 w%, as shown in figure 7.3. For pure films of the molecular glass **7g**, the maximum of the transition is at 346 nm. These values are notably lower than in solution (351 nm). This hypsochromic shift at higher concentrations could be the result of the formation of H-aggregates between the azobenzene chromophores in the solid state, analogous to similar observations in azobenzene-containing side-chain polymers ^[159,165,180]. These observations support the picture that at higher concentrations of compound **7g**, the azobenzene units are closer to each other and, therefore, show more cooperative interactions. The chromophores can reorient faster and exhibit a higher refractive-index modulation. As expected, the stability of the inscribed holographic grating also increases with increasing content of the molecular glass due to the cooperative effects.

7.2 Blends with an azobenzene-containing homopolymer

The second model system investigated, are blends of the molecular glass **7g** and homopolymer **17** which contains azobenzene side groups ^[181]. The chemical structure of the repeating units of the homopolymer **17** is the same as the azobenzene groups in diblock copolymer **18**.

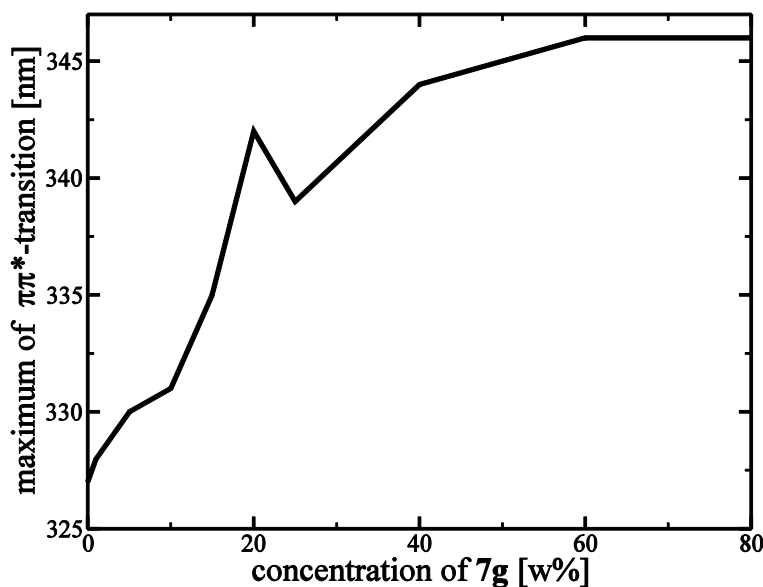


Figure 7.4. Position of the maximum of the $\pi\pi^*$ -transition in blends of homopolymer **17** and molecular glass **7g** as a function of the concentration of the latter.

The blends were prepared by doctor-blading thin films from solution. All samples were amorphous and showed good optical quality without light

scattering. Different weight fractions of the molecular glass between 0 and 80 w% were employed.

The position of the maximum of the $\pi\pi^*$ -transition in the blends shows a red shift with increasing content of the molecular glass, as shown in figure 7.4. For the pure homopolymer, the maximum is at 327 nm and in blends containing 80 w% of the molecular glass at 346 nm. The latter value is the same as for the pure molecular glass. The pure homopolymer is known to be liquid-crystalline and therefore forms stable holographic gratings. With increasing content of molecular glass, the liquid-crystalline phase is destroyed also the molecular aggregation is suppressed. This leads to the shift of the absorption maximum as discussed above.

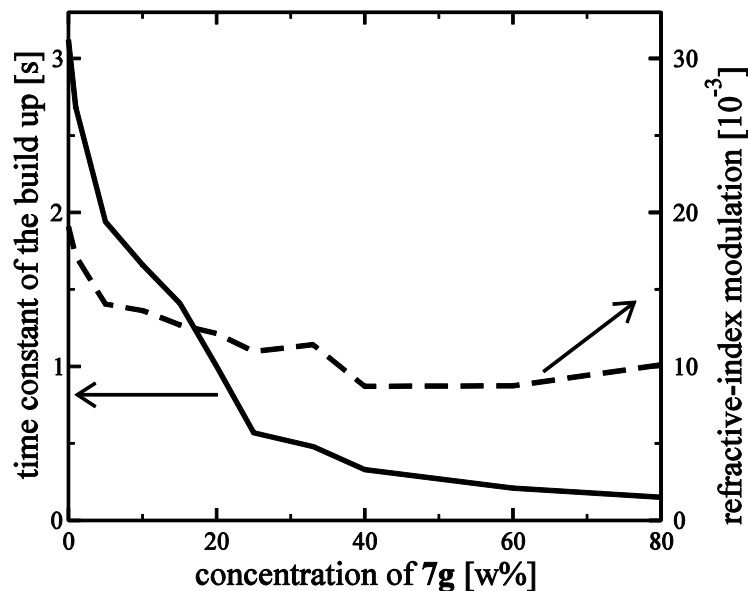


Figure 7.5. Maximum refractive-index modulation and time constant of the build-up of the holographic gratings in blends of homopolymer **17** and molecular glass **7g** as a function of the concentration of the latter.

The decrease of the refractive-index modulation -as shown in figure 7.5- can be explained by the difference between the maximum refractive-index modulations of the two materials. In contrast to the molecular glass, the azobenzene chromophores in the homopolymer are attached via long spacers. This enables the formation of a liquid-crystalline phase and an increase of the anisotropy and the order parameter, as discussed in chapter 5. The pure homopolymer **17** has a refractive-index modulation of 0.019 which is higher by a factor 2.5 than the value of 0.0076 for the molecular glass **7g**. By blending both materials, a linear decrease of the refractive-index modulation would be expected. The observed nonlinear variation is caused by the

destruction of the liquid-crystalline phase since the amorphous state of the homopolymer has a lower refractive-index modulation than the liquid-crystalline phase.

The build-up of the refractive-index modulation in the blends can also be fitted with equation 32. The obtained time constants of the build-up are plotted in figure 7.5. With increasing content of the molecular glass, they decrease by more than a factor of 10.

The material sensitivity of the blends -as discussed in section 2.2.3- depends on the refractive-index modulation and the time constant τ_1 . With the assumption that the temporal increase of the refractive-index modulation is the same for all blends, the sensitivity is directly proportional to the refractive-index modulation and indirectly proportional to τ_1 . When the content of the molecular glass is varied in this concentration series, the time constant varies more strongly than the refractive-index modulation, leading to an increase of the sensitivity by a factor of 10, as shown in figure 7.6.

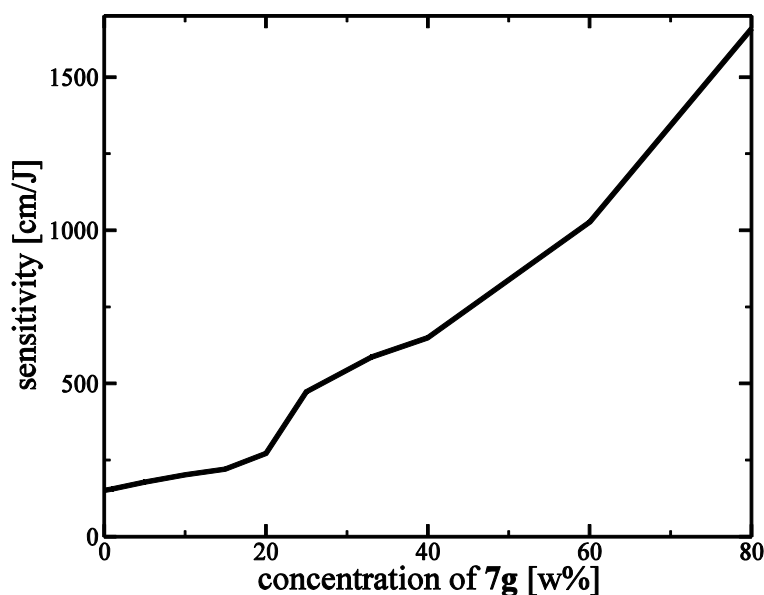


Figure 7.6. Material sensitivity of blends of homopolymer **17** and molecular glass **7g** as a function of the concentration of the latter.

The observed decrease of the time constant τ_1 and the resulting increase of the sensitivity are caused by the photo-sensitivity of **7g**. A more detailed discussion of the mechanism is given in the next section. All other possible mechanisms besides photo-induction can be excluded, as shown in the following: Changes of the thermal parameters, in particular a decrease of the glass transition temperature of the blend, would also lead to the observed results. But the glass transition temperature of **7g** is 11 °C higher than the T_g

of the homopolymer (47 °C). Therefore, the glass transition temperature of the blend should increase as compared to that of the pure homopolymer. If only this thermal effect played a role, this would lead -in contrast to the experimental observation- to an increase of the time constant. Additionally, no evidence for changes of the thermal properties was found in DSC experiments. In order to investigate, whether the observed shortening of the time constants in the blends is due to changes in the free volume caused by the low-molecular-weight compound, the non-photo-addressable low-molecular-weight compound **20** shown in figure 7.7 was used as a blending material. Compound **20** has a molecular weight of 907 g/mol and is, therefore, of similar size as **7g**, its T_g is at 83 °C. In holographic experiments, a blend containing 10 w% of compound **20** and 90 w% of homopolymer **17** was investigated. The refractive-index-modulation of the blend decreased slightly as compared to pure **17**, since the concentration of the azobenzene is lower, but the time constant of the build-up increased by a factor of 3 in this blend.

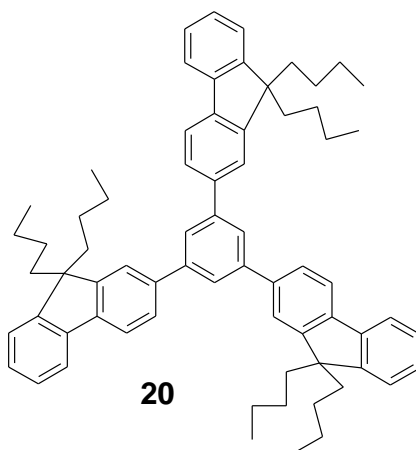


Figure 7.7. Chemical structure of the non-photo-active low-molecular-weight compound **20**.

The temporal behavior of the refractive-index modulation during the first hour after the inscription is shown in figure 7.8. The pure photo-addressable polymer exhibits long-term-stable gratings whose refractive-index modulation shows post-development due to its liquid-crystalline phase. A drawback of the blending approach is that the liquid-crystalline phase is destroyed in blends with high concentrations of molecular glass **7g**. In all blends containing more than 25 w% of the molecular glass, the inscribed refractive-index modulation was not long-term stable. With increasing content of the molecular glass, the refractive-index modulation decays faster. But in all blends containing 25 w% or less of **7g**, the slope of the refractive-index modulation was still positive after 2.5 days. This means that the inscribed gratings are long-term stable. Hence, the blend containing 25 w% of **7g** shows the largest improvement of

the holographic properties without losing its long-term stability. For this composition, τ_1 decreases by more than a factor of 5 and the sensitivity increases by more than a factor of 3 as compared to the pure homopolymer.

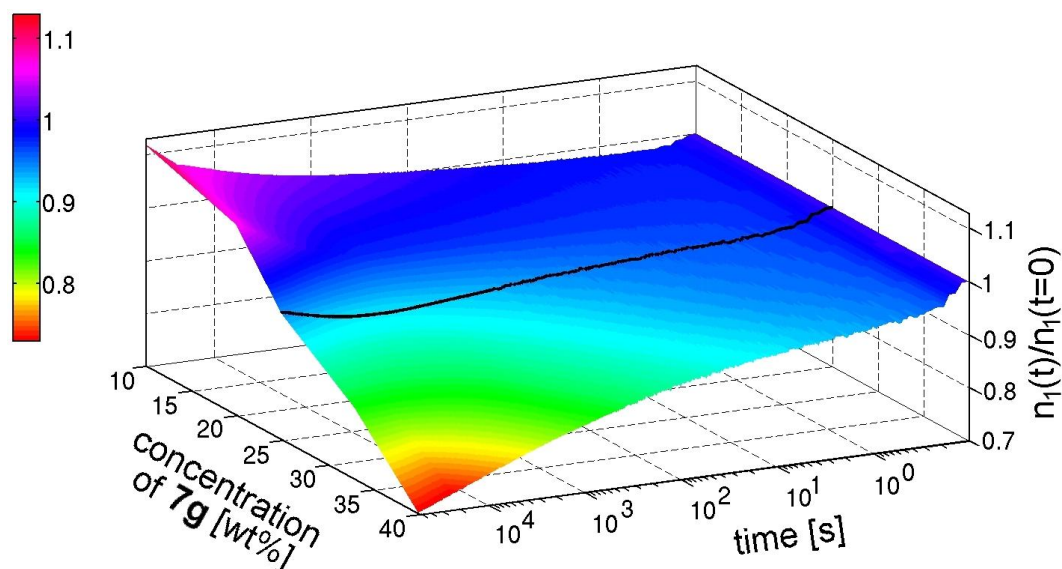


Figure 7.8. Stability of the refractive-index modulation of volume phase gratings inscribed in blends containing the molecular glass **7g** and the photo-addressable homopolymer **17** as a function of time and of the content of **7g**. The refractive-index modulation has been normalized with respect to its value at the time when the writing laser was turned off. Note the logarithmic time axis.

With a blend containing 20 w% of the molecular glass, experiments were also performed at elevated constant temperatures. At higher temperatures, the time constant of the build-up decreased further, but at the expense of the stability. At 40 °C, the gratings are no longer stable.

7.3 Blends with an azobenzene-containing diblock copolymer

A series of blends containing the compounds **7g** and diblock copolymer **18** were prepared by doctor-blading. The concentration of **7g** ranged from 0 to 40 weight %^[182]. The blends were not annealed, only the remaining solvent was removed. Due to the low concentration of the azobenzene chromophores bound to the minority block of **18**, a big fraction of the azobenzene moieties in the blend belongs to the molecular glass in most cases. For the blend containing 40 w% **7g** for example, 83 % of the azobenzene chromophores are bound to the molecular glass and only 17 % to the polymer. The fit according to equation 32 was not satisfactory for these blends, as will be discussed below. Therefore, the writing times to the maximum of the refractive-index

modulation are given in this section as a measure for the writing speed. They are equivalent to the time constant of the build-up discussed in the previous sections. The refractive-index modulation grows in the concentration series due to the increased overall content of azobenzene per volume. The blend containing 40 w% **7g** has a higher concentration of azobenzene groups by a factor of 3.5 as compared to pure **18**. Similar as in the case of the homopolymer, also the azobenzene moieties bound to the polymer backbone of **18** via spacers result in higher refractive-index modulations normalized to the azobenzene content than the azobenzene groups bound to molecular glass **7g**. Therefore, the refractive-index modulation grows only by a factor of 2.5 from 0 to 40 w%. The writing time, however, decreases by more than a factor of seven, as shown in figure 7.9.

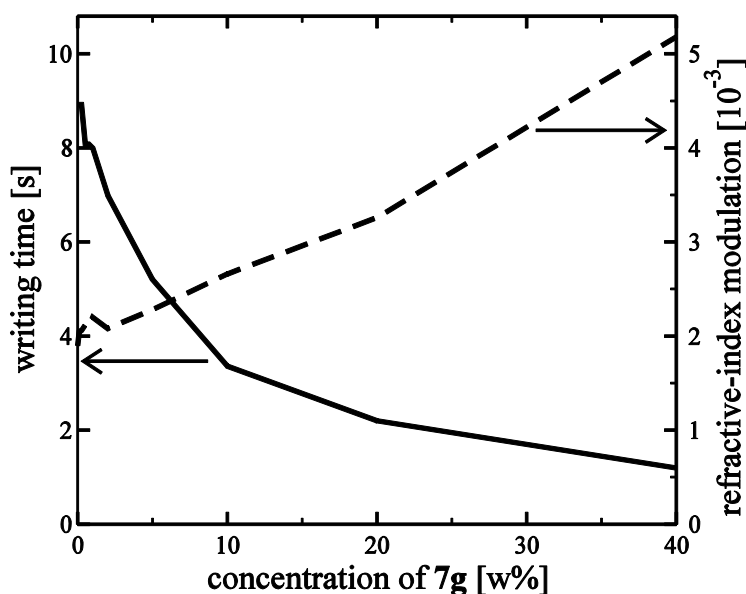


Figure 7.9. Maximum refractive-index modulation and writing time of the holographic gratings in blends of diblock copolymer **18** and molecular glass **7g** as a function of the concentration of the latter.

For the 40 w% blend, the sensitivity increases by a factor of 37 as compared to the pure block copolymer, as shown in figure 7.10. The inscribed gratings are stable in blends with a concentration of less than 2 w% of the molecular glass. For this concentration, only 13 % of all azobenzene chromophores belong to the molecular glass. The sensitivity in this blend is higher by a factor of 1.7 as compared to the pure diblock copolymer.

This experiment proves that the assumption outlined at the beginning of this chapter is valid. It is possible to increase the sensitivity of diblock copolymers by blending with a molecular glass. The underlying mechanism can be understood with the help of the previous sections in which the holographic

responses of the inert and photo-active block were investigated separately. The improved sensitivity is not due to molecules of **7g** located in the inert PS matrix of **18**. As mentioned above, already for 2 w% of the molecular glass in the diblock copolymer, there is a remarkable increase in sensitivity. Even if all the molecular glass were embedded in the PS block, the concentration of **7g** in this block would be around 2.4 w% in this example. From section 7.1 it is known that the writing time to the maximum of a refractive-index modulation of **7g** diluted in PS at this concentration is longer by two orders of magnitude than for pure **18**. Hence, the formation of the refractive-index grating of the molecular glass in the inert block of the diblock copolymer cannot be the reason for the observed increase in sensitivity. Furthermore, it does not just originate from the increased refractive-index modulation alone, which is smaller than the increase in sensitivity by more than a factor of 10.

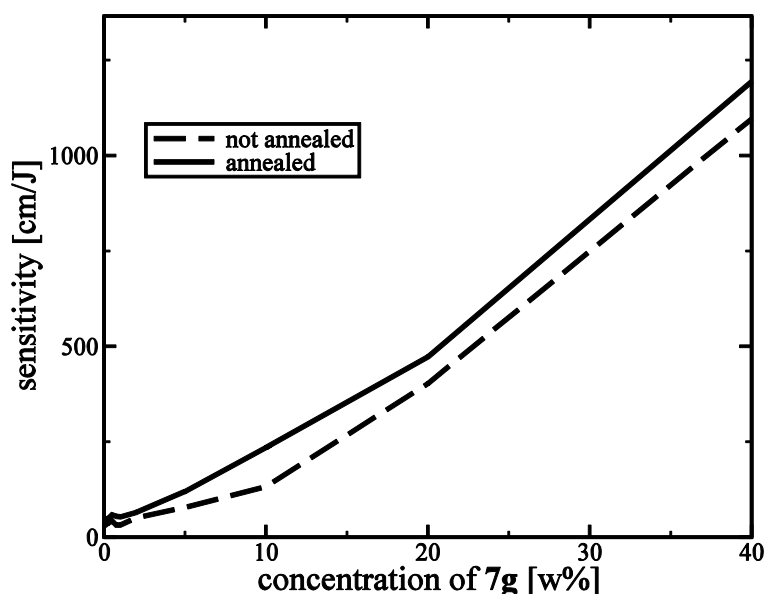


Figure 7.10. Material sensitivity of blends of diblock copolymer **18** and molecular glass **7g** as a function of the concentration of the latter.

About 18.5 w% of diblock copolymer **18** consist of the azobenzene-containing minority phase, the remaining 81.5 w% are the majority phase. At this ratio of the blocks, the minority phase forms cylinders. By adding molecular glass **7g**, a change of the morphology to a lamellar phase may, in principle, occur due to swelling of the minority block. A lamellar phase, however, is expected only for a relative content of the minority block of about 35 w%. With the assumption that all of the molecular glass is present in the minority block, only in blends containing more than 20 w% **7g**, the morphology of the diblock copolymer is expected to change from cylindrical to lamellar. But the increase in sensitivity starts already in blends with 1 w%.

At this low content, no phase change is expected to occur; therefore, an influence of the morphology can also be excluded.

Since all other mechanisms can be ruled out, the observed increase in sensitivity must be light-induced and it must occur in the photo-sensitive block of the diblock copolymer. It is known that the azobenzene chromophores bound to the molecular glass without spacer reorient faster than the azobenzene groups of the polymer. It is believed that the movement of the chromophores of the molecular glass facilitates the reorientation of the azobenzene chromophores of the polymer by creating free volume and by photo-softening effects. Additionally, the azobenzene chromophores of the polymer are reoriented with the faster orienting chromophores of **7g** due to cooperative interactions. This is schematically shown in figure 7.11. The strong influence of cooperative effects in a side-chain polymer with azobenzene chromophores and mesogenic units by steric and dipolar interactions has already been demonstrated in literature ^[43,51,183]. Hence, light-induced cooperative motions can also exist between azobenzene-containing molecular glasses and photo-addressable polymers.

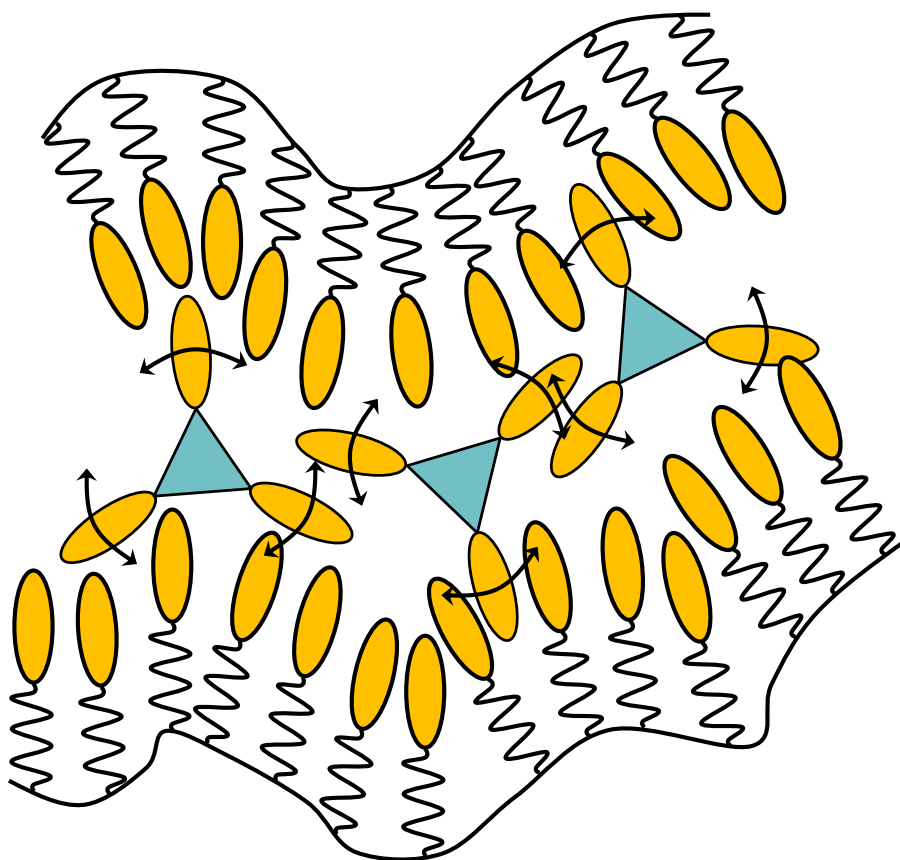


Figure 7.11. Schematic view of azobenzene-containing minority segments of a diblock copolymer with molecules of a molecular glass former.

As was discussed above, only the molecules of the molecular glass in the photo-active block can increase the sensitivity. The molecules which are diluted in the majority block of PS do not improve the sensitivity and are therefore useless. If the distribution of the molecular glass in the two blocks of the diblock copolymer were statistical, one would expect that only about 18.5 % of the molecules of **7g** enter the minority block. But it would be advantageous that all molecules of the molecular glass are inside the photo-active block.

The content of molecular glass in the minority and majority block can be determined from the experimental data. Inside the photo-sensitive block, the azobenzene chromophores of the polymer and of the molecular glass are present. In the inert block, there are only the chromophores of the molecular glass. The build-up of the refractive-index modulation in the blends occurs separately in the two blocks. Their sum yields the total refractive-index modulation of the blend:

$$n_1 = [0.825(1-z) + (1-q)z]n_{1maj} \left(1 - \exp \left(- \left(\frac{t}{\tau_{maj}} \right)^{0.9} \right) \right) + [0.175(1-z) + qz]n_{1min} \left(1 - \exp \left(- \left(\frac{t}{\tau_{min}} \right)^{0.9} \right) \right) \quad (37)$$

with:

- z weight fraction of **7g** in the blend
- q fraction of the molecules of **7g** in the minority block
- n_{1maj} maximum refractive-index modulation in the majority block
- n_{1min} maximum refractive-index modulation in the minority block
- τ_{maj} time constant of the build-up in the majority block
- τ_{min} time constant of the build-up in the minority block

The weight fraction z ranges from 0 to 40 w%. The parameter q is the fraction of the molecules of the molecular glass which are inside the minority block divided by the total amount of molecules of the molecular glass. The time constants of the build-up τ_{maj} and τ_{min} and the maximum refractive-index modulations n_{1maj} and n_{1min} were obtained from the two model system discussed in sections 7.1 and 7.2. The value of τ_{maj} , τ_{min} , n_{1maj} , and n_{1min} depend also on the parameters q and z , since these two parameters determine

the concentration of the molecular glass in the respective block. In addition to equation 32, weighting factors in the square brackets have to be introduced to account for the volume fractions of the two systems, which influence their relative contribution to the overall refractive-index modulation. The values 0.825 and 0.175 are the percentage of the majority and the minority block, respectively. If many molecules of the molecular glass are inside the minority block (high value of q), the relative volume fraction of this system increases to more than 0.175, while the other decreases. The parameter q can be determined by fitting the experimental build-up data of the refractive-index modulation in the blends with equation 37. For a statistical distribution of **7g** in **18**, one would expect $q = 0.175$. The fits yield the estimate $q \approx 45\%$, which is higher by a factor of 2.5. This suggests that the molecular glass enters mainly the photo-addressable minority block rather than the polystyrene matrix.

When the samples of pure **18** are annealed, the writing time decreases by 25 % while the refractive-index modulation remains constant. The minority phase is amorphous and annealing leads to a more distinct phase separation between the two blocks^[184]. The associated enhancement of the cooperative effects leads to the observed decrease of the writing time in the annealed samples of **18**. These observations are in contrast to literature data of a diblock copolymer containing additional mesogenic units in the minority block^[51]. For this compound it was found that annealing leads to an increase of both the writing time and the refractive-index modulation. The mesogenic units favor the build-up of a liquid-crystalline phase in the minority block. In this case, annealing additionally increases the order parameter of this liquid-crystalline phase, which impedes the reorientation of the azobenzene chromophores.

In the blends of **18** and **7g** the sensitivity can be increased by annealing at 80 or 170 °C for 3 hours, as shown in figure 7.10. The observed increase in sensitivity is higher than one would expect from the phase separation effect of the diblock copolymer discussed above. The results presented in this section and in sections 5.4 and 5.5 indicate that the molecular glass is not perfectly miscible in polystyrene. To further confirm this assumption, blends containing PS and **7g**, which were discussed in section 7.1, were also annealed. In the light microscope, a separation between the inert PS and the molecular glass could be seen. This separation resulted in a decrease of the time constant of the build-up of the annealed sample compared to the sample which was not annealed. Therefore, the likely explanation is that the molecular glass phase-separates from the polystyrene in the majority block of the diblock copolymer and migrates into the photo-addressable block during the annealing process. Judging from the data of **7g** in PS and in the homopolymer, it can be estimated from equation 37 that after the annealing step around 70% of the molecules of **7g** are in the photo-addressable block.

The phase separation between low-molecular-weight compound and the majority block of PS was detected with transmission electron microscopy (TEM) at the “Bayreuther Institut für Makromolekülforschung” with a Zeiss CEM 902. The contrast between the azobenzene and the polystyrene is very low in the TEM pictures due to their similar chemical structure. Staining the samples with RuO_4 did not increase this contrast. Therefore, the low-molecular-weight compound **7m** with an Iodine substituent was used. The order number of Iodine is higher than that of all other elements in the organic compounds **18** and **7m**. The higher electron density of Iodine leads to a good contrast between the low-molecular-weight compound and the diblock copolymer in the TEM pictures. A blend containing 10 w% of **7m** and 90 w% of **18** was spin-coated and annealed. Then the film was detached from the glass substrate, embedded in epoxy resin, and thin slices were prepared with a microtome. The samples were then investigated with TEM, as shown in figure 7.12. The black areas are the regions of high electron density, i.e. high density of the low-molecular-weight compound **7m**. Their shape, size and distance are typical for the cylindrical morphology of diblock copolymer **18**. Hence, it can be concluded that the low-molecular-weight compound accumulates inside the photo-active block, as is also indicated by the previous experiments.

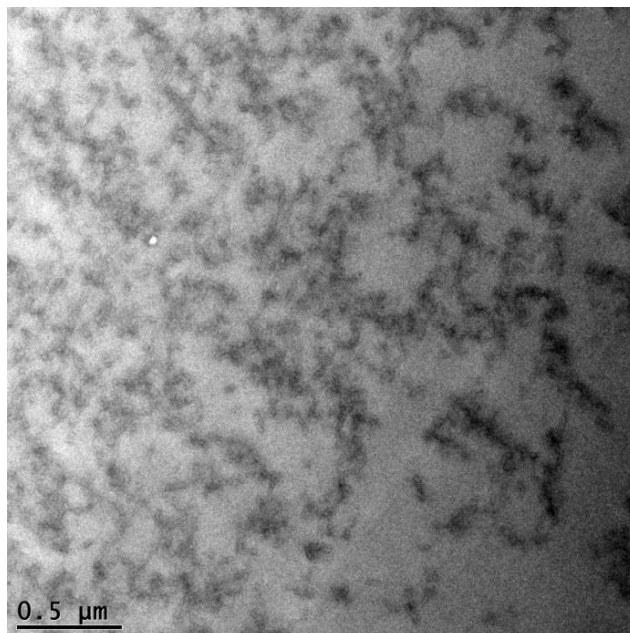


Figure 7.12. TEM picture of diblock copolymer **18** and iodine-containing low-molecular-weight compound **7m**.

7.4 Temperature dependence of blends with a diblock copolymer

An additional tool for increasing the sensitivity of blends of diblock copolymer **18** and molecular glass **7g** is to inscribe the holographic gratings at elevated temperatures. A blend containing 10 w% **7g** and 90 w% **18** was used to study the holographic properties at temperatures up to 80 °C. The results are shown in figure 7.13. The writing times decrease at higher temperatures due to the increased mobility. The refractive-index modulation also decreases, but the relative change is much smaller. This leads to an increase in sensitivity from 130 cm/J at 22 °C to 560 cm/J at 60 °C. The disadvantage is that the refractive-index modulation decays more rapidly at elevated temperatures. Subsequent cooling to room temperature after the inscription process can prevent the decay, however, and lead to long-term-stable holographic gratings. Therefore, the material sensitivity of the blends can be generally improved at higher temperatures, as was already shown in section 5.4. The activation energy for the decay of the gratings can be calculated as 31 kJ/mol, which is the same value as for pure **7g** (see section 6.6).

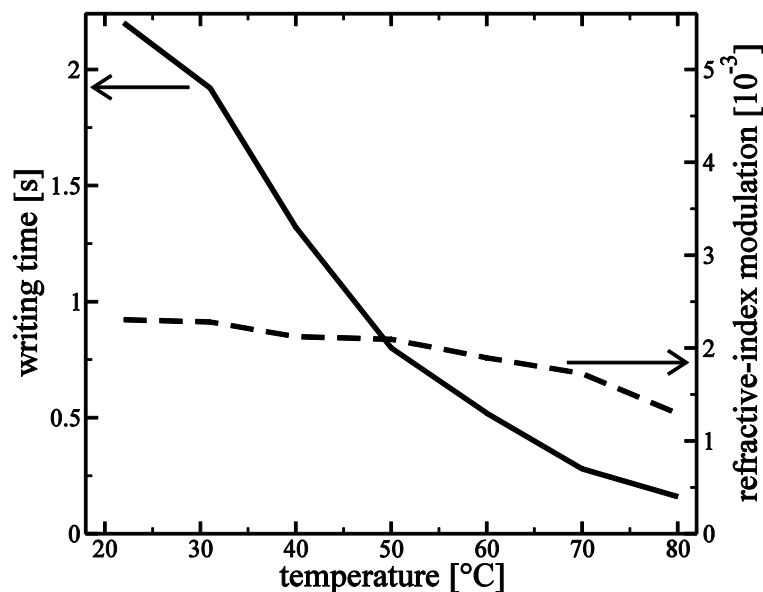


Figure 7.13. Temperature dependence of the maximum refractive-index modulation and the writing time in an annealed blend consisting of 10 w% **7g** and 90 w% **18**.

7.5 Blends with a diblock copolymer containing mesogenic units

Diblock copolymer **19** is similar to **18**, but the minority block contains additional mesogenic units. It had been demonstrated that stable, rewritable

holographic gratings can be angle-multiplexed in a compound very similar to **19** [51,52]. Due to those promising results, blends of **7g** and **19** are investigated in this section. The mesogenic units lead to a liquid-crystalline phase which enhances the stability of the orientation of the chromophores. Since the mesogenic units must be oriented by the azobenzene via cooperative motions, however, the mechanism of reorientation in pure **19** leads to a drastic increase of the writing times to the maximum of the refractive-index modulation as compared to pure **18**.

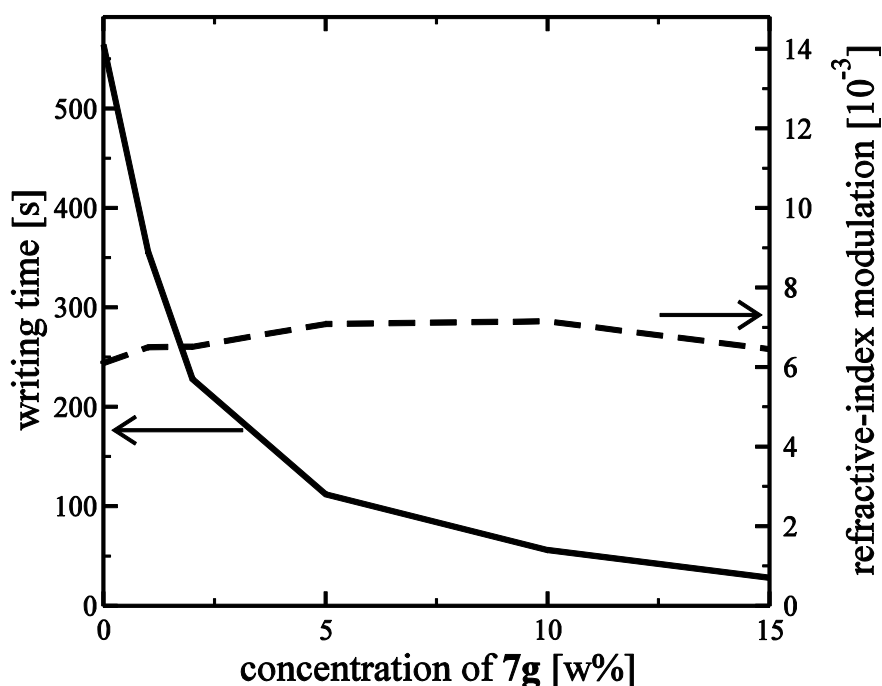


Figure 7.14. Maximum refractive-index modulation and writing time of the holographic gratings in blends of diblock copolymer **19** and molecular glass **7g** as a function of the concentration of the latter.

A series of blends of the compounds **7g** and **19** were prepared by spin-coating and all samples were annealed. As was already discussed in section 7.3, annealed samples of **19** show a higher refractive-index modulation and longer writing times as compared to the samples without annealing. The concentration of **7g** in the blends ranged from 0 to 15 w%. In all blends containing **7g**, stable holographic gratings can be inscribed. The stretched-exponential fit is not satisfactory for these systems, as was already discussed in section 7.3. For the comparison of the writing speeds in the blends, the writing time to the maximum of the refractive-index modulation is again used. The writing time decreases by more than a factor of ten as shown in figure 7.14, whereas the refractive-index modulation remains nearly constant. The sensitivity as a function of the content of **7g** increases strongly, as shown in

figure 7.15. Compared to pure **19**, the material sensitivity increases by more than a factor of 25 in the 15 w% blend and the gratings are still stable.

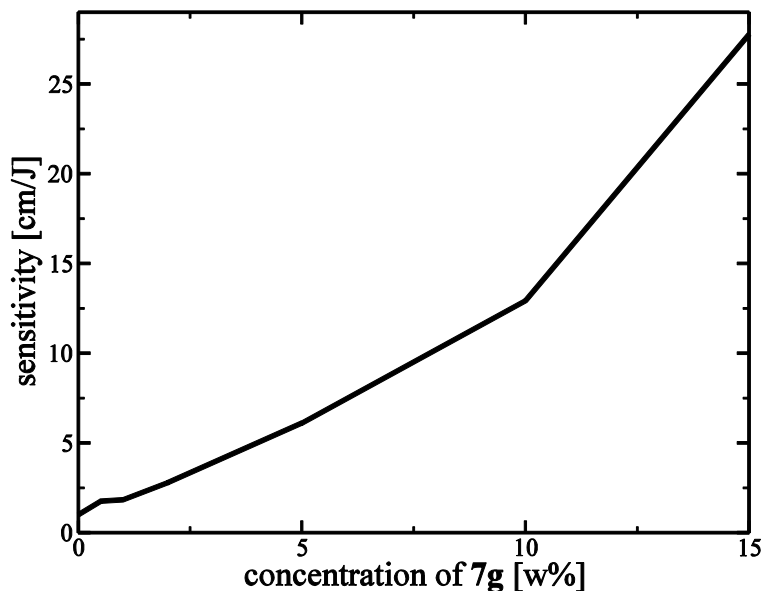


Figure 7.15. Material sensitivity of blends of diblock copolymer **19** and molecular glass **7g** as a function of the concentration of the latter.

7.6 Angular multiplexing

For holographic data storage, more than one hologram should be inscribed in the same volume of the sample. In a diblock copolymer similar to **19**, up to 200 holographic gratings were angle-multiplexed at the same spot of the sample ^[161]. To test, if the blends of molecular glass **7g** and diblock copolymer **19** are also suitable for angular multiplexing, thick samples were prepared by injection molding. The blend consisted of 99.5 w% PS, 0.1 w% **7g**, and 0.4 w% **19**.

Due to the decreased azobenzene concentration in the thick samples, the sensitivity is also lower. The increase in sensitivity of this blend as compared to a blend containing only the diblock copolymer and PS was in the thick samples less pronounced than in the thin samples discussed in the previous section. This can be explained by the strong dilution of the azobenzene-containing materials with polystyrene. The molecular glass then enters the minority phase with a smaller probability. Most of the molecular glass is located in the polystyrene where it cannot accelerate the writing speed. By appropriate annealing programs, it should be possible improve this situation.

The optical density of the thick samples at the writing wavelength of 488 nm was 0.28, lower than the optimum value^[38] by a factor of two. Additionally, the sample quality was imperfect. Inside the samples there were tiny air bubbles and contaminations and the surface was rough due to the rough surface of the injection molder. All these effects lead to strong light scattering. Therefore, the gratings were angle-multiplexed in *sp*-configuration, as discussed in section 6.7. The writing times were optimized with the help of equation 36. As shown in figure 7.16, 80 holographic gratings can be angle-multiplexed in the same volume element. By increasing the optical density and the optical quality of the sample, it should be possible to further increase the number of angle-multiplexed gratings in the blends. The dynamic range was calculated as 0.09 and the sensitivity as 0.002 cm/J. The inscribed holographic gratings are stable and show no decay during two days.

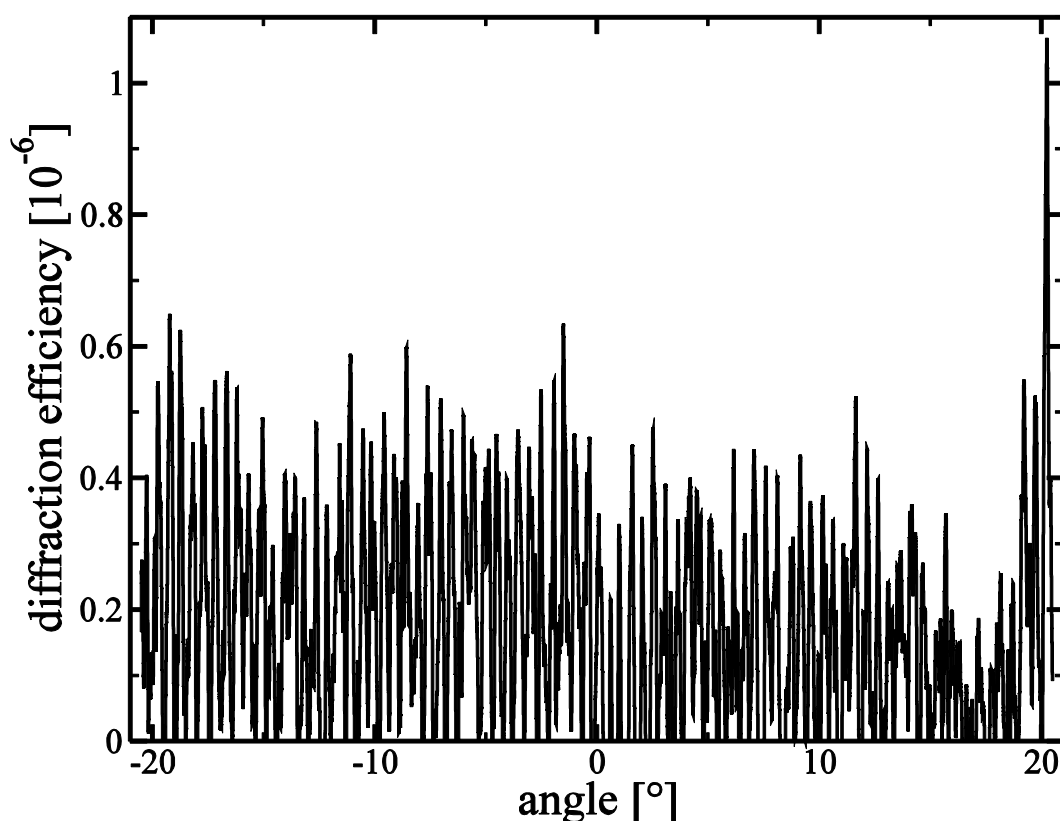


Figure 7.16. Angular multiplexing of 80 holographic gratings in a thick sample of a blend containing 99.5 w% PS, 0.1 w% **7g**, and 0.4 w% **19**.

Hence, the basic concept discussed in this chapter is also successful for diblock copolymers with azobenzene and mesogenic units in the photo-active block. Holographic gratings can be inscribed in blends containing these diblock copolymers and a molecular glass with higher sensitivity as compared

to the pure diblock copolymer. All advantages of the latter material such as stability or the possibility of angular multiplexing are also present in the blend. It is indeed possible to combine the advantages of both classes for improved holographic performance.

7.7 Storage of two-dimensional data

In HDS, two-dimensional data pages containing many bits rather than plane waves are usually inscribed. Typically the data pages are divided into squares. The squares can be either black or white representing a digital “0” or “1”, respectively. The maximum number of bits per page which can be inscribed and read out in a thick sample containing 99.5 w% PS, 0.1 w% **7g**, and 0.4 w% **19** was 2700, as shown in the checkerboard pattern in figure 7.17. In this case, the number of pixels per page is not limited by the resolution of the SLM or the CCD but by the sample quality. Especially light scattering becomes a much more severe problem in the two-dimensional data set-up than it is for the plane-wave holograms.

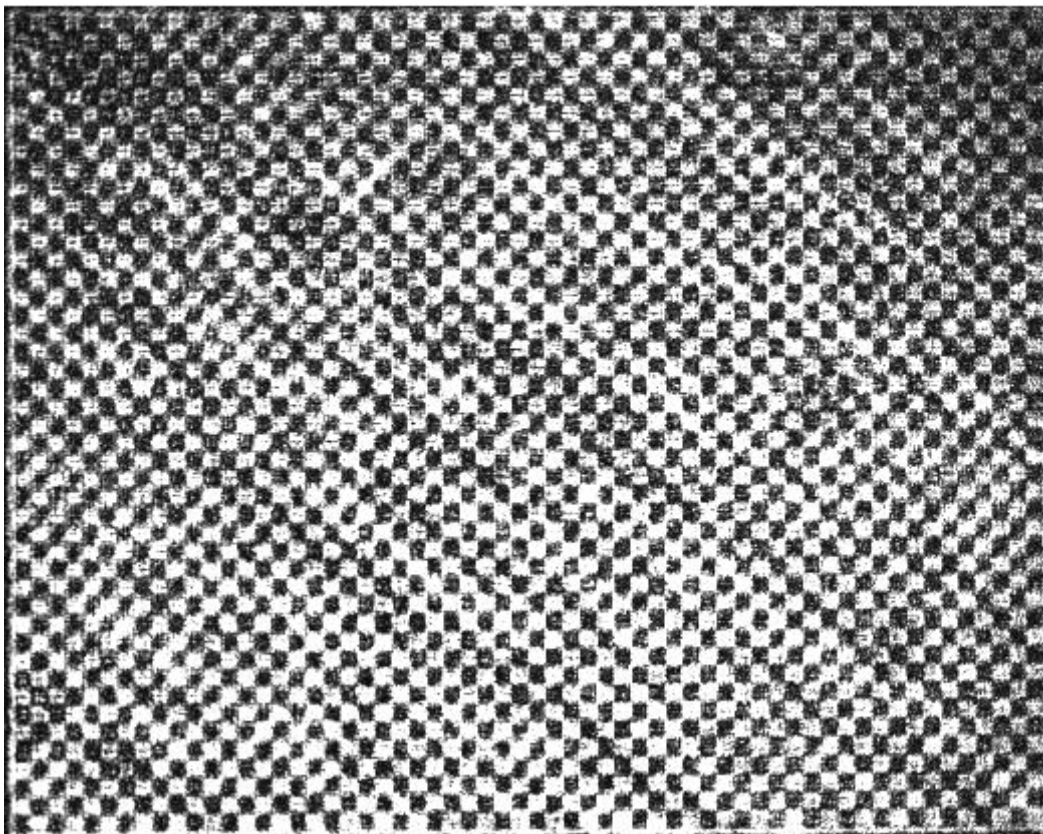


Figure 7.17. Checkerboard pattern with 60×45 squares holographically inscribed and reconstructed in a sample containing 99.5 w% PS, 0.1 w% **7g**, and 0.4 w% **19**.

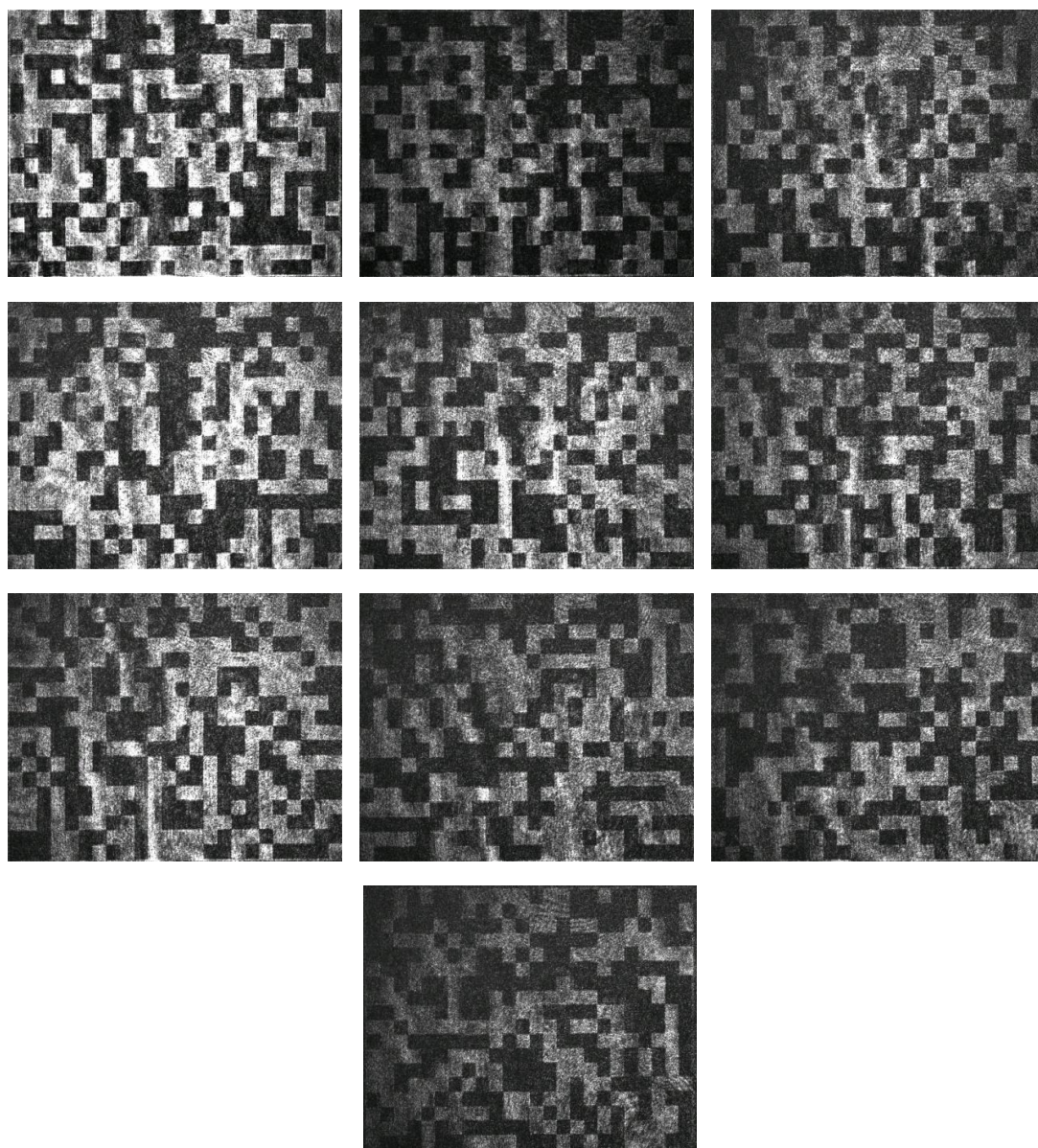


Figure 7.18. 10 data pages of each 24×18 squares inscribed and reconstructed in a sample containing 99.5 w% PS, 0.05 w% **7g**, and 0.45 w% **19**.

Also with these two-dimensional data pages, angular multiplexing is possible. The number of bits per page multiplied by the number of angle-multiplexed pages yields the maximum number of bits that can be inscribed in a section of the samples. But these two factors cannot arbitrarily be increased, since they are correlated with each other. With increasing number of pages, the diffraction efficiency per page decreases. According to equation 23, the diffraction efficiency of each angle-multiplexed hologram is inversely proportional to the square of the total number of holograms. If the diffraction efficiency decreases, also the maximum number of bits decreases, since the

signal-to-noise ratio and the integration time of the CCD determine the upper limit for the number of bits per page that can be read out. In a systematic set of experiments with a thick sample containing 99.5 w% PS, 0.05 w% **7g**, and 0.45 w% **19**, it was found that the maximum number of bits which can be stored in a volume element and accurately read out without errors, is achieved when ten pages with 432 bits each are inscribed, as shown in figure 7.18. The writing angle between the pages was varied by 2°. The 4320 bits were inscribed with a data rate of 75 b/s and the storage density was 2200 b/mm².

7.8 Blends with liquid-crystalline low-molecular-weight compounds

The concept of increasing the sensitivity of azobenzene-containing materials by blending them with molecular glass **7g** was not only tested for diblock copolymers but also for the latent liquid-crystalline material **8i**. For this purpose, the pure material **8i** was compared to a blend consisting of 90 w% **8i** and 10 w% **7g**. In the blend, molecules of **7g** act as impurities which reduce the order parameter in the liquid-crystalline phase. The gratings inscribed in the pure material as well as in the blend are stable; only the degree of post-development decreases for the blend as listed in table 7.1. The time constant of the build-up of the holographic grating decreases when **7g** is added as expected. The latter accelerates the reorientation of the azobenzene chromophores of **8i** and, therefore, the time constant becomes shorter. But at the same time also the refractive-index modulation decreases by almost a factor of two. Since the decrease of the refractive-index modulation is stronger than the increase in writing speed, the sensitivity is smaller in the blend as compared to the pure material.

Table 7.1. Results of holographic measurements.

	τ_1 [s]	n_1 [10 ⁻³]	sensitivity [cm/J]	rel. value of n_1 4000 s after the inscription [%]
100 w% 8i	1	56	1323	116
90 w% 8i and 10 w% 7g	0.75	32	1008	108

8 Surface relief gratings

Upon illumination of an azobenzene-containing sample with a holographic light grating, a grating in the volume and, additionally, a surface relief grating can develop. In the previous chapters, the experimental conditions were chosen that the SRGs did not develop and solely the holographic volume grating could be investigated. In the experiments described in the following, the experimental parameters -especially the polarization configuration and the illumination time- have been changed as compared to the previous chapters. Therefore, besides a volume grating, also SRGs develop which are the topic of this chapter.

The phenomenon of SRG formation has been mainly investigated in polymers carrying azobenzene moieties as side groups ^[27,29,30,156,159]. Surface relief gratings can also be generated in supramolecular materials ^[185,186], sol-gel-based azobenzene-containing materials ^[186], or polyelectrolytes with azobenzene groups bound by ionic interactions ^[185]. Furthermore, SRG formation was recently also demonstrated in photochromic molecular glasses ^[54,57,58,64,65] with modulation heights ranging between 280 and 490 nm. Kim et al. showed that the photoinduced growth of SRGs can be more efficient in thin films of a molecular glass as compared to polymers, since the mass transport is not hindered by entanglements of the polymer chains ^[54,63].

In this chapter, holographic gratings are inscribed in spin-coated films of pure molecular glasses with two writing beams at 488 nm and an intensity of each beam of 1 W/cm². In a systematic set of experiments, the polarization configuration of the two writing beams was varied. Additionally, the substituent at the azobenzene moiety of the molecular glasses was varied by using compounds **6a**, **6c**, **6d**, **6e**, and **6g**, which leads to a change of the optical properties. These comparative investigations lead to new insights into the formation of surface relief gratings and to an enhancement of their height.

8.1 Temporal evolution of the diffraction efficiency

During illumination of the sample films with two superimposed laser beams, in general, a refractive-index modulation in the bulk and a surface relief grating are created and both contribute to the light diffraction. Figure 8.1 shows a typical example of the time-dependent diffraction efficiency during inscription. As shown in the Figure 8.1b, the diffraction efficiency of the volume grating grows faster than that of the SRG. Here, the volume grating reaches its maximum after about 5 seconds, whereas the maximum of the SRG is reached only after some minutes, depending on the polarization

configuration of the writing beams and the material. After 60 seconds of inscription, the DE of the SRG is always larger by at least one order of magnitude in the applied set-up. Therefore, the influence of the volume hologram can be neglected at later times. Typical values of the maximum DEs of volume gratings in the experiments are around 0.1%, whereas the DEs of SRGs reach 30%, i.e., more than two orders of magnitude higher.

To simulate of the temporal evolution of the diffraction efficiency, both processes must be taken into account. Therefore, equations 11 and 26 have to be combined. This was first described by Reinke^[174]. Later-on the theory was expanded by Sobolewska and Miniewicz^[187]. The formula of the latter group was applied to simulate the measured diffraction efficiencies:

$$\eta(t) = J_1^2 \left\{ 2\pi \left[(n_1(t) d_0)^2 + (\Delta n d(t))^2 + 2 n_1(t) d_0 \Delta n d(t) \cos(\Delta\varphi) \right]^{\frac{1}{2}} \left[\lambda \cos(\theta) \right]^{-1} \right\} \quad (38)$$

with:

- d_0 thickness of the film
- n_1 refractive-index modulation
- Δn amplitude of the refractive-index change between sample and air
- d height of the SRG from peak to valley
- $\Delta\varphi$ phase difference between volume and surface relief grating

The growth of the height of the surface relief grating can be described by:

$$d(t) = d_{\max} \left[1 - \exp\left(\frac{-t}{\tau_3}\right) \right] \quad (39)$$

with:

- d_{\max} maximum height of the surface relief grating
- τ_3 time constant of the build-up of the SRG

The build-up of the refractive-index modulation of the volume grating follows the law:

$$n_1(t) = n_{1\max} \left[1 - \exp\left(\frac{-t}{\tau_1}\right) \right] \quad (40)$$

with:

- $n_{1\max}$ maximum value of the refractive-index modulation
- τ_1 time constant of the build-up of the refractive-index modulation of the volume grating

For describing the build-up of the refractive-index grating, the stretching exponent in equation 32 was set to 1. This simplification had only a minor influence on the results but made the fitting procedure more efficient. Figure 8.1 shows the temporal growth of the measured total diffraction efficiency η . The fit according to equation 38 matches the experimental data very well. From the calculations, a phase difference $\Delta\varphi = 180^\circ$ between the volume grating and the SRG can be obtained for the polarization settings *pp*, $\pm 45^\circ$, $++45^\circ$, *rlcp*, and *rscp*. This phase difference is expected from the theoretical considerations discussed in section 2.4.1. This means that the direction of the material transport in these molecular glasses with positive values of χ' is from the dark to the bright regions, as predicted by equation 28. The diffraction efficiency of the SRG quickly compensates the initial orientational diffraction efficiency and then becomes the dominating contribution. For *pp*, $\pm 45^\circ$, and *rlcp*, which exhibit a fast SRG build-up, the diffraction efficiency reaches zero after some seconds, as shown in the figure 8.1b, for the other two polarizations it reaches a local minimum. For *ss* and *sp*, no phase difference could be determined.

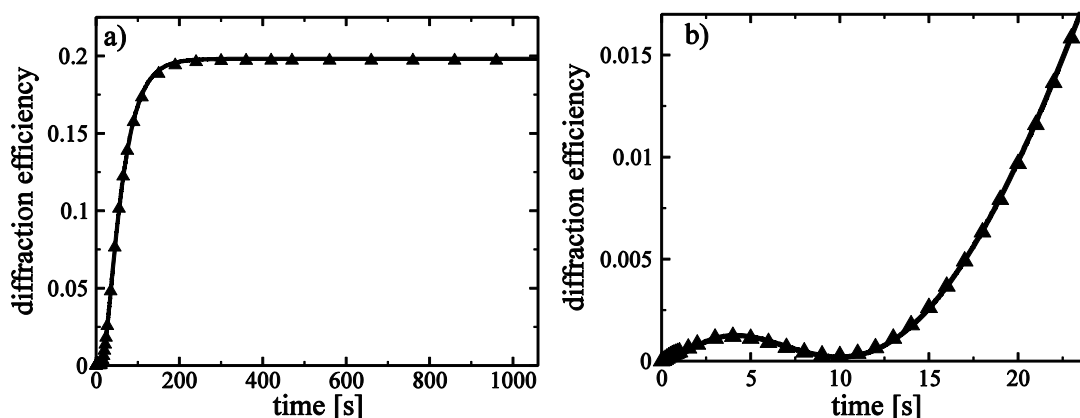


Figure 8.1. Temporal evolution of the diffraction efficiency η (black triangles) as measured on a film of compound **6c** a) during the whole hologram inscription and b) in the first seconds. Writing was performed with the polarization configuration $\pm 45^\circ$. The black curve represents the fit with equation 38. In the first seconds of the writing process, the diffraction efficiency due to reorientation of the azobenzene chromophores in the bulk is visible. Later on the influence of the SRG dominates.

Equation 38 can, in general, be used to calculate the modulation height of the SRG from the measured diffraction efficiency η . In the case of high SRGs, however, the DE of the SRG becomes larger than that of the volume grating by more than two orders of magnitude. Therefore, the latter is neglected at long writing times and equation 26 is used. For high SRGs, equation 26 and equation 38 obviously yield the same result.

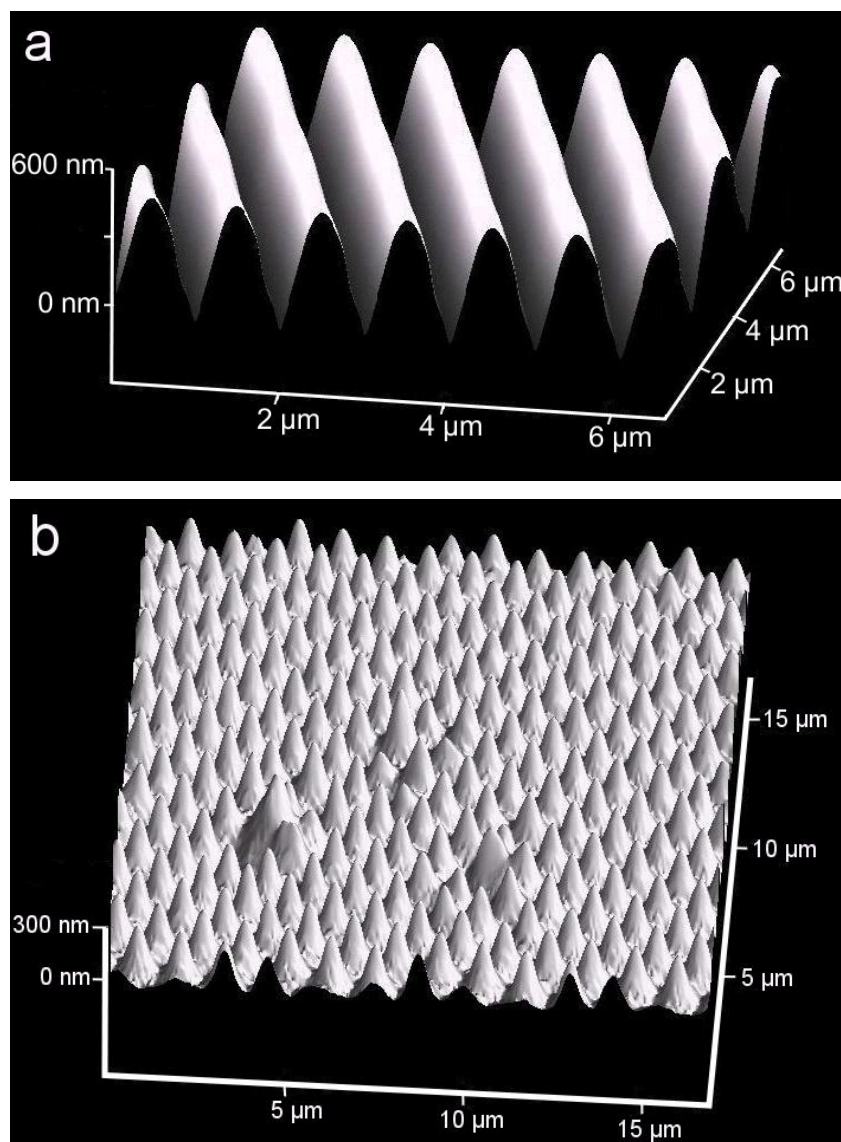


Figure 8.2. AFM image recorded in tapping mode of a) a sinusoidal SRG pattern inscribed in compound **6g** and b) an egg-crate in compound **6g** which was formed by two inscription processes between which the sample was rotated by 90°.

In order to verify the calculated modulation heights, the long-term-stable surface relief gratings were independently measured with atomic force

microscopy. Figure 8.2 shows the AFM image of an SRG on a thin film of the molecular glass **6g**. Its shape is nearly sinusoidal with a modulation depth of 610 nm and a spacing of 1 μm ^[188,189]. This amplitude is significantly higher than the values reported in the literature for any photochromic molecular glass to date ^[26,190].

8.2 Influence of the polarization of the writing beams

Holographic measurements were performed in compounds **6a**, **6c**, **6d**, **6e**, and **6g** with different polarization configurations of the writing beams. The differences of the resulting SRG heights can be explained by the different

strengths of the gradient force f_x . The term $E_x \left(\frac{\partial}{\partial x} E_x \right)$, which is proportional to f_x , is calculated for each polarization configuration. This term can be written as the product of a periodic function of x , which is the same in all seven settings, and an amplitude $|A|$ which depends on the polarization configuration. The normalized values of $|A|$ are summarized in table 8.1. In the *ss* and *sp* configuration, either E_x or its derivative is zero, so f_x is zero and no significant SRG is observed. The settings $\pm 45^\circ$, $++45^\circ$, *rlcp*, and *rrcp* have all the same normalized value $|A| = 0.5$ and, hence, they generate comparable maximum heights of the SRG, as listed in table 8.1 and graphically displayed in figure 8.3.

Table 8.1. Parameters of SRG formation for different polarization configurations of the writing beams.

polarization configuration	<i>ss</i>	<i>pp</i> ^{a)}	$++45^\circ$	<i>rrcp</i>	$\pm 45^\circ$	<i>rlcp</i>	<i>sp</i>
$ A \propto f_x$	0	1	0.5	0.5	0.5	0.5	0
normalized average maximum height of SRG ^{b)}	0.05	1	0.83	0.92	0.77	0.77	0.12
normalized average height of the SRG after 60 s ^{b)}	0.09	1	0.38	0.41	0.96	0.93	0.07
maximum growth rate of 6g [nm/s]	0.9	17.7	10.6	9.5	21.2	20.7	1.3
time to reach maximum growth rate of 6g [s]	67	29	49	49	16	16	70

^{a)} For all normalized quantities, the value of *pp* has been arbitrarily set to 1.

^{b)} Heights are given as an average of all materials for the corresponding polarization configuration.

The biggest value $|A| = 1$ is obtained with two *p*-polarized laser beams. Consequently, this configuration yields the highest SRGs of all polarizations.

One can assume that the maximum SRG height is reached when f_x is balanced by the surface energy. If the surface energy varies with the height in a nonlinear fashion, the height obtained with *pp* is not twice as large as the height of, e.g., *rlcp*. The generation of high SRGs obtained with the polarization settings $++45^\circ$ and *rrcp* has not been reported before, perhaps due to the required long writing times which necessitate a very good stability of the holographic set-up. The data presented above demonstrate that the influence of the polarization configuration on the formation of SRGs can be explained with the gradient force model.

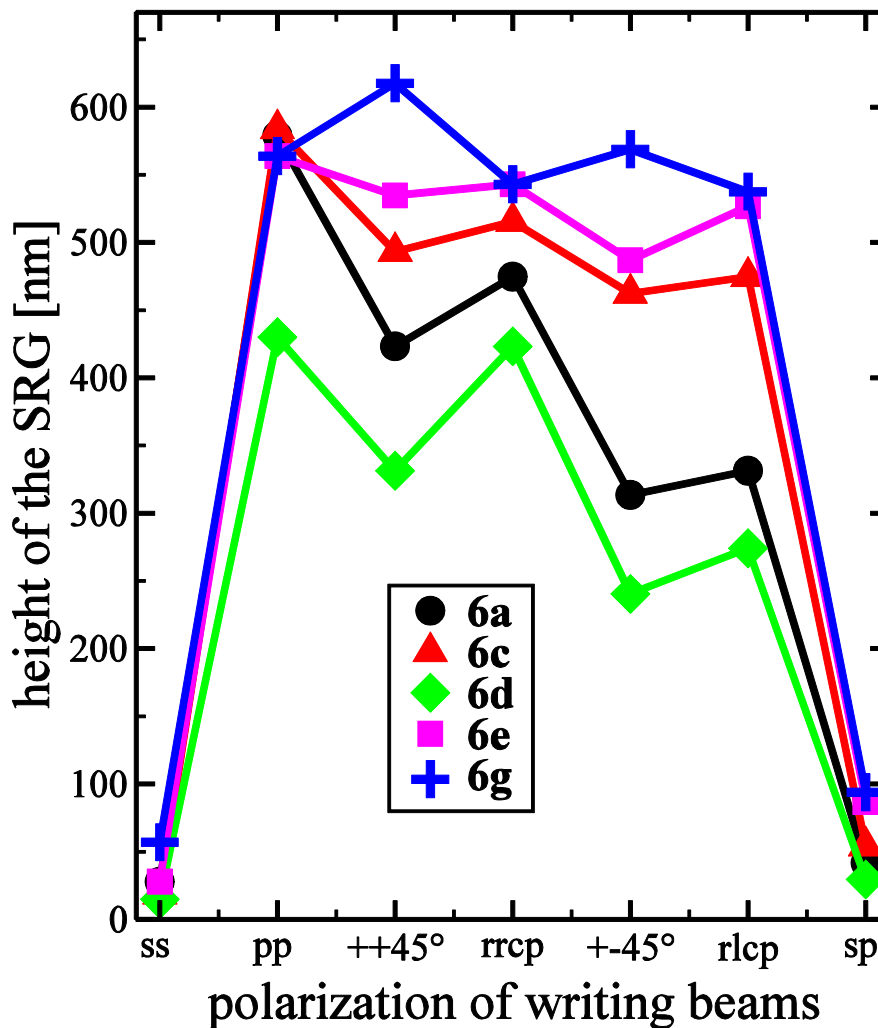


Figure 8.3. Maximum height of the SRGs of all five materials as calculated from the DE (equation 26) for the different polarization settings. The lines are a guide to the eye.

According to Kumar, an important factor for the build-up of the SRGs is the plastification of the material caused by repeated *trans-cis-trans* isomerization cycles ^[141]. A softening of the material accelerates the macroscopic material

transport below T_g . In the case of polarization gratings, such a plastification can take place throughout the material, because the light intensity in the sample is homogeneous. Intensity holograms, on the contrary, show no plastification in the dark regions and, therefore, their SRGs build-up more slowly. This effect can also be seen in table 8.1 where the amplitudes of the SRGs after 60 seconds of illumination are listed. If polarization configurations which lead to the same value of f_x are compared, the settings $\pm 45^\circ$ and *rlcp* (polarization gratings) result in much higher SRGs after 60 seconds than the settings $++45^\circ$ and *rrecp* (intensity gratings). The intensity grating *pp* creates an SRG height comparable to that of the polarization gratings after 60 seconds of irradiation, but it has twice the value of f_x , which is in agreement with the slower SRG build-up by intensity gratings. Also the maximum SRG growth rate of each material, i.e., the maximum slope of the holographic growth curve, which is proportional to the sensitivity, is much higher for the polarization gratings as compared to the intensity gratings. Additionally, the final SRG amplitude is reached after a shorter period of time for polarization gratings. On the other hand, intensity holograms on the average generate a slightly higher maximum amplitude of the SRGs. A possible reason might be that the light intensity in the illuminated areas is higher so that nonlinear effects (e.g., a nonlinear dependence of the plastification on the light intensity) give rise to higher values of f_x and, hence, to larger surface modulations.

8.3 Influence of the substituents

Tailoring the azobenzene moieties with different substituents and introducing them into molecular glasses opened a way to study the effects of substituents on the formation of SRGs, since molecular glasses are perfect model systems for comparative investigations. Although these investigations can give new insights into the formation of SRGs, few reports have been published on this topic. The formation of ester linkages between the triphenylamine core and the side groups leads to a decoupling of core and chromophore and allows an easy access to a large variety of compounds in order to tailor the required material properties. For a systematic study of structure-property relations regarding the formation of SRGs in azobenzene-containing molecular glasses, compounds **6a**, **6c**, **6d**, **6e**, and **6g** were investigated.

The focus of the comparison of the five molecular glasses is on three important parameters: the absorption coefficient at the writing wavelength, the electrical susceptibility and the volume of the chromophore. The optical densities per μm thickness at 488 nm, which are proportional to the absorption constants, can be measured by UV-Vis absorption spectroscopy and are listed in table 8.2. Larger absorption leads, due to the increased rate of

trans-cis-trans isomerization cycles, to a stronger plastification of the material and, therefore, to an increased height of the SRGs.

The wavelength of 488 nm of the writing laser is in the long-wavelength wing of the $n\pi^*$ -absorption band. Since k and n_0 are related via the Kramers-Kronig relations, an increase of the optical density, either by a shift of the absorption maximum to longer wavelengths or by an increase of the height of the absorption band, leads to an increase of the refractive-index. Both constants can be measured by ellipsometry. Since n_0 is larger than k by two orders of magnitude and usually decreases more slowly with increasing distance from the absorption maximum, the refractive index yields the main contribution to the real part of the susceptibility. The relative susceptibilities of the five materials, which determine the driving force f_x for material transport, are listed in table 8.2. They are correlated with the maximum SRG heights.

The volume or “bulkiess” of the chromophores basically has the opposite effect. With increasing size, the isomerization rate is expected to slow down, since the molecule requires a larger free volume in its environment. Also the macroscopic material transport is decelerated, because larger molecules are transported more slowly than smaller chromophores.

Compound **6a** exhibits the lowest absorption constant and susceptibility and also the lowest resulting modulation height. With increasing values of these parameters the SRGs become higher. The SRGs on compound **6d** show a slow growth rate and, in addition, they reach only a small modulation height. Steric-hindrance effects caused by the lateral methyl group are a possible explanation.

Table 8.2. Parameters of SRG formation of five molecular glasses.

molecular glass	6a	6c	6d	6e	6g ^{a)}
normalized $OD/\mu\text{m}$ at 488 nm	0.71	0.82	0.85	1.04	1
normalized χ' at 488 nm	0.69	0.79	0.76	1.03	1
normalized average maximum height of SRG ^{b)}	0.73	0.84	0.58	0.89	1
normalized average height of SRG after 60 s ^{b)}	0.48	0.48	0.21	0.66	1
average writing time to maximum [s] ^{b)}	201	272	356	121	87
(normalized average writing time) ⁻¹ [1/s] ^{b)}	0.43	0.32	0.18	0.72	1
maximum growth rate with pp [nm/s]	7.9	7.2	4.2	11	17
time to reach maximum growth rate with pp [s]	40	47	64	40	27

^{a)} For all normalized quantities, the value of **6g** has been arbitrarily set to 1.

^{b)} Heights and writing times for each material are an average of the polarization configurations.

The influence of the substituents follows this trend already in the early stages of SRG formation. When comparing materials **6a**, **6c**, and **6d**, the latter has the lowest SRG height after a writing time of 60 seconds because of the methyl group, whereas **6a** and **6c** show the same height. **6a** has a lower absorption coefficient than **6c** but also a smaller volume, so the two effects compensate each other. **6g** features very fast SRG formation. The inverse writing times up to the maximum SRG height show the same variation with absorption constant and susceptibility as the SRG height after 60 s. Also the growth rate for *pp* polarization behaves in a very similar way. Regarding the SRG formation rate, **6g** is the material with the fastest build-up, followed by **6e**, **6a** (smallest volume), **6c**, and **6d** (methyl group). This detailed comparison of the influence of different substituents of low-molecular-weight glass formers based on azobenzene chromophores shows that the influence of the material on the formation of SRGs can also be explained by the gradient force.

The glass transition temperatures of all materials are well above room temperature; the lowest one is at 89 °C and the highest at 122 °C. Therefore, no clear correlation between T_g and the maximum SRG height can be found when the gratings are inscribed at room temperature. On the other hand, they do play a role when the experiments are performed at elevated temperatures, as will be demonstrated in the following.

8.4 Influence of the temperature

SRGs inscribed in films of molecular glasses are expected to be stable at room temperature, if their glass transition temperatures are several ten degrees higher. Few experiments have been performed to investigate the stability of SRGs at elevated temperatures. One exception is the study by Kim et al. in which the diffraction efficiency of SRGs on a molecular glass was monitored during the application of a constant heating rate. The authors found that the DE drastically drops when T_g is reached^[54].

In this section, the temperature-dependent growth and decay behavior of SRGs on molecular glasses is presented. Especially the stability of the SRGs is of interest for applications in the field of replica molding, since the prepolymer for the replica must be cured at elevated temperatures. In contrast to the dynamical method of Kim et al., the formation and decay of SRGs at constant temperature is investigated.

First, the reversibility of SRG formation was tested. A grating was inscribed up to its maximum height at room temperature and then the sample was heated above the glass transition temperature and kept at this temperature until the SRG had decayed to zero. After cooling to room temperature, a new grating was inscribed at the same spot. This procedure was repeated several

times. No significant changes with respect to the writing time or maximum SRG height between the different cycles were found. Therefore, it can be assumed that the molecular glasses do not undergo recrystallization, ablation, or decomposition processes. These results are in agreement with those of Kim et al.

In figure 8.4 the growth of the SRG height is shown for compound **6c** in the temperature range between 22 °C and 110 °C. Writing was performed with two *p*-polarized beams. The heights were again calculated from the measured DE according to equation 26. Some general features can be seen. The SRG with highest modulation was inscribed at the lowest temperature. As expected, the maximum SRG amplitude drops strongly in the vicinity of T_g , but even above T_g , an SRG can still be detected. The initial slope of the height as a function of time is almost constant in the temperature range from 60 °C to 100 °C, so the SRG growth rate is not significantly enhanced by the increased molecular mobility. Below 60 °C, however, the initial growth rate is continuously increasing with temperature.

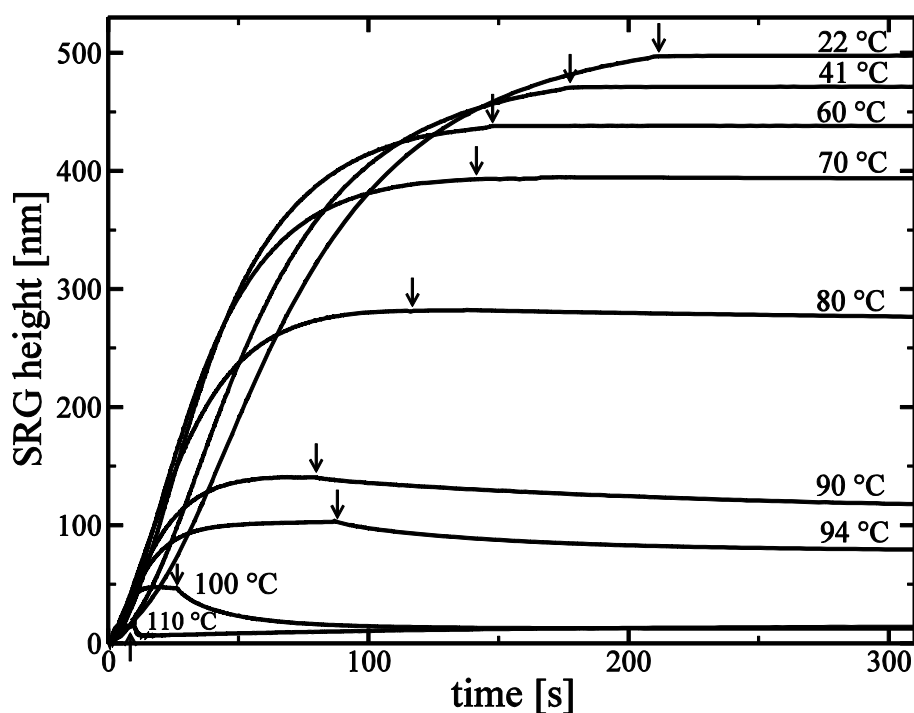


Figure 8.4. SRG build-up and initial decay at different temperatures for thin films of **6c**. The arrows indicate the times when the writing laser was turned off.

The temperature dependence of the maximum achievable SRG height is plotted in figure 8.5. The crossover from constant amplitudes at low temperatures to the strong decrease indicates the beginning softening of the material. The crossover temperature at 65 °C is significantly lower (by 34

degrees) than the glass transition temperature of 99 °C as measured by DSC. One of the reasons for this difference is the light-induced increase of the local temperature by the writing laser which is discussed later.

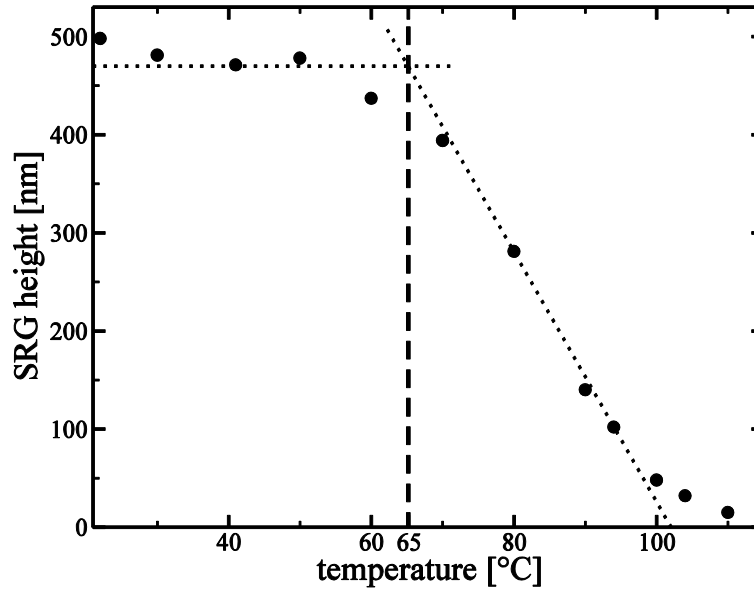


Figure 8.5. Temperature-dependent variation of the maximum SRG heights for **6c** (circles). The dotted lines represent the behavior at low temperatures and in the region of the strong decrease. Their intersection (dashed line) indicates the onset of softening of the material.

For the temporal decay of the holograms, neither a bi-exponential nor a stretched exponential function yields a satisfactory fit to the experimental data. Hence, the heat deposited by the writing laser must have an additional influence. Light absorption by the chromophores can cause the local temperature of the illuminated spot to increase so that a temperature gradient with its environment is produced. After turning the laser off, the temperature starts to equilibrate. The light-induced heating has its biggest effects at temperatures near T_g , and the time to reach thermal equilibrium increases at lower temperatures. Below 70 °C the SRGs are stable, which indicates that the local increase of temperature is no longer sufficient to cause a softening of the glass.

The light-induced heating effect is taken into account by the following decay function, which yields very good fits to the data:

$$d(t) = d_{\max} \cdot \exp\left(\frac{-t}{t_2 - t_1 \cdot \exp(-t/t_3)}\right) \quad (41)$$

with:

- d_{\max} maximum grating height
- (t_2-t_1) decay time at the initial (locally increased) temperature
- t_2 decay time at equilibrium temperature
- t_3 thermal relaxation time

By comparing the time constants (t_2-t_1) and t_2 at the external equilibrium temperatures, one can estimate the light-induced increase of the local temperature to be approximately 15 °C.

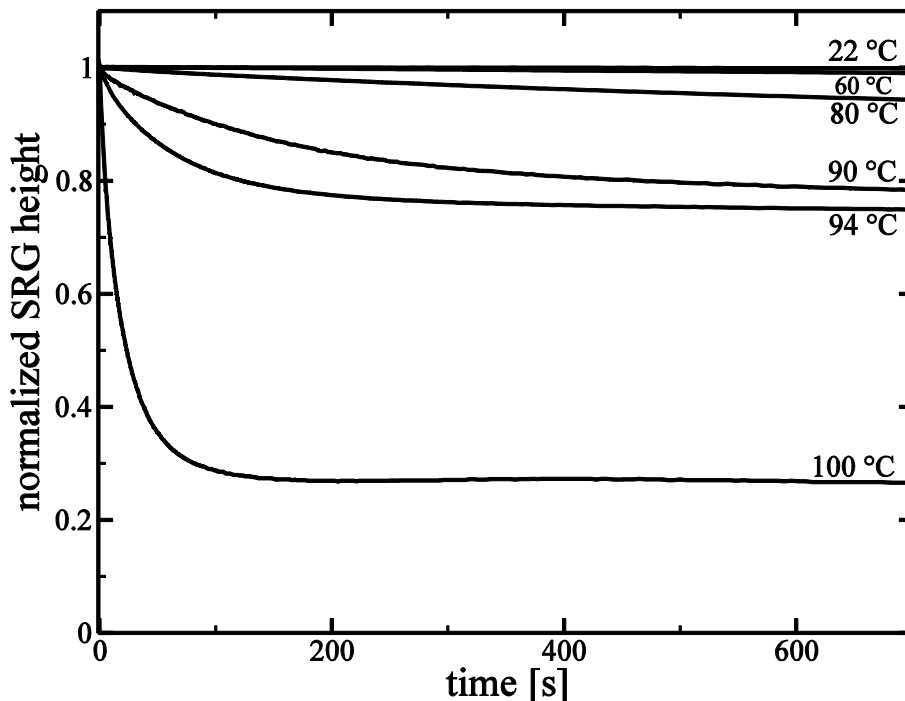


Figure 8.6. Temporal decay of the SRG height after the end of the writing process at different temperatures for thin films of **6c**.

The decay of the SRGs after the end of writing can be used to determine the T_g of the material. In figure 8.6, the temporal decay of the relative height after 1000 s has been plotted and in figure 8.7 the residual height at the end of this period as a function of temperature. Since thermal equilibrium had not yet been reached after 1000 s in all cases, the temperatures were calculated from the temperature dependence of the time constants t_1 , t_2 , and t_3 as discussed above. The transition from solid-like behavior with constant SRG heights at low temperatures to rapid decay at high temperatures is well visible. The

intersection indicates a glass point of 92 °C, which is close to the T_g measured by DSC of 99 °C.

In contrast, the temperature at which the maximum achievable SRG height begins to drop, is lower by more than 25 °C, as shown in figure 8.5. This is attributed in part to the laser-induced local heating effects.

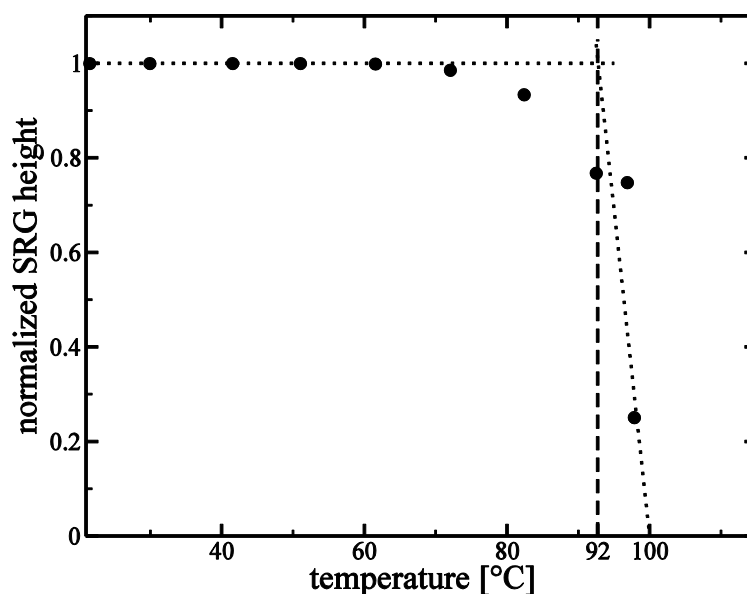


Figure 8.7. Temperature-dependent residual SRG height after 1000s for **6c** (circles). The dotted lines represent the constant height at low temperatures and the rapid decay at high temperatures, respectively. Their intersection (dash-dotted line) indicates the glass transition temperature.

A thermally induced post-development of SRGs did not take place in these purely amorphous molecular glasses. As was demonstrated above, the height of the SRGs always decays at elevated temperatures. Applying more complex temperature profiles did not change the situation. This proves that a liquid-crystalline phase is required for a thermal post-development^[82] similar to that presented in section 5.4.

8.5 Influence of the matrix

To determine the influence of the matrix surrounding the molecular glass on the formation of SRGs, a concentration series of compound **6l** was prepared. The samples varied by the amount and type of the added polymer (Ultem or PS) and the preparation method (doctor-blading and spin-coating), as listed in table 8.3. The thickness of the samples ranged from 100 to 380 nm. The maximum SRG height -as measured by AFM- was up to twice the film thickness, which is the maximum for a sinusoidal grating indicating a very

efficient build-up of the grating. With increasing concentration of the molecular glass, the SRG height increases and the writing time to the maximum decreases, as can be seen in the concentration series of **6l** in Ultem. This can be explained by an increase of the cooperative effects and the stronger plastification, when the azobenzene chromophores are higher concentrated. This effect was already reported several times ^[82,134,135,155,191]. In the spin-coated samples, the SRGs formed faster and with higher amplitude as compared to the doctor-bladed films with the same amount of Ultem. This observation can be explained by the surface quality of the film. In Dektak and AFM measurements it was found that the surface roughness was worse for the doctor-bladed films as compared to spin-coated films. Since the formation of SRGs requires a free and flat surface, a rough surface leads to low SRGs and long writing times.

When comparing the matrix polymers, a slower build-up of the SRG would be expected in Ultem as compared to PS, since the former has the higher glass transition temperature. The films with polystyrene had a worse surface than the films with Ultem, however. The arithmetic average roughness was up to 50 nm in films with PS, preventing even the exact determination of the SRG height. Due to the bad surface quality, the SRGs in polystyrene are lower than in Ultem. Therefore, the influence of the different inert materials could not be compared directly since it was obscured by the surface effects. To circumvent this problem, blends containing 50 w% of **6g** and 50 w% Ultem or PS were additionally investigated. Here, the quality of the surface was comparable in both cases. The writing times were longer as compared to pure **6g**. The writing time for this molecular glass in Ultem was twice as long as in polystyrene.

Table 8.3. Parameters of SRG formation in various samples of **6l**.

	concentration of 6l [w%]	sample preparation method	writing time [s]	height of the SRG [nm]
6l in PS	50	doctor-blading	7000	nm
6l in Ultem	40	doctor-blading	8600	190
6l in Ultem	60	doctor-blading	8000	220
6l in Ultem	80	doctor-blading	2200	240
6l in Ultem	90	doctor-blading	2600	250
6l in PS	50	spin-coating	760	nm
6l in Ultem	60	spin-coating	8800	390
6l in Ultem	90	spin-coating	790	390
6g in PS	50	spin-coating	3200	nm
6g in Ultem	50	spin-coating	6700	300

The possibility to inscribe SRGs in blends of azobenzene-containing molecular glasses and Ultem offers the possibility to produce high-temperature-stable SRGs due to the high T_g of Ultem. In a blend consisting of 50 w% **6g** and 50 w% Ultem, an SRG with a grating height of 300 nm was inscribed, as shown in figure 8.8a. Then the molecular glass was removed by washing the sample in toluene, which is a selective solvent for **6g**. The color of the sample changed from yellow-orange to transparent, indicating that most of **6g** was washed away. The remaining Ultem still showed the periodic structure of the initial SRG with the grating period of 1 μm and a height of 270 nm. Its shape became more irregular, however, as shown in figure 8.8b. The SRG in the remaining Ultem was then studied in holographic experiments. A diffraction efficiency resulting from the SRG was still present and it was stable at a temperature of 100 $^{\circ}\text{C}$, which is 10 $^{\circ}\text{C}$ above the glass transition temperature of **6g**. This proves that only the remaining Ultem determines the thermal properties and the stability of the SRG. The maximum temperature to which this sample could be heated was limited by the holographic set-up but the SRG should be stable up to the glass transition temperature of Ultem which is at 215 $^{\circ}\text{C}$.

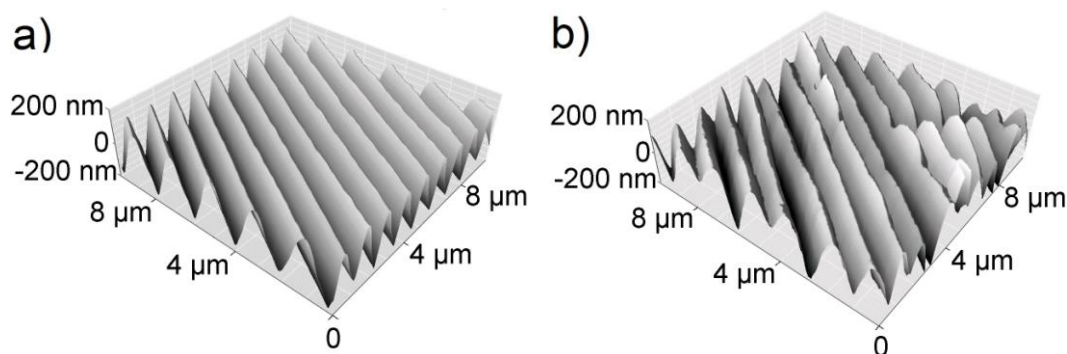


Figure 8.8. AFM pictures recorded in non-contact mode of a) a surface relief grating inscribed in a blend consisting of 50 w% **6g** and 50 w% Ultem, b) the same SRG when compound **6g** had been eroded away by washing the film with toluene and only Ultem was left.

The fact that SRGs can be formed in blends of the molecular glasses with Ultem leads to the conclusion that the low-molecular-weight compounds include the inert polymer in the macroscopic material transport resulting in SRGs. As figure 8.8 shows, the shape of the SRG formed by the remaining Ultem is similar to that of the initial blend. Another evidence that the molecular glass can induce macroscopic motions in the Ultem matrix is obtained from AFM measurements. If only the molecules of the molecular glasses had moved in a blend, the hardness of the peaks and valleys of the SRGs would be different since a separation of the compounds would have

taken place. But the hardness in the two areas as determined by AFM measurements is the same.

8.6 Replication of surface relief gratings

The holographic inscription of surface relief gratings is an all-optical single-step process without any need for post treatment. For most of the proposed applications, the SRGs have to be transferred to another polymer surface, however. This is usually performed by embossing. The possibility to emboss the SRGs on the surface of the azobenzene-containing material directly to other polymers depends on the required embossing temperature and is therefore limited by the glass transition temperature of the molecular glass. However, replica molding can be used to circumvent this problem. Compound **6e** was used for the master because of its high glass transition temperature. The SRGs on the glass film are stable at 60 °C during several hours -needed for the thermal curing process- so that an exact replica can be produced.

First, a grating was written on the surface of compound **6e**, and its height and period were confirmed by atomic force microscopy. The prepolymer used for the replica molding was a commercially available PDMS silicone elastomer, which is characterized by good thermal stability, optical transparency, and low interfacial free energy. The prepolymer was prepared by mixing the silicone elastomer base and the curing agent in a 10:1 w% ratio. Replica molding was accomplished by casting the liquid prepolymer onto the master samples with the inscribed SRG structures. Afterwards the prepolymer was cured at 60 °C for 4 h, cooled to room temperature, and the replicas were separated from the samples. Then the surface structure of the replica was measured with AFM. For polymer imprinting, the replica of the SRG and a polycarbonate sheet were placed on top of each other and inserted between two Kapton films of 125 μm thickness. These layers were sandwiched between two steel plates. The whole set-up was placed in a laboratory press, and the polymer was heated to 180 °C and pressed with a force of 5 kN for two minutes. Finally, also the imprinted polymer structure was characterized by AFM. All three gratings (master, replica, and imprint) show the same spacing of 0.95 μm. Their amplitudes decrease slightly from 580 nm (master) and 560 nm (replica) to 430 nm (imprint). Master and replica have sinusoidal cross sections, and also the polymer imprint shows only slight distortions as shown on the right-hand side of figure 8.9. With this technique it should be possible to transfer the holographically produced SRGs to large surface areas. This can open up the way to new applications, for example for changing the haptic properties of polymer surfaces.

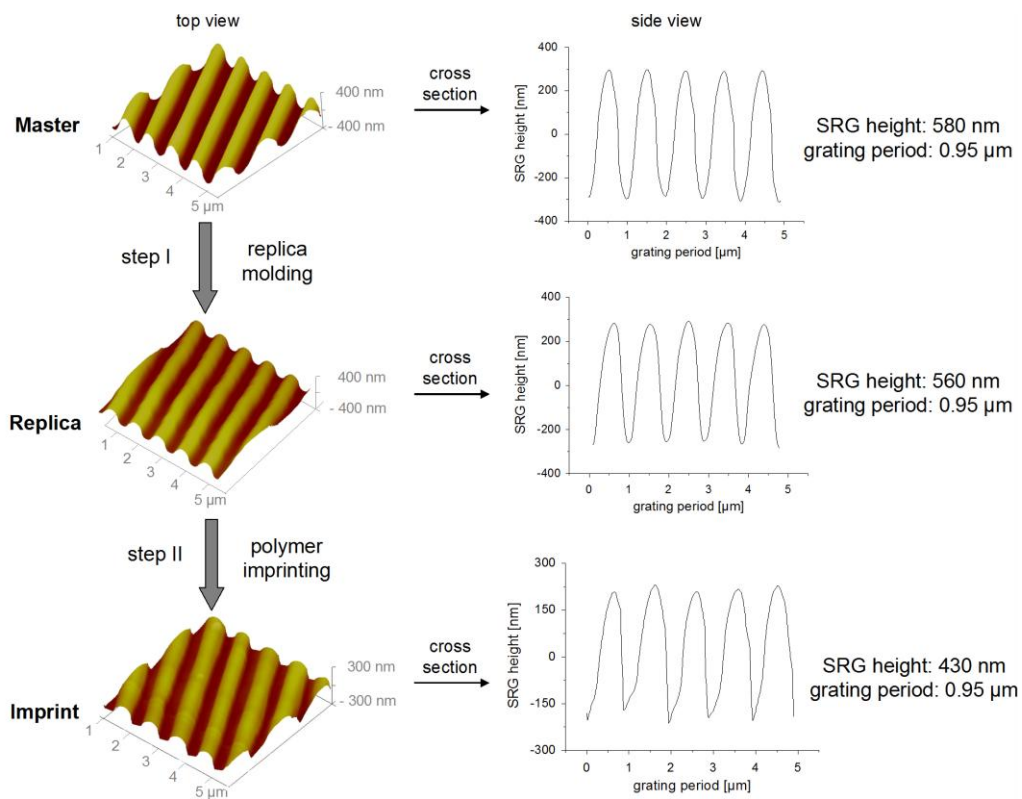


Figure 8.9. Example of replica molding of an SRG. The panels show AFM measurements of the original SRG structure (top), the replica (middle), and the polymer imprint (bottom). Left: 3D surface plots; right: cross sections.

9 Summary

In the present thesis, holographic volume and surface relief gratings in azobenzene-containing low-molecular-weight compounds are investigated to obtain a broader understanding of this new class of material.

Azobenzene chromophores undergo light-induced *trans-cis-trans* isomerization cycles leading to a reorientation of the long axis of the chromophores. If linearly polarized light is incident on the sample, these isomerizations result in a reorientation of this axis perpendicular to the light polarization. A holographic light grating, which can be formed by the interference of two coherent laser beams, leads to the inscription of a refractive-index modulation in the material.

The most common approach in the literature to obtain an azobenzene-containing material for holographic applications is to covalently bind the chromophores to a polymer. However, the azobenzene chromophores can also be covalently attached to a low-molecular-weight compound. In contrast to polymers, this class of materials features a well-defined molecular structure, monodispersity, and no undefined or undesired end groups. Therefore, they are ideal candidates for comparative investigations. The azobenzene-containing low-molecular-weight compounds studied in this thesis consist of different building blocks: the core unit, the azobenzene chromophores with substituents, and the spacer and the linkage group between chromophore and core unit. These components can be used in a modular-design principle to synthesize a large library of low-molecular-weight compounds. Some of the compounds are molecular glasses; they form a stable amorphous phase at room temperature.

Surprisingly, some of the investigated low-molecular-weight compounds form also a liquid-crystalline phase besides the amorphous phase as evidenced by polarized microscopy. The formation of this phase depends mainly on the length of the spacer and the substituent at the chromophore. If these liquid-crystalline compounds are prepared as solid films, however, they are quenched to an amorphous state. Upon reorientation of the azobenzene chromophores by illumination with a holographic light grating, a phase transition from the amorphous to an ordered state can be induced. This phase change in the latent liquid-crystalline low-molecular-weight compounds is very interesting for applications, since it yields the possibility to combine the advantages of amorphous (fast inscription of holographic gratings) and liquid-crystalline compounds (long-term stability of holographic gratings). The latent liquid-crystalline low-molecular-weight compounds show a post-

development of the refractive-index modulation after the writing process. This post-development effect is enhanced at elevated temperatures and can be used to increase the refractive-index modulation inscribed at room temperature. The inscription of holographic gratings at elevated temperatures leads to a shortening of the writing times by almost one order of magnitude as compared to room temperature due to the increased mobility of the chromophores. The holographic gratings are even stable at temperatures higher than the glass transition temperature, which further proves the light-induced formation of an ordered domain. Latent liquid-crystalline materials can also be obtained with bisazobenzene-functionalized low-molecular-weight compounds. The higher anisotropy of this chromophore leads to a more stable liquid-crystalline phase than for the azobenzene chromophore, even without spacer.

In contrast to their polymeric counterparts, molecular materials are expected to show a faster response to light because of the absence of polymer chain entanglements. Therefore, molecular glasses can be used as blending material for photo-addressable polymers to improve the photo-sensitivity of the blend as compared to the pure polymer. The influence of the core and the substituent was investigated in low-molecular-weight compounds which do not form liquid-crystalline phases. A cyclohexane core with three methoxy-substituted azobenzene chromophores was found to be the best combination of the structural components leading to the highest sensitivity. This optimized molecular glass has a sensitivity of more than 1800 cm/J, which is, by a factor of 5, higher than the sensitivity of diblock copolymers with comparable azobenzene concentration.

An azobenzene-containing diblock copolymer for holographic data storage consists of an inert majority block and a minority block containing the covalently bound photo-sensitive azobenzene chromophores. In a blend containing such a diblock copolymer and a few weight percent of the optimized molecular glass the latter is present in the both blocks and the holographic response of both blocks is independent of each other. For a deeper understanding, the molecular glass blended with polystyrene was measured as a model system for the molecular glass in the inert block of the diblock copolymer. It was found that with decreasing content of molecular glass, the time constant of the build-up of the refractive-index modulation increased by two orders of magnitude due to the loss of cooperative effects caused by the dilution. The molecular glass in an azobenzene-containing homopolymer served as model system for the molecular glass in the photo-sensitive block of the diblock copolymer. In a concentration series, the sensitivity grew with higher content of molecular glass.

The results were confirmed by measurements on blends containing the optimized molecular glass and a diblock copolymer. Also here, the sensitivity increased with increasing content of the molecular glass, mainly because the

writing time to the maximum of the refractive-index modulation decreased. The increase of the sensitivity is much larger than the observed rise of the refractive-index modulation due to the higher concentration of azobenzene chromophores. It was demonstrated that the shorter writing times are not caused by thermal effects, the molecules of the molecular glass in the inert block, or by changes of the free volume or the morphology, but that they are due to the azobenzene chromophores of the molecular glass in the minority block. They reorient faster than the chromophores attached to the polymer backbone and, thereby create free volume. Additionally, they can assist the reorientation of the azobenzene chromophores bound to the polymer by cooperative effects, i.e. dipolar and steric interactions. Both effects result in shorter writing time and higher sensitivity of the system. The temporal behavior of the refractive-index modulation of the blend containing a diblock copolymer and a molecular glass can be fitted with the help of the two model systems described above. From these fits, the content of the molecular glass in the minority block can be calculated. In an unannealed sample, around 45 % of all molecules of the molecular glass enter the photo-sensitive block of the polymer. This is more by a factor of 2.5 than one would expect from a statistical distribution. By annealing the blend, this amount can be increased to 70 %, since the molecular glass is not perfectly miscible with polystyrene. This is very advantageous, since only the molecules of the molecular glass in the minority block lead to an increase of the sensitivity. In a blend containing two weight percent of the molecular glass, the inscribed gratings are still long-term stable and the sensitivity increases by a factor of 1.7 as compared to the pure diblock copolymer. When the molecular glass is blended with a diblock copolymer with mesogenic units in the photo-active block, the sensitivity of the blend can even increase by a factor of 25 and the blend still has all the advantages of the pure polymer. To prove the applicability for holographic data storage, up to 80 plane-wave holograms or ten data pages each containing 432 bits were angle-multiplexed at the same spot of a thick sample of a blend.

Upon illumination of an azobenzene-containing material with a holographic light grating, besides the volume grating, also a surface relief grating can develop. This macroscopic material transport below the glass transition temperature is more efficient in molecular glasses than in polymers due to the lack of polymer chain entanglement. Surface modulations with heights of up to 600 nm were achieved in molecular glasses. The temporal evolution of the diffraction efficiency can be simulated by taking into account the contributions of the volume grating, the surface modulation, and the phase difference between both components. It was found that the build-up of the surface relief grating depends on the electrical susceptibility of the material at the optical frequency of the laser and the polarization of the laser beams. These experimental findings are in agreement with the gradient force model.

According to this theory, the macroscopic material transport results from the forces on the polarized material in the electrical field gradient caused by the holographic light grating. The formation of surface relief gratings can be maximized or almost completely suppressed, depending on the material and the polarization configuration. With experiments at elevated temperatures, the glass transition temperature of the compound as well as the heating of the sample caused by the beams of the writing laser can be determined.

For many applications it is important that the holographically produced surface relief gratings can be transferred to polymer surfaces. Replica molding can be used to easily copy the surface modulations to e.g. polycarbonate. Furthermore, surface relief gratings can also be inscribed in blends consisting of a molecular glass and an inert polymer. With an appropriate solvent the azobenzene-containing material can be washed away after the inscription. The shape of the surface modulation of the remaining polymer is similar to the initially inscribed surface relief grating in the blend. This proves that the motion of the glass molecules induces a corresponding motion of the polymer chains over macroscopic distances.

In summary, low-molecular-weight compounds are very versatile materials with many possible applications since they can:

- form surface relief gratings very efficiently,
- form volume gratings with high sensitivity,
- be used as blending material to increase the sensitivity of diblock copolymers,
- have latent liquid-crystalline properties and, therefore, undergo a phase change from amorphous to an ordered domain upon light irradiation.

10 Zusammenfassung

In der vorliegenden Arbeit wurden holographische Volumen- und Oberflächengitter in azobenzolhaltigen niedermolekularen Verbindungen untersucht, um ein vertieftes Verständnis dieser neuen Materialklasse zu erhalten.

Lichtinduzierte *trans-cis-trans*-Isomerisierungszyklen von Azobenzol-Chromophoren führen zu einer Reorientierung der langen Molekülachse. Bei Bestrahlung mit linear polarisiertem Licht führen die Isomerisierungen zu einer Orientierung dieser Achse senkrecht zur Polarisation des einfallenden Lichts. Ein holographisches Gitter, das durch die Interferenz von zwei kohärenten Laserstrahlen erzeugt wird, ergibt eine Brechungsindexmodulation im Material.

Beim gängigsten Ansatz ein azobenzolhaltiges Material für holographische Anwendungen zu erhalten, werden die Chromophore kovalent an ein Polymer gebunden. Die Azobenzol-Chromophore können jedoch ebenso kovalent an eine niedermolekulare Verbindung gebunden werden. Im Gegensatz zu Polymeren hat diese Materialklasse eine wohldefinierte molekulare Struktur, ein definiertes Molekulargewicht und keine unbestimmten oder unerwünschten Seitengruppen. Daher sind niedermolekulare Verbindungen ideale Kandidaten für vergleichende Untersuchungen. Die azobenzolhaltigen niedermolekularen Verbindungen, die Gegenstand dieser Arbeit sind, bestehen aus verschiedenen Bausteinen: Kerngruppe, Azobenzol-Chromophor mit Substituent und zwischen Kern und Chromophor ein Spacer und eine Verbindungsgruppe. Diese Komponenten können in einem Baukasten-Prinzip benutzt werden, um eine große Vielzahl niedermolekularer Verbindungen zu synthetisieren. Einige dieser Verbindungen sind molekulare Gläser; sie bilden eine stabile amorphe Phase bei Raumtemperatur.

Einige der untersuchten niedermolekularen Verbindungen können neben der amorphen auch eine flüssigkristalline Phase ausbilden. Die Entstehung dieser Phase hängt überwiegend von der Länge des Spacers und dem Substituenten ab. Wenn aus diesen flüssigkristallinen Verbindungen jedoch ein Film hergestellt wird, führt dies auf Grund der schnellen Verfestigung zu einem amorphen Zustand. Durch die Reorientierung der Azobenzol-Chromophore in einem holographischen Lichtgitter kann ein Phasenübergang von amorph zu einer geordneten Phase induziert werden. Dieser Phasenübergang in den latent flüssigkristallinen niedermolekularen Verbindungen ist sehr interessant für Anwendungen, da es dadurch möglich ist, die Vorteile von amorphen (schnelles Einschreiben der holographischen Gitter) und flüssigkristallinen

Verbindungen (Langzeitstabilität der holographischen Gitter) zu kombinieren. Die latent flüssigkristallinen Verbindungen zeigen eine Nachentwicklung der Brechungsindexmodulation nach Beendigung des Schreibvorgangs. Dieser Effekt der Nachentwicklung ist bei höheren Temperaturen stärker ausgeprägt und kann verwendet werden, um eine bei Raumtemperatur erzeugte Brechungsindexmodulation zu vergrößern. Das Einschreiben von holographischen Gittern bei erhöhten Temperaturen führt wegen der größeren Mobilität der Chromophore zu einer Verkürzung der Schreibzeit um eine Größenordnung. Die eingeschriebenen holographischen Gitter sind noch bei Temperaturen oberhalb der Glasübergangstemperatur stabil. Dies ist ein weiterer Beweis für die lichtinduzierte Entstehung einer geordneten Phase. Latent flüssigkristalline Verbindungen können auch mit Bisazobenzol-Chromophoren synthetisiert werden. Die höhere Anisotropie dieser Chromophore führt auch ohne Spacer-Gruppe zu einer stabilen flüssigkristallinen Phase.

Im Vergleich zu azobenzolhaltigen Polymeren mit ihren Kettenverschlaufungen weisen niedermolekulare Verbindungen eine höhere Photosensitivität auf. Durch Zumischen von molekularen Gläsern zu photoadressierbaren Polymeren kann dadurch die Photosensitivität des Blends im Vergleich zum reinen Polymer erhöht werden. In amorphen niedermolekularen Verbindungen, die auf Grund des Fehlens der Spacer-Einheiten keine flüssigkristalline Phase ausbilden können, wurde der Einfluss des Kerns und des Substituenten auf die Photosensitivität untersucht. Ein Cyclohexanring mit drei Methoxy-substituierten Azobenzol-Chromophoren erwies sich als die beste Kombination der Bausteine. Die Sensitivität von 1800 cm/J dieses optimierten molekularen Glases ist um den Faktor fünf größer als in Diblockcopolymeren mit vergleichbarer Azobenzolkonzentration.

Ein azobenzolhaltiges Diblockcopolymer für die holographische Datenspeicherung besteht aus einem inerten Majoritätsblock und einem Minoritätsblock, an den die Azobenzol-Chromophore kovalent gebunden sind. In einem Blend, der solch ein Polymer und wenige Gewichtsprozent des optimierten molekularen Glases enthält, ist letzteres sowohl im Minoritäts- als auch im Majoritätsblock vorhanden. Die Ausbildung holographischer Gitter in diesen beiden Bereichen ist unabhängig voneinander. Für ein tieferes Verständnis wurde eine Mischung aus dem molekularen Glas und Polystyrol als Modellsystem für das molekulare Glas im inerten Block des Diblockcopolymeren untersucht. Mit abnehmender Konzentration des molekularen Glases stieg die Zeitkonstante des Aufbaus der Brechungsindexmodulation um zwei Größenordnungen an, da durch die Verdünnung die kooperativen Effekte der Chromophore verloren gehen. Analog dazu diente eine Mischung aus dem molekularen Glas und einem azobenzolhaltigen Homopolymer als Modellsystem für das molekulare Glas

im photosensitiven Block. In einer Konzentrationsserie erhöhte sich die Sensitivität bei steigender Konzentration des molekularen Glases.

In einem Blend, bestehend aus Diblockcopolymer und molekularem Glas, wurde die Sensitivität umso höher, je mehr molekulares Glas enthalten war. Dieser Anstieg der Sensitivität ist viel größer als die beobachtete Zunahme der Brechungsindexmodulation auf Grund der höheren Konzentration der Azobenzol-Chromophore. Die Erhöhung der Sensitivität ist auf eine erhebliche Verkürzung der Schreibzeiten zurückzuführen. Es konnte gezeigt werden, dass dies nicht durch thermische Effekte, das molekulare Glas im inerten Block, eine Änderung des freien Volumens oder eine Morphologieänderung des Blockcopolymer verursacht wird, sondern eindeutig durch das molekulare Glas im Minoritätsblock. Dessen Azobenzol-Chromophore reorientieren sich schneller und generieren dadurch zusätzliches freies Volumen. Daneben können sie die Umorientierung der an das Polymer gebundenen Chromophore durch kooperative Effekte -Dipol- und sterische Wechselwirkungen- unterstützen. Die zeitliche Entwicklung der Brechungsindexmodulation des Blends kann mit Hilfe der beiden oben genannten Modellsysteme beschrieben werden. Aus den Fits lässt sich die Konzentration des molekularen Glases im Minoritätsblock berechnen. In einer ungetemperten Probe sind circa 45 % der Moleküle des molekularen Glases im photoaktiven Block des Polymers enthalten. Diese Konzentration ist 2,5-mal größer als man es bei einer statistischen Verteilung erwarten würde. Durch Tempern des Blends lässt sich diese Konzentration auf 70 % steigern, da das molekulare Glas in Polystyrol nicht perfekt mischbar ist. Dieses Verhalten ist sehr vorteilhaft, da nur die Moleküle des molekularen Glases im Minoritätsblock zu einer Erhöhung der Sensitivität führen. In einem Blend mit zwei Gewichtsprozent des molekularen Glases sind die eingeschriebenen Gitter langzeitstabil und die Sensitivität ist um einen Faktor 1,7 größer als im reinen Diblockcopolymer. Wenn man das molekulare Glas mit einem Diblockcopolymer mischt, das außer den Azobenzol-Chromophoren auch mesogene Seitengruppen im photoaktiven Block enthält, steigt die Sensitivität um einen Faktor 25 an und alle Vorteile des reinen Diblockcopolymer bleiben erhalten.

Bis zu 80 langzeitstabile Hologramme konnten an derselben Stelle in eine dicke Probe eines Blends per Winkelmultiplexing eingeschrieben und wieder ausgelesen werden. Außerdem konnten 10 Datenseiten mit je 432 Bits in Experimenten zur holographischen Datenspeicherung abgespeichert und rekonstruiert werden.

Wenn ein azobenzolhaltiges Material mit einem holographischen Lichtgitter bestrahlt wird, so kann, abhängig von den experimentellen Bedingungen, außer einem Volumengitter auch ein Oberflächengitter entstehen. Der zugehörige makroskopische Materialtransport unterhalb der Glasübergangs-

temperatur ist in molekularen Gläsern effizienter als in Polymeren, da keine Kettenverschlaufungen vorliegen. Oberflächenreliefgitter mit einer Höhe von bis zu 600 nm konnten in molekularen Gläsern erzeugt werden. Die zeitliche Entwicklung der Beugungseffizienz kann simuliert werden, wenn man die Beiträge des Volumengitters und des Oberflächengitters sowie eine Phasendifferenz zwischen beiden berücksichtigt. Der Aufbau des Oberflächengitters hängt von der elektrischen Suszeptibilität des Materials bei der optischen Frequenz des Schreiblasers und der Polarisation der Laserstrahlen ab. Diese Befunde stehen im Einklang mit dem Gradienten-Kraft-Modell. Diese Theorie erklärt den Materialtransport als Ergebnis der Kräfte, die das elektrische Feld des holographischen Lichtgitters auf das polarisierte Material ausübt. Die Entstehung von Oberflächengittern kann durch die Auswahl des Materials und die Polarisationskonfiguration der Schreibstrahlen optimiert oder auch nahezu vollständig unterdrückt werden. Durch Experimente bei erhöhten Temperaturen kann sowohl die Glasübergangstemperatur der Verbindung als auch die Temperaturerhöhung der Probe durch die Laserstrahlen bestimmt werden.

Für viele Anwendungen ist es wichtig, dass die holographisch hergestellten Oberflächengitter auf Polymeroberflächen übertragen werden können. Es wurde gezeigt, dass sich die Oberflächenmodulationen mittels „Replica-Molding“ auf eine Polykarbonat-Oberfläche transferieren lassen. Oberflächengitter können auch in einem Blend, bestehend aus molekularem Glas und einem inerten Polymer, eingeschrieben werden. Nach dem Einschreiben ist es möglich, das molekulare Glas mit einem selektiven Lösungsmittel auszuwaschen. Die Form der Oberfläche des verbleibenden Polymers ist ähnlich der ursprünglichen Oberflächenmodulation im Blend. Dies beweist dass die optisch inerten Polymer-Ketten der Bewegung der Moleküle des molekularen Glases über makroskopische Distanzen folgen.

Zusammenfassend kann man sagen, dass niedermolekulare Verbindungen sehr vielseitige Materialien mit vielen möglichen Anwendungen sind, da sie:

- sehr effektiv Oberflächengitter aufbauen können
- Volumengitter mit hoher Photosensitivität bilden können
- als Blend-Material benutzt werden können, um die Photosensitivität von Diblockcopolymeren zu erhöhen
- einen lichtinduzierten Phasenübergang von amorph zu einer geordneten Phase durchlaufen können.

11 Appendix A: Liquid-crystalline polymers

Most azobenzene-containing systems studied in the past show either high sensitivity but unstable refractive-index modulation like molecular glass **7g**, or low sensitivity but long-term-stable refractive-index modulation like polymer **19**. Due to this trade-off between writing speed and stability it is not possible to optimize both properties separately. This situation is related with the different phases of the materials. The amorphous systems are fast, but the orientation of the azobenzene moiety is only stable in liquid-crystalline systems which are inherently slow. Combining the favorable properties of both groups of materials would be of great advantage. This approach is possible with molecular glasses performing a phase change, as was already shown in chapter 5; but also polymers with this property can be synthesized, as will be discussed in this section.

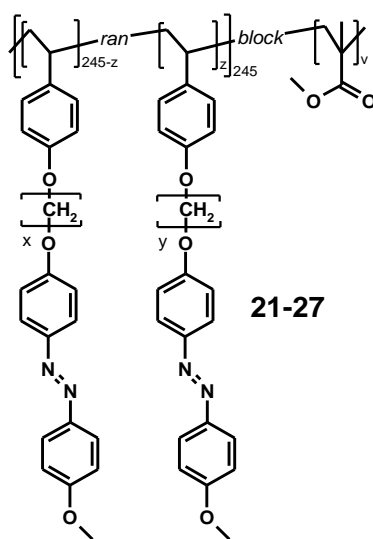


Figure 11.1. Chemical structure of the polymers **21-27**.

A systematic study was conducted on homopolymer **21** and the corresponding diblock copolymers **22-27** which are shown in figure 11.1. Their characteristic data are listed in table 11.1. The inert majority block of the diblock copolymers consists of poly(methyl methacrylate) (PMMA). The homopolymer **21** has a spacer length of 8 CH_2 units and the diblock copolymers **22-24** have spacer lengths of 6, 8, and 10 units, respectively.

Additionally, a mixture of two randomly distributed spacer lengths in the photo-active block was synthesized. The combination of spacer lengths 6/8, 4/8, and 4/8 are used in polymers **25-27**. The overall number of side chains of each spacer length is the same. Due to the relatively large size of the photo-active block, all diblock copolymers form a lamellar morphology.

Table 11.1. Characteristic data of the polymers **21-27**.

	<i>v</i>	<i>x</i>	<i>y</i>	<i>z</i>	M_n^a [kg/mol]	M_w^a [kg/mol]	<i>PDI</i>	T_{LC-ISO}^b [°C]	T_{ISO-LC}^b [°C]	Azo block [w%] ^c
21	0	8	--	0	120	126	1.05	156	142	100
22	880	6	--	0	249	261	1.05	152	141	53
23	880	8	--	0	266	282	1.06	142	128	54
24	880	10	--	0	293	306	1.04	142	133	54
25	880	6	8	123	305	317	1.04	147	131	50
26	880	4	8	123	300	322	1.07	142	130	51
27	880	4	6	123	291	394	1.04	155	141	51

^{a)} measured by GPC

^{b)} measured by DSC at 10 °C/min

^{c)} measured by ¹H-NMR.

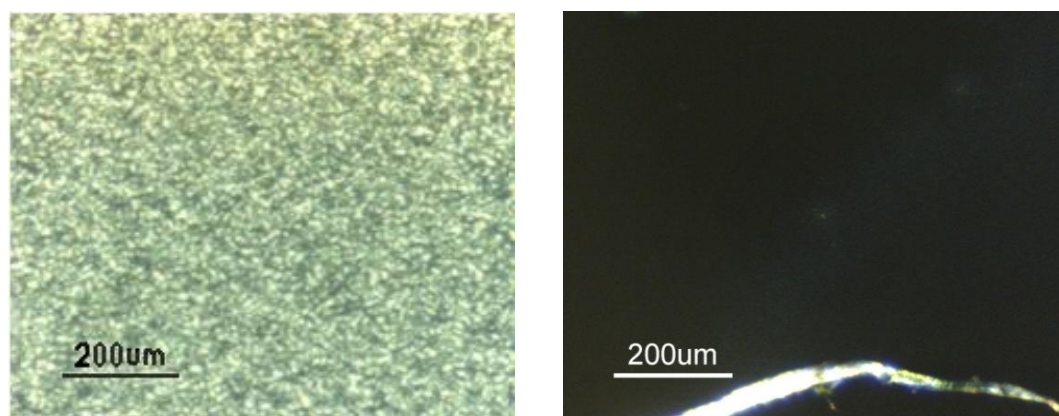


Figure 11.2. Polmic pictures of homopolymer **21** a) heated to 170 °C for 1 h and annealed at 120°C for 2 h, b) quenched by heating to 170°C and subsequent rapid cooling below room temperature.

The glass transition temperature of the majority block of the diblock copolymers is around 100 °C as determined by DSC. All polymers exhibit a smectic liquid-crystalline phase, as listed in table 11.1 and shown in figure 11.2a. The existence of this phase was evidenced by X-ray diffraction, DSC, and polmic. But the formation of the smectic phase can also be suppressed

and the samples can be quenched to an amorphous state, as shown in figure 11.2b. This is achieved by heating the sample above the clearing temperature and subsequent rapid cooling below T_g , e.g. by placing the hot film on a copper block which is cooled by liquid nitrogen.

The maximum of the $\pi\pi^*$ -transition was located between 341 and 346 nm for all annealed diblock copolymers as listed in table 11.2. Quenching results in a small red shift. As discussed in sections 7.1 and 7.2, this can be explained by the destruction of the molecular aggregates in the liquid-crystalline phase. In turn, this also indicates an amorphous phase in the quenched samples.

For the holographic experiments, the samples were spin-coated on glass slides and annealed. The measurements were performed with the standard holographic set up. Two *s*-polarized plane waves at 488 nm with an intensity of each 1 W/cm^2 are brought to interference in the plane of the sample. In contrast to all previous experiments, the results of the holographic experiments -especially the maximum of the refractive-index modulation and the writing times to the maximum of the refractive-index modulation- showed a big variance. The minimum and the maximum value of the two parameters differed by up to a factor of 5. In order to obtain more reliable results, the samples were measured several times (depending on the variance three to eleven times) and the average of the experiments was calculated. In the beginning, the results of holographic experiments with annealed samples are discussed.

The sizes of the smectic domains of each material are subject to a distribution. In homopolymer **21**, the size of these domains can reach the wavelength of the light causing strong light scattering. The director of the smectic domains becomes more stable with increasing domain size. The light-induced movement of the azobenzene chromophores is not sufficient to reorient the director of the largest domains. Additionally, the force between the neighboring azobenzene chromophores can cause an already reoriented azobenzene chromophore to orient back along the director. This leads to the rapidly decaying holographic gratings observed in the homopolymer. But at elevated temperatures, the director can reorient more easily due to the higher mobility. Then it is also possible to reorient the director of the large domains by the light-induced reorientation of the azobenzene chromophores. This mechanism explains the observed increase of the refractive-index modulation of the homopolymer at higher temperatures.

The average domain size in the diblock copolymers is much smaller due to its lamellar morphology. Here all domains are small enough so the director can be reoriented by the reorientation of the azobenzene. Therefore, the achievable refractive-index modulation in the diblock copolymer is not half that of the homopolymer -as one would expect solely from the azobenzene concentration- but, on the contrary, it is even larger. Additionally, the

inscribed refractive-index modulation in the diblock copolymers is stable after a slight decay in the first minutes. The holographic performance of liquid-crystalline diblock copolymers is, therefore, superior to that of the homopolymer.

Table 11.2. Optical and holographic properties of the polymers **21-27**. ann: annealed, quen: quenched.

	maximum of $\pi\pi^*$ - transition [nm]	maximum of $n\pi^*$ - transition [nm]	writing time to max. of n_1 [s]	$n_{1\max}$ [10^{-3}]	$n_1(4000\text{s})$ / $n_{1\max}$ [%]	$n_1(60\ 000\text{s})$ / $n_{1\max}$ [%]
21 ann	324	436	120±70	5.8±1.1	78	65
22 ann	344	405	3200±1800	6.7±1.5	96	98
23 ann	345	407	3900±900	7.4±1.3	92	90
24 ann	346	408	20000±7000	7.1±1.4	96	97
25 ann	346	404	1000±50	10.3±1.7	97	101
26 ann	345	403	370±30	6.8±0.3	96	99
27 ann	341	409	390±90	6.6±0.7	95	92
21 quen	346	nm	100±30	13.6±9.3	77	nm
22 quen	346	408	33±4	3.7±0.5	90	nm
23 quen	347	409	90±30	2.9±0.6	79	nm
24 quen	347	407	1400±500	6.6±1.3	94	96
25 quen	348	415	170±50	5.8±1.6	96	98

With increasing spacer length, the azobenzene chromophores can move independently of the back bone and the anisotropy of the side group increases. Therefore, the smectic phase is more stable and has a higher order parameter. This leads to longer writing times and an increase of the refractive-index modulations of the annealed diblock copolymers as listed in table 11.2.

Combining two different spacer lengths leads to a lower order parameter in the smectic domains, since the side chains do not match as perfectly as with the same spacer length. This leads to writing times which are one order of magnitude shorter than in the diblock polymers with only one spacer length, while the refractive-index modulation remains nearly constant. With the combination of different spacer lengths, the sensitivity to light can therefore be increased.

As was discussed above, the samples can also be quenched to an amorphous state. By holographic illumination with two polarized light beams, it should be possible to transform the initially amorphous samples to their smectic state,

similar as for the low-molecular-weight compounds discussed in chapter 5. Holographic gratings inscribed in the quenched material were long-term stable and showed post-development. This indicates the formation of a liquid-crystalline phase. Additionally, the sample was investigated by polmic. The illuminated spot was very bright between crossed polarizers, indicating not only a preferred orientation but also the formation of a smectic phase. On the contrary, the rest of the sample remained dark indicating an amorphous phase. Thus, a liquid-crystalline phase can be induced by the holographic light grating and stable holographic gratings can be inscribed. In the initially amorphous sample, the reorientation occurs faster leading to writing times more than one order of magnitude shorter as compared to the annealed samples, whereas the refractive-index modulation does not change so strongly. Therefore, the sensitivity to light increases in the quenched samples. This proves the potential of these phase-change materials to combine the advantages of both amorphous and liquid-crystalline samples.

Quenched samples of a diblock copolymer with a mixture of spacer lengths show the best holographic properties as discussed above. The holographic performance can be further increased at elevated temperatures. The temperature dependence of compound **25** was tested, as shown in figure 11.3 and figure 11.4. Even at 120 °C, which is 20 °C above the glass transition temperature of the PMMA matrix, the inscribed gratings were long-term stable. This again confirms the light-induced formation of a liquid-crystalline phase. Additionally, the refractive-index modulation showed a post-development effect which increased at elevated temperatures, as shown in figure 11.4b. At 120 °C, the refractive-index modulation 4000 s after the end of the writing process had increased to 180 % as compared to its value directly after the writing process. The maximum refractive-index modulation $n_{1\max}$ decreased by a factor of three when heating from 22 °C to 120 °C. In this temperature range, the writing time decreased by three orders of magnitude. Since the material sensitivity cannot be clearly determined for these materials, the rate defined as the maximum refractive-index modulation divided by the writing time was used as a measure for the sensitivity. Between 22 °C to 120 °C, the rate increased by two orders of magnitude. The rate of the quenched diblock copolymer **25** at 120 °C is a factor of 1000 higher than the annealed diblock copolymer **25** at room temperature and higher than that of the annealed diblock copolymer **23** at room temperature by a factor of 5000. This indicates the enormous potential of these phase change materials.

In order to test, whether the sensitivity of these polymers can be further increased by molecular glass **7g**, a blend consisting of 10 w% of the glass and 90 w% of **25** was prepared. In the blends, the scatter of the writing times was larger than the expected decrease of the writing times by adding the molecular glass. The average data of all experiments indicate, however, that the blends indeed have an even higher sensitivity than the pure materials. The approach

discussed in chapter 7 therefore seems to be applicable to these liquid-crystalline polymers as well.

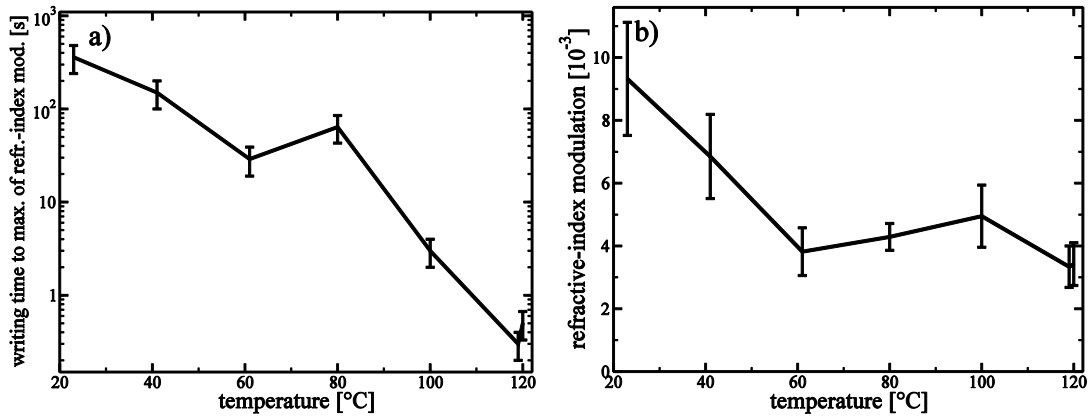


Figure 11.3. a) Writing times and b) maximum refractive-index modulation as a function of temperature for a quenched sample of **25**. Note the logarithmic scale of the ordinate axis in part (a).

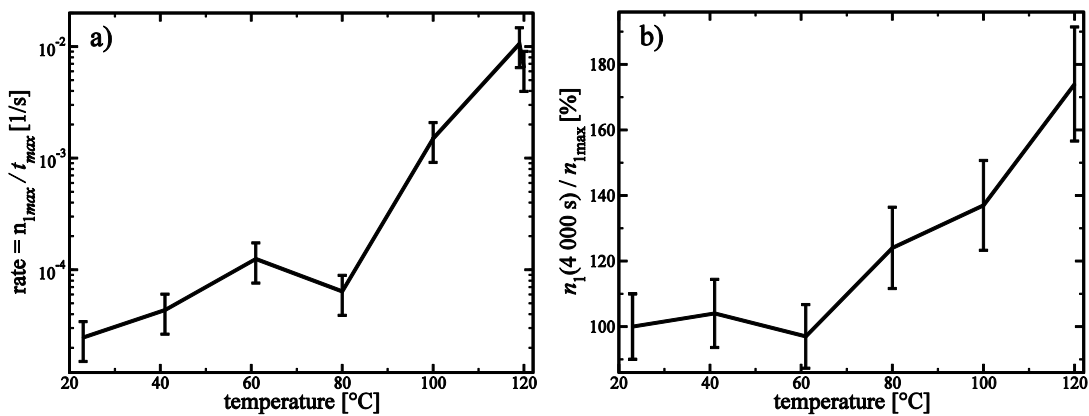


Figure 11.4. a) Rate of the inscription of the holographic gratings and b) normalized refractive-index modulation after 4000 s as a function of temperature for a quenched sample of **25**. Note the logarithmic scale of the ordinate axis in part (a).

12 Appendix B: Determination of the glass transition temperature of the minority segment of diblock copolymers

The glass transition temperature of the photo-active minority block has a strong influence on the holographic response; hence it is of big interest to know its exact value, but the determination can be difficult. Especially when its relative weight fraction is very small, established methods like DSC cannot be used for sensitivity reasons. The holographic response, however, depends only on the processes in the minority block. Therefore, holography is sensitive to the T_g of the minority block and can be used to determine it^[160]. For this purpose a block copolymer similar to **18** was investigated. **18'** consists also of an inert polystyrene majority block and a minority block containing the same azobenzene groups as **18**. This polymer has an average molecular weight of 56 000 g/mol, a polydispersity of 1.03, and the weight fraction of the minority block was 10.6 %. Homogeneous thin films were prepared by doctor-blading and annealing at 120 °C for 20 h under high vacuum. This ensures that residual solvent is removed and any kind of preferential orientation, for example by shearing, in the minority segment can be excluded. The film thickness is approx. 1 μm . Two *s*-polarized laser beams, each with a wavelength of 514 nm and an intensity of 1 W/cm², were used to generate the holographic intensity gratings. Recording was performed in the temperature range of 295 to 323 K. In order to verify the results, all holographic measurements were repeated several times and an accuracy of the determined parameters of $\pm 5\%$ was achieved.

In figure 12.1 the growth curves of the refractive-index modulation are shown. It can be clearly seen that with increasing temperature, the maximum achievable refractive-index modulation decreases, but this maximum is reached after shorter writing times. At 313 K, the maximum of the refractive-index modulation is less than one half of the value at 295 K. On the other hand, at temperatures below room temperature, the values do not significantly increase.

In figure 12.2, the temporal decay of the normalized refractive-index modulation at different temperatures is shown. In order to compare the decay curves, the refractive-index modulations are normalized to unity at time zero when the writing laser was turned off. As expected, the decay occurs on

different time scales resulting from different mechanisms. It is widely accepted that the decay comprises several independent processes^[42,160] so its normalized value can be described by the following function:

$$n_{1norm} = Ce^{-k_C t} + De^{-k_D t} + Ee^{-k_E t} \quad (42)$$

with:

C, D, E relative amplitudes of the fast, intermediate, and slow decay component

k_C, k_D, k_E corresponding rate constants

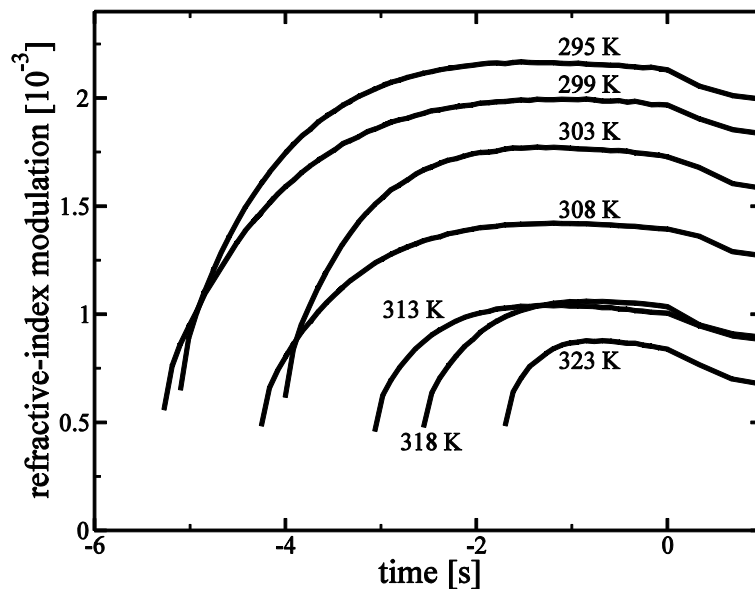


Figure 12.1. Growth of the refractive-index modulation in the temperature range of 295 to 323 K. The writing laser was turned off at time zero.

The fast decay component C is mainly attributed to the thermal *cis-trans* back isomerization, which is significantly accelerated at higher temperatures, as can be seen from the steeper slope in figure 12.2. The subsequent slower component D may be attributed to a partial loss of the in-plane orientation due to the free volume which is present at this temperature. The slowest component E results from the reorientation of whole segments of the polymer backbone.

Fitting of the experimental decay curves with equation 42 yields the rate constants of the different decay processes. The results are summarized in table 12.1. For rate constant k_E , reliable values can only be obtained at elevated temperatures. It is several orders of magnitude smaller than k_C and k_D and can therefore be neglected at lower temperatures.

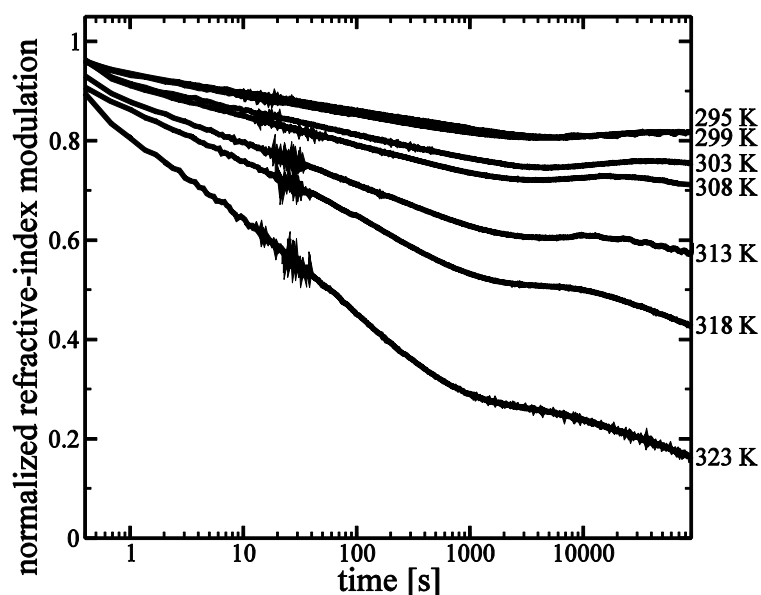


Figure 12.2. Long-term stability of the inscribed holographic gratings at different temperatures. Note the logarithmic time axis.

Table 12.1. Characteristic data obtained from the temperature-dependent measurements.

T [K]	E [%]	k_C [s^{-1}]	k_D [s^{-1}]	k_E [s^{-1}]
277	67	$3.8 \cdot 10^{-3}$	$3.1 \cdot 10^{-4}$	--
295	65	$1.8 \cdot 10^{-2}$	$1.3 \cdot 10^{-3}$	--
299	64	$1.4 \cdot 10^{-2}$	$1.9 \cdot 10^{-3}$	--
303	55	$4.8 \cdot 10^{-2}$	$2.0 \cdot 10^{-3}$	--
308	52	$4.2 \cdot 10^{-2}$	$1.9 \cdot 10^{-3}$	--
313	36	$9.1 \cdot 10^{-2}$	$2.8 \cdot 10^{-3}$	$1.0 \cdot 10^{-5}$
318	26	$9.1 \cdot 10^{-2}$	$3.8 \cdot 10^{-3}$	$3.1 \cdot 10^{-5}$
323	7	$2.0 \cdot 10^{-1}$	$8.2 \cdot 10^{-3}$	$1.5 \cdot 10^{-4}$

Assuming an Arrhenius-like behavior, the activation energies of the relaxation processes can be obtained from a plot of $\ln(k)$ vs. $1/T$, as shown in figure 12.3. The activation energies for the rate constants k_C , k_D , and k_E are calculated as 62, 48, and 229 kJ/mol, respectively. The activation energies of k_C and k_D are similar, but their absolute values differ by more than an order of magnitude. The latter is in good agreement with the results of Song et al. ^[192]. From the activation energy of k_E , the time after which the term E has dropped to a value of $1/e$ at room temperature can be estimated to be approximately 260 - 300

days. This is in good agreement with the time scale of the stability of holographic gratings which had been previously determined for block copolymers with methoxy-azobenzene side groups ^[51].

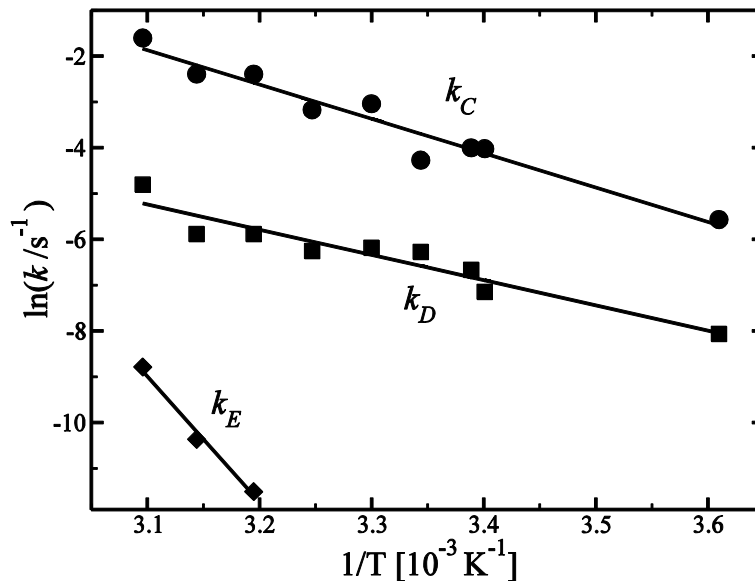


Figure 12.3. Logarithm of the three rate constants k_C , k_D , and k_E as a function of $1/T$.

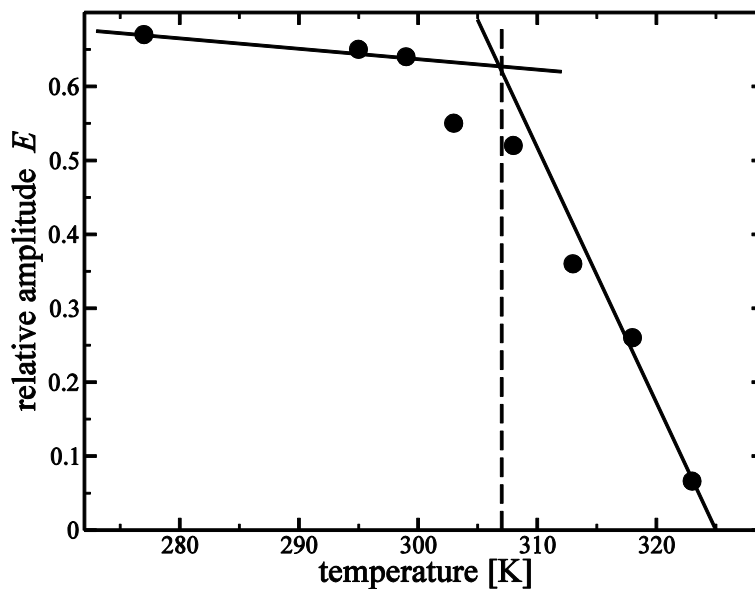


Figure 12.4. Relative amplitude E of the slow decay component as a function of temperature. The glass transition temperature can be estimated from the intersection of the asymptotic lines.

At the glass transition temperature, most parameters -including the stability of the holographic gratings- show a distinct change of the temperature

dependence. This was also the case for the parameters determined from equation 42. Thus, the glass transition temperature can be estimated by plotting e.g. E as a function of temperature, as shown in figure 12.4. The glass transition of the minority phase, which is indicated by the intersection of the asymptotic lines, is determined to be (307 ± 5) K. This value is lower than that of the azobenzene-functionalized homopolymer determined by DSC, but it is in good agreement with the results of ^2H NMR which was performed on a deuterated compound **18'** ^[160]. Additionally, the glass transition temperature of the minority block of **18'** was determined by dynamic mechanical thermal analysis (DMTA) as 327 K. Since DMTA is a non-equilibrium method, in contrast to the other two techniques, it usually yields higher T_g values.

13 Appendix C: Publications

Dynamic behavior of the minority phase of photoaddressable block copolymers

Kreger, K., Löffler, C., Walker, R., Wirth, N., Bingemann, D., Audorff, H., Rössler, E. A., Kador, L., Schmidt, H.-W.

Macromolecular Chemistry and Physics, **208** (14), p. 1530-1541 (2007)

Polarization dependence of the formation of surface relief gratings in azobenzene-containing molecular glasses

Audorff, H., Walker, R., Kador, L., Schmidt, H.-W.

Journal of Physical Chemistry B, **113** (11), p. 3379-3384 (2009)

Synthesis and structure-property relations of a series of photochromic molecular glasses for controlled and efficient formation of surface relief nanostructures

Walker, R., Audorff, H., Kador, L., Schmidt, H.-W.

Advanced Functional Materials, **19** (16), p. 2630-2638 (2009)

Holographic studies of azobenzene-containing low-molecular-weight organic glasses

Audorff, H., Walker, R., Schmidt, H.-W., Kador, L.

Proceedings of SPIE, **7233**, p. 00/1-00/12 (2009)

Optimization of the photochromic response of photoaddressable polymers with azobenzene-containing molecular glasses

Walker, R., Audorff, H., Kador, L., Schmidt, H.-W.

Proceedings of SPIE, **7358**, p. 03/1-03/9 (2009)

Stable holographic gratings with small-molecular trisazobenzene derivatives

Kreger, K., Wolfer, P., Audorff, H., Kador, L., Stingelin-Stutzmann, N., Smith, P., Schmidt, H.-W.

Journal of the American Chemical Society, **132** (2), p. 509-516 (2010)

Blends of azobenzene-containing diblock copolymers and molecular glasses for holographic data storage

Audorff, H., Walker, R., Kador, L., Schmidt, H.-W.

Proceedings of SPIE, **7730**, p. 0X/1-0X/8 (2010)

Blends of azobenzene-containing polymers and molecular glasses as stable rewritable holographic storage materials

Walker, R., Audorff, H., Kador, L., Schmidt, H.-W.

Proceedings of SPIE, **7619**, p. 0H/1-0H/9 (2010)

Holographic gratings and data storage in azobenzene-containing block copolymers and molecular glasses

Audorff, H., Kreger, K., Walker, R., Haarer, D., Kador, L., Schmidt, H.-W.

in: *Advances in Polymer Science*, **228**, p. 59-121 Springer (2010)

Photo-induced molecular alignment of trisazobenzene derivatives

Wolfer, P., Audorff, H., Kreger, K., Kador, L., Schmidt, H.-W., Stingelin-Stutzmann, N., Smith, P.

Accepted in *Journal of Materials Chemistry* (2011)

Holographic investigations of azobenzene-containing low molecular weight compounds in pure materials and binary blends with polystyrene

Audorff, H., Walker, R., Schmidt, H.-W., Kador, L.

Submitted to *Chemistry - A European Journal*

Improving the holographic recording sensitivity of photoaddressable azobenzene-containing polymers with molecular glasses

Walker, R., Audorff, H., Kador, L., Schmidt, H.-W.

Intended for *Advanced Materials*

Stable holographic volume gratings with novel photochromic bisazobenzene-based low molecular weight compounds

Walker, R., Audorff, H., Kador, L., Schmidt, H.-W.

Intended for *Chemistry of materials*

14 References

- [1] IDC. "The Digital Universe decade - Are you ready?" <http://www.emc.com/collateral/demos/microsites/idc-digital-universe/iview.htm> (2010).
- [2] Kim, J., Kim, M., Hong, S., Milster, T. "Characteristics of the depth of focus in a high-NA optical system with a SIAX for data storage" *Proc. SPIE* **7730** p. 77300M/1-77300M/8 (2010).
- [3] Kim, J.-H., Lee, S.-H., Seo, J.-K. "High density recording with SIL-based near-field optical recording" *Proc. SPIE* **7730** p. 77300K/1-77300K/8 (2010).
- [4] Shi, X., Hesselink, L. "Design of a C aperture to achieve $\lambda/10$ resolution and resonant transmission" *J. Opt. Soc. Am.* **21** (7), p. 1305-1317 (2004).
- [5] Zijlstra, P., Chon, J., Gu, M. "Five-dimensional optical recording mediated by surface plasmons in gold nanorods" *Nature* **459** p. 410-413 (2009).
- [6] Hesselink, L., Orlov, S., Bashaw, M. "Holographic data storage systems" *Proc. IEEE* **92** (8), p. 1231-1280 (2004).
- [7] van Heerden, P. "Theory of optical information storage in solids" *Appl. Opt.* **2** (4), p. 393-400 (1963).
- [8] Hammond, A. "Optical data storage: mass memories for future computers?" *Science* **180** p. 287-289 (1973).
- [9] Maiman, T. "Stimulated optical radiation in ruby" *Nature* **187** (4736), p. 493 (1960).
- [10] Ashley, J., Bernal, M., Burr, G., Coufal, H., Guenther, H., Hoffnagle, J., Jefferson, C., Marcus, B., Macfarlane, R., Shelby, R., Sincerbox, G. "Holographic data storage" *IBM J. Res. Dev.* **44** (3), p. 341-368 (2000).
- [11] Psaltis, D., Mok, F. "Holographic memories" *Sci. Am.* **273** p. 70-86 (1995).
- [12] Buse, K., Adibi, A., Psaltis, D. "Non-volatile holographic storage in doubly doped lithiumniobate crystals" *Nature* **393** p. 665-668 (1998).
- [13] Schilling, M., Colvin, V., Dhar, L., Harris, A., Schilling, M., Katz, H., Wysocki, T., Hale, A., Blyler, L., Boyd, C. "Acrylate oligomer-based photopolymers for optical storage applications" *Chem. Mater.* **11** (2), p. 247-254 (1999).

- [14] Barbastathis, G., Psaltis, D. "Volume holographic multiplexing methods" in: *Holographic data storage* p. 21-62 Springer-Verlag (2000).
- [15] Waldman, D., Butler, C., Raguin, D. "CROP holographic storage media for optical data storage greater than 100 bits/microm²" *Proc. SPIE* **5216** p. 10-25 (2003).
- [16] Schnoes, M., Ihas, B., Dhar, L., Michaels, D., Setthachayanon, S., Schomberger, G., Wilson, W. "Photopolymer use for holographic data storage" *Proc. SPIE* **4988** p. 68-76 (2003).
- [17] InPhase. "Drives & Media" http://www.inphase-technologies.com/products/mediaf486.html?subn=3_2 (2010).
- [18] Curtis, K., Dhar, L., Hill, A., Wilson, W., Ayres, M. "Holographic data storage - from theory to practical systems" Wiley (2010).
- [19] Rau, H. "Photoisomerization of azobenzenes" in: *Photochemistry and Photophysics* **9**, p. 323-328 CRC Press (1990).
- [20] Ringsdorf, H., Schmidt, H.-W. "Electro-optical effects of azo dye containing liquid crystalline copolymers" *Macromol. Chem.* **185** p. 1327-1334 (1984).
- [21] Eich, M., Wendorff, J., Ringsdorf, H., Schmidt, H.-W. "Nonlinear optical self diffraction in a mesogenic side chain polymer" *Macromol. Chem.* **186** (12), p. 2639-2647 (1985).
- [22] Meng, X., Natansohn, A., Rochon, P. "Azo polymers for reversible optical storage. 13. Photoorientation of rigid side groups containing two azo bonds" *Polymer* **38** (11), p. 2677-2682 (1997).
- [23] Eich, M., Wendorff, J., Peck, B., Ringsdorf, H. "Reversible digital and holographic optical storage in polymeric liquid crystals" *Macromol. Rapid Comm.* **8** (1), p. 59-63 (1987).
- [24] Cimrova, V., Neher, D., Kostromine, S., Bieringer, T. "Optical anisotropy in films of photoaddressable polymers" *Macromolecules* **32** (25), p. 8496-8503 (1999).
- [25] Rochon, P., Batalla, E., Natansohn, A. "Optically induced surface gratings on azo aromatic polymer films" *Appl. Phys. Lett.* **66** (2), p. 136-138 (1995).
- [26] Kim, D.-Y., Tripathy, S., Li, L., Kumar, J. "Laser-induced holographic surface relief gratings on nonlinear optical polymer films" *Appl. Phys. Lett.* **66** (10), p. 1166-1168 (1995).
- [27] Schulz, B., Huber, M., Bieringer, T., Krausch, G., Zilker, S. "Length-scale dependence of surface relief gratings in azobenzene side-chain polymers" *Synth. Met.* **124** (1), p. 155-157 (2001).

-
- [28] Helgert, M., Wenke, L., Hvilsted, S., Ramanujam, P. "Surface Relief measurements in side-chain azobenzene polyesters with different substituents" *Appl. Phys. B* **72** (4), p. 429-433 (2001).
- [29] Yager, K., Tanchak, O., Godbout, C., Fritzsche, H., Barrett, C. "Photomechanical effects in azo-polymers studied by neutron reflectometry" *Macromolecules* **39** (26), p. 9311-9319 (2006).
- [30] Carvalho, L., Borges, T., Cardoso, M., Mendonca, C., Balogh, D. "Molecular weight effect on the photoinduced birefringence and surface relief gratings formation of a methacrylate azopolymer" *Eur. Polym. J.* **42** (10), p. 2589-2595 (2006).
- [31] Lefin, P., Fiorini, C., Nunzi, J.-M. "Anisotropy of the photoinduced translation diffusion of azo-dyes" *Opt. Mater.* **9** (1-4), p. 323-328 (1998).
- [32] Barrett, C., Rochon, P., Natansohn, A. "Model of laser-driven mass transport in thin films of dye-functionalized polymers" *J. Chem. Phys.* **109** (4), p. 1505-1516 (1998).
- [33] Pedersen, T., Johansen, P. M., Holme, N., Ramanujam, P., Hvilsted, S. "Mean-field theory of photoinduced formation of surface reliefs in side-chain azobenzene polymers" *Phys. Rev. Lett.* **80** (1), p. 89-92 (1998).
- [34] Henneberg, O., Geue, T., Saphiannikova, M., Pietsch, U., Rochon, P., Natansohn, A. "Formation and dynamics of polymer surface relief gratings" *Appl. Surf. Sci.* **182** (3-4), p. 272-279 (2001).
- [35] Yang, K., Yang, S., Kumar, J. "Formation mechanism of surface relief structures on amorphous azo-polymer films" *Phys. Rev. B* **73** (16), p. 165204/1-165204/14 (2006).
- [36] Yager, K., Barrett, C. "Photomechanical surface patterning in azo-polymer materials" *Macromolecules* **39** (26), p. 9320-9326 (2006).
- [37] Imlau, M., Bieringer, T., Odoulov, S., Woike, T. "Holographic data storage" in: *Nanoelectronics and Information Technology* p. 659-686 Wiley (2003).
- [38] Minabe, J., Maruyama, T., Yasuda, S., Kawano, K., Hayashi, K., Ogasawara, Y. "Design of dye concentrations in azobenzene-containing polymer films for volume holographic storage" *Jpn. J. Appl. Phys.* **43** (7B), p. 4964-4967 (2004).
- [39] Ringsdorf, H., Schmidt, H.-W., Baur, G., Kiefer, R., Windscheid, F. "Orientational ordering of dyes in the glassy state of liquid-crystalline side group polymers" *Liq. Cryst.* **1** (4), p. 319-325 (1986).
- [40] Brown, D., Natansohn, A., Rochon, P. "Azo polymers for reversible optical storage. 5. Orientation and dipolar interactions of azobenzene side groups in copolymers and blends containing methyl methacrylate structural units" *Macromolecules* **28** (18), p. 6116-6123 (1995).

- [41] Ho, M.-S., Natansohn, A., Barrett, C., Rochon, P. "Azo polymers for reversible optical storage. 8. The effect of polarity of the azobenzene groups" *Can. J. Chem.* **73** p. 1773-1778 (1995).
- [42] Ho, M.-S., Natansohn, A., Rochon, P. "Azo polymers for reversible optical storage. 7. The effect of the size of the photochromic groups" *Macromolecules* **28** (18), p. 6124-6127 (1995).
- [43] Meng, X., Natansohn, A., Barrett, C., Rochon, P. "Azo polymers for reversible optical storage. 10. Cooperative motion of polar side groups in amorphous polymers" *Macromolecules* **29** (13), p. 946-952 (1996).
- [44] Natansohn, A., Rochon, P., Gosselin, J., Xie, S. "Azo polymers for reversible optical storage. 1. Poly[4'-[[2-(acryloyloxy)ethyl]ethylamino]-4-nitroazobenzene]" *Macromolecules* **25** (8), p. 2268-2273 (1992).
- [45] Anderle, K., Birenheide, R., Werner, M., Wendorff, J. "Molecular addressing? Studies on light-induced reorientation in liquid-crystalline side chain polymers" *Liq. Cryst.* **9** (5), p. 691-699 (1991).
- [46] Natansohn, A., Rochon, P., Pézolet, M., Audet, P., Brown, D., To, S. "Azo polymers for reversible optical storage. 4. Cooperative motion of rigid groups in semicrystalline polymers" *Macromolecules* **27** (9), p. 2580-2585 (1994).
- [47] Natansohn, A., Rochon, P., Meng, X., Barrett, C., Buffeteau, T., Bonenfant, S., Pézolet, M. "Molecular addressing? Selective photoinduced cooperative motion of polar ester groups in copolymers containing azobenzene groups" *Macromolecules* **31** (4), p. 1155-1161 (1998).
- [48] Audorff, H., Kreger, K., Walker, R., Haarer, D., Kador, L., Schmidt, H.-W. "Holographic gratings and data storage in azobenzene-containing block copolymers and molecular glasses" in: *Advances in Polymer Science* **228**, p. 59-121 Springer (2010).
- [49] Breiner, T., Kreger, K., Hagen, R., Häckel, M., Kador, L., Müller, A., Kramer, E., Schmidt, H.-W. "Blends of poly(methacrylate) block copolymers with photoaddressable segments" *Macromolecules* **40** (6), p. 2100-2108 (2007).
- [50] Häckel, M., Kador, L., Kropp, D., Frenz, C., Schmidt, H.-W. "Holographic information storage in azobenzene-containing diblock copolymers" *Proc. SPIE* **5939** p. 593908/1-593908/10 (2005).
- [51] Häckel, M., Kador, L., Kropp, D., Frenz, C., Schmidt, H.-W. "Holographic gratings in diblock copolymers with azobenzene and mesogenic side groups in the photoaddressable dispersed phase" *Adv. Funct. Mat.* **15** (10), p. 1722-1727 (2005).

-
- [52] Häckel, M., Kador, L., Kropp, D., Schmidt, H.-W. "Polymer blends with azobenzene-containing block copolymers as stable rewritable volume holographic media" *Adv. Mater.* **19** (2), p. 227-231 (2007).
- [53] Gimeno, S., Forcen, P., Oriol, L., Pinol, M., Sanchez, C., Rodriguez, F., Alcalá, R., Jankova, K., Hvilsted, S. "Photoinduced optical anisotropy in azobenzene methacrylate block copolymers: Influence of molecular weight and irradiation conditions" *Eur. Polym. J.* **45** (1), p. 262-271 (2009).
- [54] Kim, M.-J., Seo, E.-M., Vak, D., Kim, D.-Y. "Photodynamic properties of azobenzene molecular films with triphenylamines" *Chem. Mater.* **15** (21), p. 4021-4027 (2003).
- [55] Ando, H., Tanino, T., Nakano, H., Shirota, Y. "Photoinduced surface relief grating formation using new polymers containing the same azobenzene chromophore as a photochromic amorphous molecular material" *Mater. Chem. Phys.* **113** (1), p. 376-381 (2009).
- [56] Shirota, Y., Moriwaki, K., Yoshikawa, S., Ujike, T., Nakano, H. "4-[Di(biphenyl-4-yl)amino]azobenzene and 4,4'-bis[bis(4'-tert-butylbiphenyl-4-yl)amino]azobenzene as a novel family of photochromic amorphous molecular materials" *J. Mater. Chem.* **8** (12), p. 2579-2581 (1998).
- [57] Fuhrmann, T., Tsutsui, T. "Synthesis and properties of a hole-conducting, photopatternable molecular glass" *Chem. Mater.* **11** (8), p. 2226-2232 (1999).
- [58] Nakano, H., Takahashi, T., Kadota, T., Shirota, Y. "Formation of a surface relief grating using a novel azobenzene-based photochromic amorphous molecular material" *Adv. Mater.* **14** (16), p. 1157-1160 (2002).
- [59] Ishow, E., Lebon, B., He, Y., Wang, X., Bouteiller, L., Galmiche, L., Nakatani, K. "Structural and photoisomerization cross studies of polar photochromic monomeric glasses forming surface relief gratings" *Chem. Mater.* **18** (5), p. 1261-1267 (2006).
- [60] Shirota, Y. "Organic materials for electronic and optoelectronic devices" *J. Mater. Chem.* **10** (1), p. 1-25 (2000).
- [61] Strohriegl, P., Grazulevicius, J. "Charge-transporting molecular glasses" *Adv. Mater.* **14** (20), p. 1439-1452 (2002).
- [62] Shirota, Y. "Photo- and electroactive amorphous molecular materials-molecular design, syntheses, reactions, properties, and applications" *J. Mater. Chem.* **15** (1), p. 75-93 (2005).
- [63] Seo, E.-M., Kim, M.-J., Shin, Y.-D., Lee, J.-S., Kim, D.-Y. "The behavior of surface relief grating formation on organic glass films containing azo chromophores" *Mol. Cryst. Liquid Cryst.* **370** p. 143-146 (2001).

- [64] Chun, C., Kim, M.-J., Vak, D., Kim, D.-Y. "A novel azobenzene-based amorphous molecular material with a spiro linked bifluorene" *J. Mater. Chem.* **13** (12), p. 2904-2909 (2003).
- [65] Ando, H., Takahashi, T., Nakano, H., Shirota, Y. "Comparative studies of the formation of surface relief grating. Amorphous molecular material vs vinyl polymer" *Chem. Lett.* **32** (8), p. 710-711 (2003).
- [66] Gabor, D. "A new microscopic principle" *Nature* **161** (4098), p. 777-778 (1948).
- [67] Kakichashvili, S. "Method for phase polarization recording of holograms" *Sov. J. Quant. Electron.* **4** (6), p. 795-798 (1974).
- [68] Collier, R., Burckhardt, C., Lin, L. "Optical Holography" Academic Press (1971).
- [69] Mehta, P., Rampal, V. "Lasers and holography" World Scientific Publishing (1993).
- [70] Hariharan, P. "Optical Holography: Principles, Techniques and Applications" Cambridge University Press (1996).
- [71] Ackermann, G., Eichler, J. "Holography: A practical approach" Wiley (2007).
- [72] van Renesse, R. "Optical document security" Artech House (2005).
- [73] Blanche, P.-A., Bablumian, A., Voorakaranam, R., Christenson, C., Lin, W., Gu, T., Flores, D., Wang, P., Hsieh, W.-Y., Kathaperumal, M., Rachwal, B., Siddiqui, O., Thomas, J., Norwood, R. A., Yamamoto, M., Peyghambarian, N. "Holographic three-dimensional telepresence using large-area photorefractive polymer" *Nature* **468** p. 80-83 (2010).
- [74] Kaspar, F. "Diffraction by thick, periodically stratified gratings with complex dielectric constant" *J. Opt. Soc. Am.* **63** (1), p. 37-45 (1973).
- [75] Magnusson, R., Gaylord, T. "Analysis of multiwave diffraction of thick gratings" *J. Opt. Soc. Am.* **67** (9), p. 1165-1170 (1977).
- [76] Magnusson, R., Gaylord, T. "Diffraction efficiencies of thin phase gratings with arbitrary grating shape" *J. Opt. Soc. Am.* **68** (6), p. 806-809 (1978).
- [77] Magnusson, R., Gaylord, T. "Diffraction regimes of transmission gratings" *J. Opt. Soc. Am.* **68** (6), p. 809-814 (1978).
- [78] Moharam, M., Gaylord, T. "Rigorous coupled-wave analysis of planar-grating diffraction" *J. Opt. Soc. Am.* **71** (7), p. 811-818 (1981).
- [79] Kogelnik, H. "Coupled wave theory for thick hologram gratings" *Bell. Syst. Tech. J.* **48** (9), p. 2909-2947 (1969).
- [80] Moharam, M., Young, L. "Criterion for Bragg and Raman-Nath diffraction regimes" *Appl. Opt.* **17** (11), p. 1757-1759 (1978).

-
- [81] Bieringer, T. "Optische Untersuchungen zu kollektiven Photoorientierung in flüssigkristallinen Seitenkettenpolymeren" PhD Thesis, Universität Bayreuth (1996).
- [82] Huber, M. "Oberflächengitter Photoadressierbarer Polymere" PhD Thesis, Universität Bayreuth (2001).
- [83] Schulze, F., Petrick, H., Cammenga, H., Klinge, H. "Thermodynamic properties of the structural analogs benzo[c]cinnoline, trans-azobenzene and cis-azobenzene" *Z. Phys. Chem.* **107** (1), p. 1-19 (1977).
- [84] Mita, I., Horie, K., Hirao, K. "Photoisomerization in polymer solids. 9. Photoisomerization of azobenzene in a polycarbonate film" *Macromolecules* **22** (2), p. 558-563 (1989).
- [85] Brown, E., Granneman, R. "Cis-trans isomerism in the pyridyl analogs of azobenzene. Kinetic and molecular orbital analysis" *J. Am. Chem. Soc.* **97** (3), p. 621-627 (1975).
- [86] Haberfield, P., Block, P., Lux, M. "Enthalpies of solvent transfer of the transition states in the cis-trans isomerization of azo compounds. Rotation vs. the nitrogen inversion mechanism" *J. Am. Chem. Soc.* **97** (20), p. 5804-5806 (1975).
- [87] Nagamani, A., Norikane, Y., Tamaoki, N. "Photoinduced hinge-like molecular motion: studies on xanthene-based cyclic azobenzene dimers" *J. Org. Chem.* **70** (23), p. 9304-9313 (2005).
- [88] Hartley, G. "Cis form of azobenzene" *Nature* **140** p. 281 (1937).
- [89] Naito, T., Horie, K., Mita, I. "Photochemistry in polymer solids: 12. Effects of main-chain structures and formation of hydrogen bonds on photoisomerization of azobenzene in various polymer films" *Polymer* **34** (19), p. 4140-4145 (1993).
- [90] Naito, T., Horie, K., Mita, I. "Photochemistry in polymer solids. 11. The effects of the size of reaction groups and the mode of Photoisomerization on photochromic reactions in polycarbonate films" *Macromolecules* **24** (10), p. 2907-2911 (1991).
- [91] Aoki, K. i., Nakagawa, M., Ichimura, K. "Self-Assembly of amphoteric azopyridine carboxylic acids: organized structures and macroscopic organized morphology influenced by heat, pH change and light" *J. Am. Chem. Soc.* **122** (44), p. 10997-11004 (2000).
- [92] Kadota, S., Aoki, K., Nagano, S., Seki, T. "Photocontrolled microphase separation of block copolymers in two dimensions" *J. Am. Chem. Soc.* **127** (23), p. 8266-8267 (2005).
- [93] Arai, K., Kawabata, Y. "Changes in the sol-gel transformation behavior of azobenzene moiety-containing methylcellulose irradiated with UV light" *Macromol. Rapid Commun.* **16** (12), p. 875-880 (1995).

- [94] Ebralidze, T., Mumladze, A. "Light-induced anisotropy in azo-dye-colored materials" *Appl. Opt.* **29** (4), p. 446-447 (1990).
- [95] Ikeda, T., Nakano, M., Yu, Y., Tsutsumi, O., Kanazawa, A. "Anisotropic bending and unbending behavior of azobenzene liquid-crystalline gels by light exposure" *Adv. Mater.* **15** (3), p. 201-205 (2003).
- [96] Yu, Y., Nakano, M., Ikeda, T. "Photomechanics: Directed bending of a polymer film by light" *Nature* **425** p. 145 (2003).
- [97] Yu, Y., Maeda, T., Mamiya, J.-i., Ikeda, T. "Photomechanical effects of ferroelectric liquid-crystalline elastomers containing azobenzene chromophores" *Angew. Chem. Int. Edit.* **46** (6), p. 881-883 (2006).
- [98] Rau, H., Yu-Quan, S. "Photoisomerization of sterically hindered azobenzenes" *J. Photochem. Photobiol. A* **42** (2-3), p. 321-327 (1988).
- [99] Rau, H. "Azo compounds" in: *Photochromism: Molecules and Systems* p. 165-192 Elsevier (1990).
- [100] Kobayashi, T., Degenkolb, E., Rentzepis, P. "Picosecond spectroscopy of 1-phenylazo-2-hydroxynaphtalene" *J. Phys. Chem.* **83** (19), p. 2431-2434 (1979).
- [101] Lednev, I., Ye, T.-Q., Hester, R., Moore, J. "Femtosecond time-resolved UV-visible absorption spectroscopy of trans-azobenzene in solution" *J. Phys. Chem.* **100** (32), p. 19998-13341 (1996).
- [102] Monti, S., Orlandi, G., Palmieri, P. "Features of the photochemically active state surfaces of azobenzenes" *Chem. Phys.* **71** (1), p. 87-99 (1982).
- [103] Lamarre, L., Sung, C. "Studies of physical aging and molecular motion by azochromophoric labels attached to the main chains of amorphous polymers" *Macromolecules* **16** (11), p. 1729-1736 (1983).
- [104] Naito, T., Horie, K., Mita, I. "The effect of polymer rigidity on photoisomerization of 4-dimethylamino-4'-nitroazobenzene" *Polym. J.* **23** (6), p. 809-813 (1991).
- [105] Paik, C., Morawatz, H. "Photochemical and thermal isomerization of azoaromatic residues in the side chains and the backbone of polymers in bulk" *Macromolecules* **5** (2), p. 171-177 (1972).
- [106] Diau, E. "A new trans-to-cis photoisomerization mechanism of azobenzene on the $S_1(n,\pi^*)$ surface" *J. Phys. Chem. A* **108** (6), p. 950-956 (2004).
- [107] Angeli, C., Cimiraglia, R., Hofmann, H.-J. "On the competition between inversion and rotation mechanism in the cis-trans thermal isomerization of diazene" *Chem. Phys. Lett.* **259** (3,4), p. 276-282 (1996).

-
- [108] Xie, S., Natansohn, A., Rochon, P. "Recent developments in aromatic azo polymers research" *Chem. Mater.* **5** (4), p. 403-411 (1993).
- [109] Ikeda, T., Tsutsumi, O. "Optical switching and image storage by means of azobenzene liquid-crystal films" *Science* **268** (5219), p. 1873-1875 (1995).
- [110] Altomare, A., Ciardelli, F., Tirelli, N., Solaro, L. "4-Venylazobenzene: polymerizability and photochromic properties of its polymers" *Macromolecules* **30** (5), p. 1298-1303 (1997).
- [111] Fujino, T., Arzhantsev, S., Tahara, T. "Femtosecond time-resolved fluorescence study of photoisomerization of trans-azobenzene" *J. Phys. Chem. A* **105** (35), p. 8123-8129 (2001).
- [112] Gegiou, D., Muszkat, K., Fischer, E. "Temperature dependence of photoisomerization. V. Effect of substituents on the photoisomerization of stilbenes and azobenzenes." *J. Am. Chem. Soc.* **90** (15), p. 3907-3918 (1968).
- [113] Ho, C.-H., Yang, K.-N., Lee, S.-N. "Mechanistic study of trans-cis isomerization of the substituted azobenzene moiety bound on a liquid-crystalline polymer" *J. Polym. Sci. Pol. Chem.* **39** (13), p. 2296-2307 (2001).
- [114] Bortulus, P., Monti, S. "Cis-trans photoisomerization of azobenzene. solvent and triplet donor effects" *J. Phys. Chem.* **83** (6), p. 648-652 (1979).
- [115] Hagen, R., Bieringer, T. "Photoaddressable polymers for optical data storage" *Adv. Mater.* **13** (23), p. 1805-1810 (2001).
- [116] Yager, K., Barrett, C. "Novel photo-switching using azobenzene functional materials" *J. Photochem. Photobiol. A* **182** (3), p. 250-261 (2006).
- [117] Barley, S., Gilbert, A., Mitchell, G. "Photoinduced reversible refractive-index changes in tailored siloxane-based polymers" *J. Mater. Chem.* **1** (3), p. 481-482 (1991).
- [118] Bredenbeck, J., Helbing, J., Behrendt, R., Renner, C., Moroder, L., Wachtveitl, J., Hamm, P. "Transient 2D-IR spectroscopy: snapshots of the nonequilibrium ensemble during the picosecond conformational transition of a small peptide" *J. Phys. Chem. B* **107** (33), p. 8654-8660 (2003).
- [119] Siewertsen, R., Neumann, H., Buchheim-Stehn, B., Herges, R., Näther, C., Renth, F., Temps, F. "Highly efficient reversible Z-E photoisomerization of a bridged azobenzene with visible light through resolved $S_1(n\pi^*)$ absorption bands" *J. Am. Chem. Soc.* **131** p. 15594-15595 (2009).

- [120] Viswanathan, N., Kim, D.-Y., Bian, S., Williams, J., Liu, W., Li, L., Samuelson, L., Kumar, J., Tripathy, S. "Surface relief structures on azo polymer films" *J. Mater. Chem.* **9** (9), p. 1941-1955 (1999).
- [121] Goldenberg, L., Gritsai, Y., Kulikovska, O., Stumpe, J. "Three-dimensional planarized diffraction structures based on surface relief gratings in azobenzene materials" *Opt. Lett.* **33** (12), p. 1309-1311 (2008).
- [122] Guo, M., Xu, Z., Wang, X. "Photofabrication of two-dimensional quasi-crystal patterns on UV-curable molecular azo glass films" *Langmuir* **24** (6), p. 2740-2745 (2008).
- [123] Zhao, D., Xu, Z., Wang, G., Cao, H., Li, W., He, W., Huang, W., Yang, Z., Yang, H. "Formation of surface relief gratings in homeotropically oriented photopolymer from a photocross-linkable organic monomer" *Phys. Chem. Chem. Phys.* **12** (7), p. 1436-1439 (2010).
- [124] Kaneko, F., Kato, T., Babab, A., Shinbo, K., Kato, K., Advincula, R. "Photo-induced fabrication of surface relief gratings in alternate self-assembled films containing azo dye and alignments of LC molecules" *Colloid Surface A* **198** p. 805-810 (2002).
- [125] Tripathy, S., Viswanathan, N., Balasubramanian, S., Kumar, J. "Holographic fabrication of polarization selective diffractive optical elements on azopolymer film" *Polym. Adv. Technol.* **11** (8-12), p. 570-574 (2000).
- [126] Rochon, P., Natansohn, A., Callender, C., Robitaille, L. "Guided mode resonance filters using polymer films" *Appl. Phys. Lett.* **71** (8), p. 1008-1010 (1997).
- [127] Delaire, J., Nakatani, K. "Linear and nonlinear optical properties of photochromic molecules and materials" *Chem. Rev.* **100** (5), p. 1817-1845 (2000).
- [128] Jiang, X.-L., Li, L., Kumar, J., Kim, D.-Y., Tripathy, S. "Unusual polarization dependent optical erasure of surface relief gratings on azobenzene polymer films" *Appl. Phys. Lett.* **72** (20), p. 2502-2504 (1998).
- [129] Watanabe, O., Tsuchimori, M., Okada, A., Ito, H. "Mode selective polymer waveguide defined by the photoinduced change in birefringence" *Appl. Phys. Lett.* **71** (6), p. 750-752 (1997).
- [130] Viswanathan, N., Balasubramanian, S., Li, L., Kumar, J., Tripathy, S. "Surface-initiated mechanism for the formation of relief gratings on azo-polymer films" *J. Phys. Chem. B* **102** (31), p. 6064-6070 (1998).
- [131] Bian, S., Liu, W., Williams, J., Samuelson, L., Kumar, J., Tripathy, S. "Photoinduced surface relief grating on amorphous poly(4-phenylazophenol) films" *Chem. Mater.* **12** (6), p. 1585-1590 (2000).

- [132] Sobolewska, A., Bartkiewicz, S., Miniewicz, A., Schab-Balcerzak, E. "Polarization dependence of holographic recording in azobenzene-functionalized polymers monitored by visible and infrared light" *J. Phys. Chem. B* **114** (30), p. 9751-9760 (2010).
- [133] Barrett, C., Natansohn, A., Rochon, P. "Mechanism of optically inscribed high-efficiency diffraction gratings in azo polymer films" *J. Phys. Chem.* **100** (21), p. 8836-8842 (1996).
- [134] Andruzzi, L., Altomare, A., Ciardelli, F., Solaro, R. "Holographic gratings in azobenzene side-chain polymethacrylates" *Macromolecules* **32** (2), p. 448-454 (1999).
- [135] Börger, V., Kulikovska, O., Hubmann, K., Stumpe, J., Huber, M., Menzel, H. "Novel polymers to study the influence of the azobenzene content on the photo-induced surface relief grating formation" *Macromol. Chem. Phys.* **206** (15), p. 1488-1496 (2008).
- [136] Zhao, Y., Ikeda, T. "Smart Light-Responsive Materials" Wiley (2009).
- [137] Holme, N., Nikolova, L., Hvilsted, S., Rasmussen, P., Berg, R., Ramanujam, P. "Optically induced surface relief phenomena in azobenzene polymers" *Appl. Phys. Lett.* **74** (4), p. 519-521 (1999).
- [138] Nakano, H. "Photoinduced surface relief grating formation on a (100) surface of a single crystal of 4-(dimethylamino)azobenzene" *J. Phys. Chem. C* **112** (41), p. 16042-16045 (2008).
- [139] Pedersen, T., Johansen, P. M. "Mean-field theory of photoinduced molecular reorientation in azobenzene liquid crystalline side-chain polymers" *Phys. Rev. Lett.* **79** (13), p. 2470-2473 (1997).
- [140] Ashkin, A. "Acceleration and trapping of particles of radiation pressure" *Phys. Rev. Lett.* **24** (4), p. 156-159 (1970).
- [141] Kumar, J., Li, L., Jiang, X.-L., Kim, D.-Y., Lee, T.-S., Tripathy, S. "Gradient force: The mechanism for surface relief grating formation in azobenzene functionalized polymers" *Appl. Phys. Lett.* **72** (17), p. 2096-2098 (1998).
- [142] Viswanathan, N., Balasubramanian, S., Li, L., Tripathy, S., Kumar, J. "A detailed investigation of the polarization-dependent surface-relief-grating formation process on azo polymer films" *Jpn. J. Appl. Phys.* **38** (10), p. 5928-5937 (1999).
- [143] Saphiannikova, M., Geue, T., Henneberg, O., Morawatz, K., Pietsch, U. "Linear viscoelastic analysis of formation and relaxation of azobenzene polymer gratings" *J. Chem. Phys.* **120** (8), p. 4039-4045 (2004).
- [144] Mechau, N., Saphiannikova, M., Neher, D. "Dielectric and mechanical properties of azobenzene polymer layers under visible and ultraviolet irradiation" *Macromolecules* **38** (9), p. 3894-3902 (2005).

- [145] Bian, S., Li, L., Kumar, J., Kim, D.-Y., Williams, J., Tripathy, S. "Single laser beam-induced surface deformation on azobenzene polymer films" *Appl. Phys. Lett.* **73** (13), p. 1817-1819 (1998).
- [146] Huang, J., Wu, S., Beckemper, S., Gillner, A., Zhang, Q., Wang, K. "All-optical fabrication of ellipsoidal caps on azobenzene functional polymers" *Opt. Lett.* **35** (16), p. 2711-2713 (2010).
- [147] Thelakkat, M., Schmitz, C., Hohle, C., Strohrriegl, P., Schmidt, H.-W., Hofmann, U., Schloter, S., Haarer, D. "Novel functional materials based on triarylamine-synthesis and application in electroluminescent devices and photorefractive systems" *Phys. Chem. Chem. Phys.* **1** (8), p. 1693-1698 (1999).
- [148] Shirota, Y., Kinoshita, M., Noda, T., Okumoto, K., Ohara, T. "A novel Class of emitting amorphous molecular materials as bipolar radical formants: 2-{4-[bis(4-methylphenyl)amino]phenyl}-5-(dimesitylboryl)thiophene and 2-{4-[Bis(9,9-dimethylfluorenyl)amino]phenyl}-5-(dimesitylboryl)thiophene" *J. Am. Chem. Soc.* **122** (44), p. 11021-11022 (2000).
- [149] Steuber, F., Staudigel, J., Stössel, M., Simmerer, J., Winnacker, A., Spreitzer, H., Weissörtel, F., Salbeck, J. "White light emission from organic LEDs utilizing spiro compounds with high-temperature stability" *Adv. Mater.* **12** (2), p. 130-133 (2000).
- [150] Dai, J., Chang, S., Hamad, A., Yang, D., Felix, N., Ober, C. "Molecular glass resists for high-resolution patterning" *Chem. Mater.* **18** (15), p. 3404-3411 (2006).
- [151] Naito, K., Miura, A. "Molecular design for nonpolymeric organic dye glasses with thermal stability: relations between thermodynamic parameters and amorphous properties" *J. Phys. Chem.* **97** (23), p. 6240-6248 (1993).
- [152] Walker, R., Audorff, H., Kador, L., Schmidt, H.-W. "Synthesis and structure-property relations of a series of photochromic molecular glasses for controlled and efficient formation of surface relief nanostructures" *Adv. Funct. Mat.* **19** (16), p. 2630-2638 (2009).
- [153] Kreger, K., Wolfer, P., Audorff, H., Kador, L., Stingelin-Stutzmann, N., Smith, P., Schmidt, H.-W. "Stable holographic gratings with small-molecular trisazobenzene derivatives" *J. Am. Chem. Soc.* **132** (2), p. 509-516 (2010).
- [154] Walker, R. "Azobenzene-functionalized molecular glasses for holographic applications" PhD Thesis, Universität Bayreuth (2010).
- [155] Schab-Balcerzak, E., Sobolewska, A., Miniewicz, A., Jurusik, J. "Chromophore concentration effect on holographic grating formation efficiency in novel azobenzene-functionalized polymers" *Polym. Eng. Sci.* **48** (9), p. 1755-1767 (2008).

-
- [156] Natansohn, A., Rochon, P. "Photoinduced motions in azo-containing polymers" *Chem. Rev.* **102** (11), p. 4139-4175 (2002).
- [157] Theißen, U. "Photoadressierbare Blockcopolymere als Material für die holographische Datenspeicherung" PhD Thesis, Universität Bayreuth (2002).
- [158] Frenz, C. "Diblock copolymers with photoaddressable chromophores for holographic data storage" PhD Thesis, Universität Bayreuth (2003).
- [159] Frenz, C., Fuchs, A., Schmidt, H.-W., Theißen, U., Haarer, D. "Diblock copolymers with azobenzene side-groups and polystyrene matrix: Synthesis, characterization and photoaddressing" *Macromol. Chem. Phys.* **205** (9), p. 1246-1258 (2004).
- [160] Kreger, K., Löffler, C., Walker, R., Wirth, N., Bingemann, D., Audorff, H., Rössler, E. A., Kador, L., Schmidt, H.-W. "Dynamic behavior of the minority phase of photoaddressable block copolymers" *Macromol. Chem. Phys.* **208** (14), p. 1530-1541 (2007).
- [161] Häckel, M. "Holographische Datenspeicherung in nanostrukturierten azobenzolhaltigen Polymeren" PhD Thesis, Universität Bayreuth (2006).
- [162] Sherif, H., Naydenova, I., Martin, S., McGimm, C., Toal, V. "Characterization of an acrylamide-based photopolymer for data storage utilizing holographic angular multiplexing" *J. Opt. A Pure Appl. Opt.* **7** (5), p. 255-260 (2005).
- [163] Goodman, J. "Introduction to Fourier Optics" Roberts & Co Publ. (2004).
- [164] Fujiwara, H. "Spectroscopic Ellipsometry" Wiley (2007).
- [165] Stumpe, J., Läsker, L., Fischer, T., Rutloha, M., Kostromine, S., Ruhmann, R. "Photo-orientation in amorphous and aligned films of photochromic liquid crystalline polymers" *Thin Solid Films* **284-285** p. 252-265 (1996).
- [166] Fischer, T., Läsker, L., Czaplak, S., Rübner, J., Stumpe, J. "Interdependence of photoorientation and thermotropic self-organization in photochromic liquid crystalline polymers" *Mol. Cryst. Liquid Cryst.* **298** p. 213-220 (1997).
- [167] Zilker, S., Bieringer, T., Haarer, D., Stein, R., van Egmond, J., Kostromine, S. "Holographic data storage in amorphous polymers" *Adv. Mater.* **10** (11), p. 855-859 (1998).
- [168] Zilker, S., Huber, M., Bieringer, T., Haarer, D. "Holographic recording in amorphous side-chain polymers. A comparison of two different design philosophies" *Appl. Phys. B* **68** (5), p. 893-897 (1999).

- [169] Kidowaki, M., Fujiwara, T., Morino, S., Ichimura, K., Stumpe, J. "Thermal amplification of photoinduced optical anisotropy of p-cyanoazobenzene polymer films monitored by temperature scanning ellipsometry" *Appl. Phys. Lett.* **76** (11), p. 1377-1379 (2000).
- [170] Rosenhauer, R., Fischer, T., Czaplá, S., Stumpe, J., Vinuales, A., Pinol, M., Serrano, J. "Photo-induced alignment of LC polymers by photoorientation and thermotropic self-organization" *Mol. Cryst. Liquid Cryst.* **364** p. 295-304 (2001).
- [171] Audorff, H., Walker, R., Kador, L., Schmidt, H.-W. "Polarization dependence of the formation of surface relief gratings in azobenzene-containing molecular glasses" *J. Phys. Chem. B* **113** (11), p. 3379-3384 (2009).
- [172] Erhard, D., Giesa, R., Altstädt, V., Schmidt, H.-W. "Charge storage performance of polyetherimide Ultem 1000 - Influence of secondary antioxidants and purification" *J. Appl. Polym. Sci.* **115** (2), p. 1247-1255 (2010).
- [173] Williams, G., Watts, D. "Non-symmetrical dielectric relaxation behaviour arising from a simple empirical decay function" *Trans. Faraday Soc.* **66** p. 80-86 (1969).
- [174] Reinke, N., Draude, A., Fuhrmann, T., Franke, H., Lessard, R. "Electric field assisted holographic recording of surface relief gratings in an azo-glass" *Appl. Phys. B* **78** (2), p. 205-209 (2004).
- [175] Barrett, C., Natansohn, A., Rochon, P. "Thermal cis-trans isomerization rates of azobenzene bound in side chain of some copolymers and blends" *Macromolecules* **27** (17), p. 4781-4786 (1994).
- [176] Burawoy, A. "Studies in the light absorption of organic compounds. VIII. Azo-compounds" *J. Chem. Soc.* **1937** p. 1865-1869 (1937).
- [177] Birnbaum, P., Linford, J., Style, D. "The absorption spectra of azobenzene and some derivatives" *Trans. Faraday Soc.* **49** (1), p. 735-744 (1953).
- [178] Pedersen, M., Hvilsted, S., Holme, N., Ramanujam, P. "Influence of the substituent on azobenzene side-chain polyester optical storage materials" *Macromol. Symp.* **137** p. 115-127 (1999).
- [179] Pu, A., Curtis, K., Psaltis, D. "Exposure schedule for multiplexing holograms in photopolymer films" *Opt. Eng.* **35** p. 2824-2829 (1996).
- [180] Tong, X., Cui, L., Zhao, Y. "Confinement effects on photoalignment, photochemical phase transition, and thermochromic behavior of liquid crystalline azobenzene-containing diblock copolymers" *Macromolecules* **37** (9), p. 3101-3112 (2004).
- [181] Walker, R., Audorff, H., Kador, L., Schmidt, H.-W. "Blends of azobenzene-containing polymers and molecular glasses as stable

- rewritable holographic storage materials" *Proc. SPIE* **7619** p. 76190H/1-76190H/9 (2010).
- [182] Audorff, H., Walker, R., Kador, L., Schmidt, H.-W. "Blends of azobenzene-containing diblock copolymers and molecular glasses for holographic data storage" *Proc. SPIE* **7730** p. 77300X/1-77300X/8 (2010).
- [183] Wiesner, U., Reynolds, N., Boeffel, C., Spiess, H. "Photoinduced reorientation in liquid-crystalline polymers below the glass transition temperature studied by time-dependent infrared spectroscopy" *Macromol. Rapid Comm.* **12** (8), p. 457-464 (1991).
- [184] Abetz, V., Simon, P. "Phase behaviour and morphologies of block copolymers" in: *Advances in Polymer Science* **189**, p. 125-212 Springer (2005).
- [185] Kulikovska, O., Goldenberg, L., Stumpe, J. "Supramolecular azobenzene-based materials for optical generation of microstructures" *Chem. Mater.* **19** (13), p. 3343-3348 (2007).
- [186] Kulikovska, O., Goldenberg, L., Kulikovsky, L., Stumpe, J. "Smart ionic sol-gel-based azobenzene materials for optical generation of microstructures" *Chem. Mater.* **20** (10), p. 3528-3534 (2008).
- [187] Sobolewska, A., Miniewicz, A. "Analysis of the kinetics of diffraction efficiency during the holographic grating recording in azobenzene functionalized polymers" *J. Phys. Chem. B* **111** (7), p. 1536-1544 (2007).
- [188] Audorff, H., Walker, R., Schmidt, H.-W., Kador, L. "Holographic studies of azobenzene-containing low-molecular-weight organic glasses" *Proc. SPIE* **7233** p. 72330O/1-72330O/12 (2009).
- [189] Walker, R., Audorff, H., Kador, L., Schmidt, H.-W. "Optimization of the photochromic response of photoaddressable polymers with azobenzene-containing molecular glasses" *Proc. SPIE* **7358** p. 735803/1-735803/9 (2009).
- [190] Nakano, H., Takahashi, T., Tanino, T., Shirota, Y. "Synthesis and photoinduced surface relief grating formation of a novel azobenzene-based photochromic amorphous molecular material" *J. Photopolym. Sci. Tec.* **20** (1), p. 87-89 (2007).
- [191] Fukuda, T., Matsuda, H., Shiraga, T., Kimura, T., Kato, M., Viswanathan, N., Kumar, J., Tripathy, S. "Photofabrication of surface relief grating on films of azobenzene polymer with different dye functionalization" *Macromolecules* **33** (11), p. 4220-4225 (1999).
- [192] Song, O., Wang, C., Pauley, M. "Dynamic processes of optically induced birefringence of azo compounds in amorphous polymers below T_g " *Macromolecules* **30** (22), p. 6913-6919 (1997).

15 Acknowledgement

Ich möchte mich bei meinem Doktorvater Prof. Dr. Lothar Kador bedanken, dass er mir die Möglichkeit gab, meine Dissertation in seiner Arbeitsgruppe zu schreiben. Lothar gab mir viele Freiheiten, er hatte immer Zeit für mich und konnte mir bei meinen Problemen stets weiterhelfen. Desweiteren hat er mir die Möglichkeit eröffnet, meine Ergebnisse auf zahlreichen nationalen und internationalen Konferenzen und Tagungen vorzustellen. Auch hat sich Lothar um die Finanzierung gekümmert und mir eine Stelle im Teilprojekt B2 („Photoadressierbare Blockcopolymere für die holographische Datenspeicherung“) des SFB 481 („Komplexe Makromolekül- und Hybridsysteme in inneren und äußeren Feldern“) besorgt. Auch nach dem Auslaufen des SFBs musste ich mir keine finanziellen Sorgen machen.

Ein ganz besonderer Dank geht an Dr. Roland Walker, meinem Kooperationspartner aus der Makromolekularen Chemie I hier in Bayreuth. Er hat einen Großteil der von mir gemessenen Proben synthetisiert, präpariert und thermisch charakterisiert. Diese Zusammenarbeit war stets harmonisch und fruchtbar. Desweiteren danke ich aus der MC I Prof. Hans-Werner Schmidt für viele neue Ideen und die Mittel für die Reparatur meines Lasers; Dr. Klaus Kreger für die Synthese der flüssigkristallinen molekularen Gläser, zahlreiche Diskussionen und die Korrektur vieler Manuskripte; Robin Pettau für die Synthese der smektischen flüssigkristallinen Polymere und Christian Probst für die Synthese der flüssigkristallinen Polymere für die Datenspeicherung.

Ebenso geht mein besonderer Dank an den anderen Kooperationspartner, Pascal Wolfer von der ETH Zürich. Auch diese Zusammenarbeit mit einem Materialwissenschaftler war äußerst erfolgreich und lieferte viele neue Ergebnisse. Bei seinen Aufenthalten in Bayreuth, per Mail und Telefon haben wir viele lehrreiche Diskussionen geführt.

Desweiteren bedanke ich mich bei allen aktuellen und ehemaligen Mitgliedern von EP IV für die gute Atmosphäre, vor allem bei Tobias Pflock, Paul Böhm, Ralf Kunz (die ich schon seit meiner Ankunft hier in Bayreuth vor 9 Jahren kenne), Marc Jendryny und Martti Pärs. Stets haben sie dafür gesorgt, dass ich nicht alleine zu Mittag essen musste. Werner Reichstein, der guten Seele von EP IV, möchte ich für die Unterstützung bei zahlreichen technischen Problemen danken. Außerdem hat er alle Erstkontakte für diverse Messungen mit Apparaten an der UBT hergestellt. Auch dem Sekretariat EP IV möchte ich für die Hilfe bei allerlei organisatorischen und bürokratischen Problemen danken. Auch die Möglichkeit der Nutzung der vorhandenen Infrastruktur von EP IV, u.a. des Chemielabors, der Spektrometer von Jürgen

und Werner Köhler und des AFMs -in das mir Dominique Ernst eine Einweisung gegeben hat- waren wichtig für das Vorankommen meiner Arbeit. Insbesondere möchte ich den ehemaligen Diplomanden der AG Kador, die mit mir die Denkwelle geteilt haben, den Freunden, die Bayreuth schon verlassen haben (Christian Reindl, Alexander Stülb, Florian Preisinger und Willi Hüttner), sowie Andreas Kohl danken für die schöne Zeit.

Desweiteren möchte ich mich an der Uni Bayreuth bedanken bei:

- Markus Hund für eine Einweisung in eines der AFMs am Lehrstuhl Physikalische Chemie II (Prof. Fery),
- Anika Ochs, Dr. Markus Drechsler und vor allem Carmen Kunert für die Messungen am TEM des SFB 481 (zentrales Teilprojekt Z2) / Bayreuther Institut für Makromolekülforschung (BIMF),
- dem BIMF für die Möglichkeit am Dektak messen zu können,
- Dr. Alexandra Sperschneider für die Einweisung am Ellipsometer im BZKG und
- den Mitarbeitern der Mechanikwerkstatt für die Herstellung und Reparatur diverser Teile meines Aufbaus

Ein besonderer Dank geht auch an Prof. Haarer und Werner Reichstein von Freshpoint Bayreuth/HAREKA. Sie gaben mir die Möglichkeit an einer anderen Anwendung von photochromen Materialien zu forschen, nämlich als Zeit-Temperatur-Integrator in den OnVu-labels.

Meinen Eltern möchte ich danken für die Unterstützung in den letzten 30 Jahren. Isabella danke ich für den Beistand in den schweren Zeiten und vieles mehr und ihrer Familie für die Gastfreundschaft in Weichendorf.

Und mein Dank geht auch an alle, die ich hier nicht namentlich erwähnt oder vergessen habe.